이학박사 학위논문

Spatiotemporal distribution and fate of sedimentary organic carbon of tidal flat ecosystem in the Yellow Sea

황해 연안 갯벌 퇴적환경내 유기탄소의 시공간 분포 및 거동특성 규명

2022년 8월

서울대학교 대학원
지구환경과학부
이 종 민

Spatiotemporal distribution and fate of sedimentary organic carbon of tidal flat ecosystem in the Yellow Sea

지도 교수 김 종 성

이 논문을 이학박사 학위논문으로 제출함

2022년 8월

서울대학교 대학원

지구환경과학부

이 종 민

이종민의 이학박사 학위논문을 인준함

2022년 8월

위 원 장 ______________________ (인)

부위원장 ______________________ (인)

위 원 ______________________ (인)

위 원 ______________________ (인)

위 원 ______________________ (인)

ABSTRACT

Recently, blue carbon ecosystems (BCEs), including salt marshes, mangrove forests, and seagrass meadows, have been highlighted for their capacity to fix high quantities of carbon under global warming. Although these conventional BCEs are widely studied for their role as highly efficient CO_2 sinks, holistic data analysis of carbon sink capacity and its controlling factors remain limited in the tidal flat ecosystems of the Yellow Sea. Thus, the current study evaluated the spatiotemporal distribution and fate of sedimentary organic carbon of tidal flat ecosystems in the Yellow Sea.

Sedimentary organic carbon in the surface sediments of typical intertidal areas were investigated to address year-round monthly distributions and site-specific sources. Target areas included four natural tidal flats (Ganghwa, Garolim, Sinan, and Suncheon) and one artificially closed estuary (Nakdong River) in South Korea during 2018. Among the parameters monitored, mud content was a key factor controlling organic matter content, across varying habitats, with significant positive correlations to total organic carbon (TOC). Elevated TOC content and heavier carbon stable isotope ratios ($\delta^{13}C$) in the sediments of Garolim and Suncheon from February to April of 2018 reflected microphybenthos blooms during winter, indicating a primary influence of marine sources. In comparison, $\delta^{13}C$ and $\delta^{15}N$ were depleted in the sediments of Nakdong River estuary during the flood season (September–October), indicating the direct influence of terrestrial organic input through freshwater discharge.

To estimate current organic carbon stocks and sequestration rates in the coastal areas of the West Sea, South Sea, and East Sea of South Korea, field surveys were conducted over 4 years combined with remote sensing technology were conducted encompassing entire intertidal areas. Twenty-one intertidal flats were targeted across seven provinces (Gyeonggi, Chungnam, Jeonbuk, Jeonnam, Gyeongnam, Gyeongbuk, and Gangwon). Organic carbon stocks measured in salt marshes (i.e., upper intertidal zone) reflected the high carbon fixation capacity of halophytes through primary production. The texture of different sediments was classified based on remotely sensed imagery, and was confirmed to be closely correlated with field-based classification data. Using field and remote sensing results, total organic carbon stocks and sequestration rates were estimated in the tidal flats of South Korea.

This investigation was conducted to address the effects of an invasive halophyte (i.e., *Spartina alterniflora*) on sedimentary organic carbon compared to native halophyte habitats (i.e., *Suaeda japonica* and *Phragmites australis*) in South Korea

and China. Out of the two countries, salt marshes in China tended to have higher organic carbon stocks compared to those in Korea, which was attributed to different rates of increase in TOC by halophyte species. *Spartina alterniflora* contributed to higher carbon accumulation rates in sediments (3.4 times), through higher primary production and greater root biomass, compared to *S. japonica* (2.5 times) and *P. australis* (2.4 times) over the same period. In addition, compared to *P. australis* and bare tidal flats, *S. alterniflora* had advantages with respect to greenhouse gas emissions, the food web, sediment erodibility, and carbon burial.

Finally, a large-scale investigation was conducted to demonstrate the distribution of total organic carbon stocks and sequestration rates of coastal sediments along the Yellow Sea. Riverine inputs of anthropogenic organic matter from aquaculture, municipal, and industrial areas contributed to the burial of sedimentary organic carbon. Out of the evaluated environmental parameters, sediment mud contents and halophytes were confirmed as key factors affecting organic carbon levels in coastal sediment. Based on the assimilated data, total organic carbon stocks (21–171 Tg C) and sequestration rates (0.08–0.61 Tg C yr^{-1}; 0.29–2.24 Tg CO_2 eq. yr^{-1}) were evaluated in the Yellow Sea. Of note, tidal flats had relatively lower carbon stocks due to having lower net primary production (NPP) compared to conventional BCEs. Nevertheless, given the extensive areal coverage and microphytobenthos (MPB), tidal flats could be significant carbon sinks, and also terminal reservoirs of detritus organic matter from adjacent vegetated coastal ecosystems. Overall, the distribution of sedimentary organic carbon varied in the sediment mud content and vegetation of tidal flats in the Yellow Sea. Furthermore, the sources affecting the differences in its origin included halophyte species and terrestrial-marine inputs. In conclusion, the present study provides a relatively large-scale baseline on the carbon dynamics of coastal sediments along the Yellow Sea, contributing to the global database of “Blue Carbon” science.

Keywords: Total organic carbon, Organic carbon stock, Organic carbon sequestration rates, Blue carbon, Net-zero carbon, Tidal flat ecosystem, Yellow Sea

Student Number: 2017-24161

TABLE OF CONTENTS

LIST OF ABBREVIATIONS

ANOVA	One-way analysis of variance
BCEs	Blue carbon ecosystems
C/N	Carbon to nitrogen ratio
CH_4	Methane
Chl-*a*	Chlorophyll-*a*
CO_2	Carbon dioxide
CRS	Constant rate of supply model
EA-IRMS	Elemental analyzer-isotope ratio mass spectrometer
ENC	Electronic navigator chart
GEMS	Gust erosion microcosm system
GIS	Geographic information system
IAEA	International atomic energy agency
IPCC	Intergovernmental Panel on Climate Change
MC	Mud content
MPB	Microphytobenthos
NDCs	Nationally Determined Contributions
NMDS	Non-metric multidimensional scaling
NPP	Net primary production
OC	Organic content
POM	Particulate organic matter
SOM	Sedimentary organic matter
SSC	Suspended sediment concentration
TN	Total nitrogen
TOC	Total organic carbon
VPDB	Vienna Peedee Belemnite
WC	Water content
$\delta^{13}C$	Carbon stable isotope ratio
$\delta^{15}N$	Nitrogen stable isotope ratio

LIST OF TABLES

LIST OF FIGURES

CHAPTER 1.

INTRODUCTION

1.1. Backgrounds

Concentrations of atmospheric carbon dioxide (CO_2) increased from 277 ppm at the beginning of the Industrial Era in 1750 to 407 ppm in 2018, about 270 years later (Joos and Spahni, 2008; Dlugokencky and Tans, 2019). The rise in atmospheric CO_2 above pre-industrial levels was caused by the release of carbon from land-use change and deforestation activities (Ciais et al., 2013). Although CO_2 emissions from fossil fuel combustion started before the Industrial Era, it became the dominant source to the atmosphere from the 1950s, and has increased to the present (Friedlingstein et al., 2019). Land-use change causes both higher CO_2 emissions and the deterioration of coastal ecosystems. Yet, these coastal ecosystems provide important natural carbon sinks for deforestation, forest fires, agricultural activities, and the clearance of natural vegetation, and so require protection (IPCC, 2007; Friedlingstein et al., 2019). The Intergovernmental Panel on climate change (IPCC) estimated that global CO_2 emissions should be reduced by 85% from CO_2 levels in 2000, to limit global average temperature rise to below 2°C (IPCC, 2007).

An emerging option to reduce CO_2 emissions is natural climate solutions, including carbon burial through reforestation and ecosystem management (Nesshover et al., 2017; Chausson et al., 2020). Natural climate solutions are more scalable and cost-effective than technological options, such as biochar production, geological sequestration, and direct air capture (McLaren, 2012; Pires et al., 2019). These technological options have limitations when deployed at large scales and when barriers exist, including environmental, social, and economic (Anderson and Peters, 2016). Natural climate solutions mainly target green carbon (terrestrial) ecosystems, largely overlooking ocean-based and coastal opportunities for carbon burial (Nellemann et al., 2010).

The potential of blue carbon ecosystems (BCEs), including mangrove forests, salt marshes, and seagrass meadows, has been highlighted for high carbon fixation capacity since 2009 (Macreadie et al., 2021). BCEs are highly productive coastal habitats that provide various ecosystem services, including coastal protection, food supply, and CO_2 fixation (mitigating climate change), influencing the livelihoods of millions (Barbier et al., 2011; Himes-Cornell et al., 2018; Friess et al., 2020). These blue carbon ecosystems could contribute to CO_2 drawdown, because they are able to remove greenhouse gases and store sequestered carbon over long periods (Lovelock and Duarte, 2019). Any disturbance to BCEs could accelerate potential greenhouse gas emissions; thus, blue carbon strategies are required that facilitate conservation and restoration (Duarte et al., 2013; Lovelock and Duarte, 2019).

Although BCEs occupy only 0.5% of the seafloor, from the intertidal flats to 50 m seabed depth, they contribute to more than 50% of global carbon burial in the oceans (Duarte et al., 2005; Mcleod et al., 2011; Krause-Jensen and Duarte, 2016) (Figure 1.1). Buried carbon in BCEs originates from both autochthonous and allochthonous sources, with quantities varying depending on the source (Duarte et al., 2013). In addition, anaerobic burial conditions contribute in limiting the decomposition of organic carbon by decreasing microbial activity (Macreadie et al., 2019). Compared to the Green carbon ecosystem, BCEs have the capacity to withstand natural disasters, such as bush fires, cyclones, and flooding, safeguarding the permanence of carbon storage from centennial to millennial timescales (Duarte et al., 2013; Sippo et al., 2018). Recently, approximately 50% of BCE global extent was estimated to be lost, accelerating reduced carbon burial and greater greenhouse gas emissions (Duarte et al., 2013; Lovelock et al., 2017). Consequently, the conversion and restoration of BCEs have been lighted as an urgent matter to attain net-zero carbon against climate change.

Mangrove forests, salt marshes, and seagrass meadows meet the criteria of BCEs as actionable in climate mitigation, and are already recognized for their value the by IPCC (Howard et al., 2017; Windham-Myers et al., 2018) (Table 1.1). In addition, these BCEs are included in Nationally Determined Contributions (NDCs), National Greenhouse Gas Inventory, and climate mitigation policies globally (Lovelock and Duarte, 2019; Pidgeon et al., 2021). While projects continue to develop BCEs, including Mangrove forests, salt marshes, and seagrass meadows, there remains debate as to whether other marine ecosystems (e.g., tidal flats, macroalgae, and benthic sediments) are BCEs (Lovelock and Duarte, 2019). Table 1.1 presents the criteria for delineating BCEs, ways to manage blue carbon research, and guidelines for contributing to climate change mitigation.

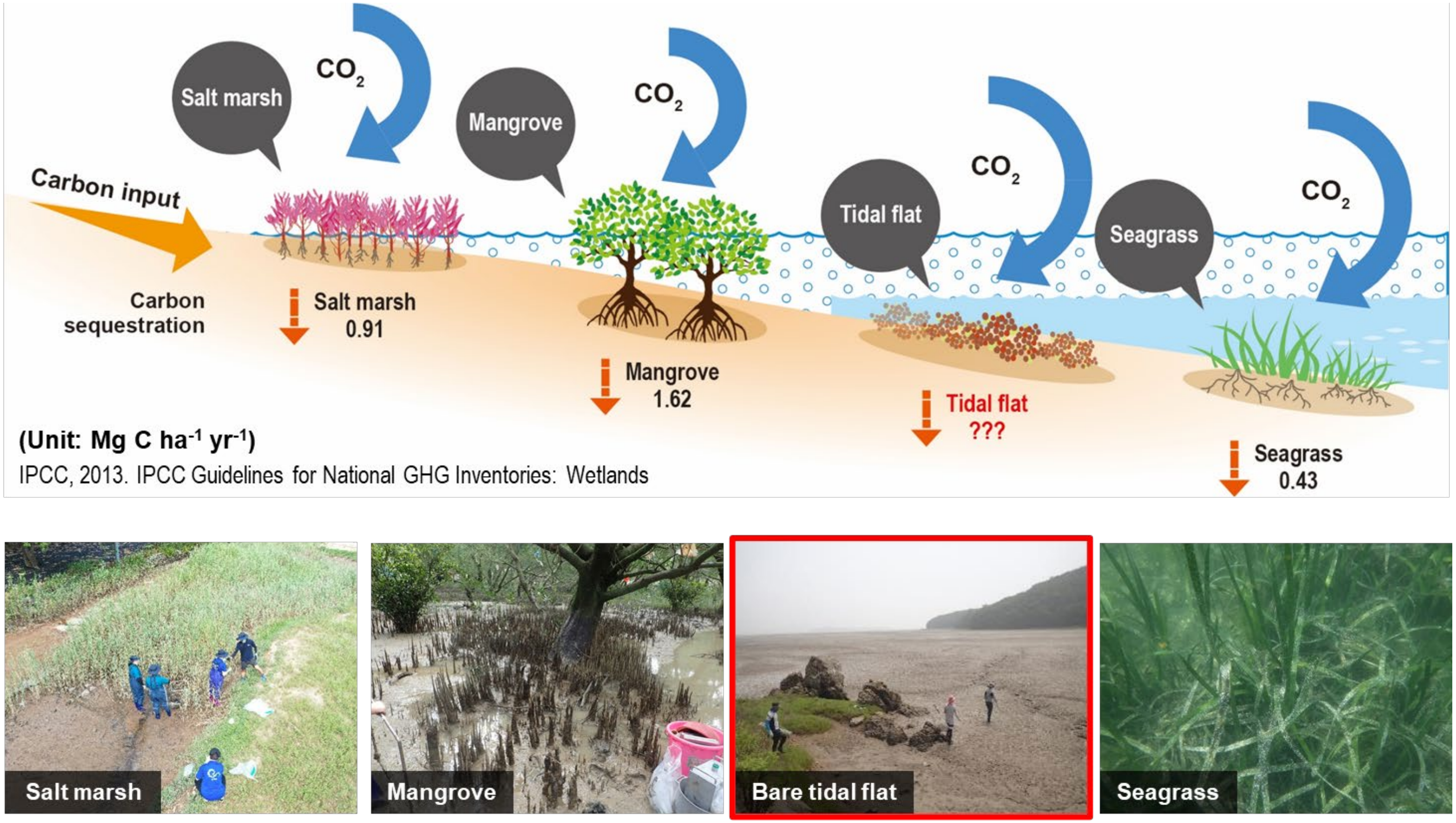

Figure 1.1
Schematic diagram of contribution of coastal environment on carbon sink.

Table 1.1.
Criteria for actionable Blue Carbon Ecosystems (BCEs) for mitigation (Lovelock and Duarte, 2019).

		Criteria for Actionable Blue Carbon Ecosystems for Mitigation					
Status	Habitat	Large scale of GHG removals or emissions	Long-term storage of fixed CO_2	Carbon loss by anthropogenic impacts	Practical management to reduce emission	Included in IPCC GHG accounting guidelines	Alignment with other policies
Actionable Blue carbon ecosystems for mitigation	Mangrove	YES	YES	YES	YES	YES	YES
	Salt marsh	YES	YES	YES	YES	YES	YES
	Seagrass	YES	YES	YES	YES	YES	YES
Emerging Blue Carbon Ecosystems	Tidal flat	?	?	YES	?	NO	YES
	Benthic sediment	?	YES	YES	?	NO	?
	Macroalgae	YES	YES	YES	YES	NO	YES
Other Ocean Ecosystems (Not actionable)	Coral reef	NO	NO	NO	NO	NO	YES
	Oyster reef	NO	?	NO	NO	NO	YES
	Phytoplankton	YES	?	?	NO	NO	NO
	Fish	NO	NO	NO	NO	NO	YES

Conventional BCEs, including mangrove forests, salt marshes, and seagrass meadows, have been widely studied for their role as highly efficient CO_2 sinks (Macreadie et al., 2021). In contrast, there is paucity of information on the status of carbon sink capacity and its controlling factors in tidal flats, one of the BCE candidates (Lin et al., 2020). Tidal flats tend to have relatively lower organic carbon stocks per unit area, due to their lower net primary production (NPP) compared to mangrove, salt marshes, and seagrasses (Chen et al., 2020; Lee et al., 2021). Yet, tidal flats could serve as important carbon reservoirs, due to their extensive areal coverage and microphytobenthos (Chen et al., 2020; Lin et al., 2020).

Recently, Murray et al. (2019) estimated that tidal flats cover 127,921 km^2 globally, with most being distributed in Asia (44% of the total). The estimated global area of tidal flats is approximately double that of salt marshes, and is comparable to mangrove areas, whereas seagrasses cover 16% of area (Davidson and Finlayson, 2019). Over the last three decades, tidal flats have been threatened by anthropogenic activities, such as reclamation and land use (Chen et al., 2016). Compared to 1984, by 2016, the global tidal flat area had noticeably decreased by 16%, with estimated losses of more than 20,000 km^2 (Murray et al., 2019). In the Yellow Sea region, around 3,800 km^2 of tidal flats have been lost from 1980 to 2010 due to reclamation (Yim et al., 2018).

Under the threat of climate change and human impacts, it is necessary to examine the spatiotemporal dynamics of sedimentary organic carbon on tidal flats. Any change to dynamic of sedimentary organic carbon on tidal flats could have significant implications on the global carbon budget, due to the large surface area of these habitats at the global scale (Chen et al., 2020; Lin et al., 2020) (Figure 1.2). However, tidal flats tend to be excluded from global carbon budget models because of a lack of studies (Lin et al., 2020). Thus, understanding of carbon dynamics in tidal flats could provide important information, contributing to the global database of “Blue Carbon” science.

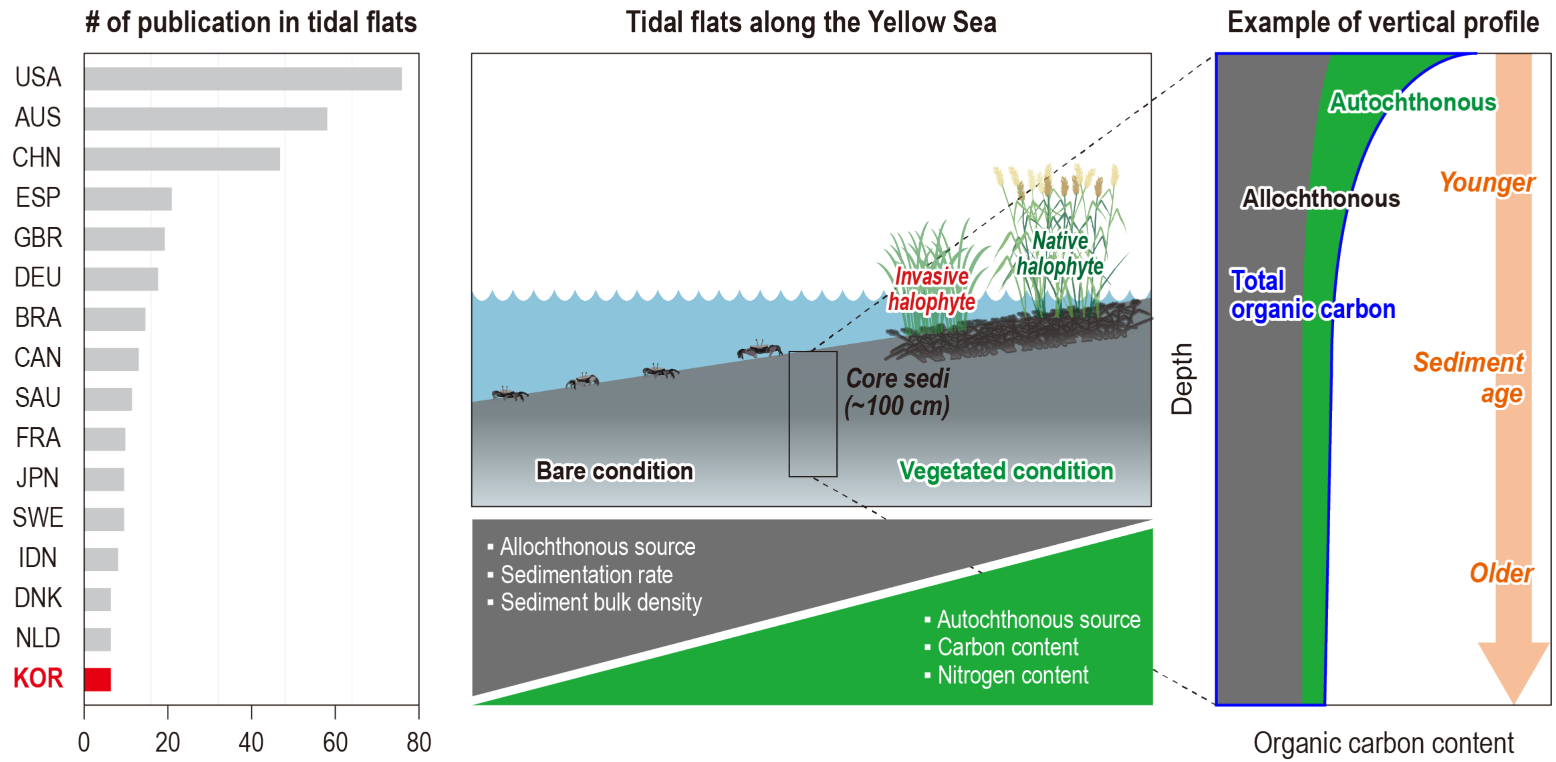

Figure 1.2
Mini review of blue carbon research about tidal flats (Scopus analysis) and conceptual diagram of sedimentary organic carbon distribution and source pattern in the Yellow Sea.

1.2. Objectives

The overarching research objective of this dissertation is "***Identifying spatiotemporal distribution and fate of sedimentary organic carbon of tidal flat ecosystems in the Yellow Sea.***" A series of case studies on sedimentary organic carbon in the tidal flat ecosystems of the Yellow Sea was conducted to advance the current scientific understanding of carbon dynamics in these systems. Sampling was designed to: **1)** identify the spatiotemporal distribution of sedimentary organic carbon in tidal flats, and **2)** elucidate environmental factors affecting the fate of sedimentary organic carbon. The specific objectives and structure of the four case studies are delineated here (Figure 1.3).

1. ***Natural and anthropogenic signatures on sedimentary organic matter across varying intertidal habitats in the waters of Korea.***

   This case study aimed to elucidate temporal variation in sedimentary organic carbon of the surface sediments in the tidal flats of South Korea. I measured organic carbon at monthly intervals in five coastal regions along the West and South Seas of South Korea (**Chapter 2**).

2. ***First national scale evaluation of organic carbon stocks and sequestration rates of coastal sediments along the West Sea, South Sea, and East Sea of South Korea***

   This case study aimed to estimate the organic carbon stocks and sequestration rates of core sediments in the tidal flats of South Korea. I investigated organic carbon at 20 coastal regions along the West and South Seas of South Korea. In addition, based on extensive field surveys, remote sensing technology, which could validate tidal flat area and sediment textural types, was integrated (**Chapter 3**).

3. ***Effect of exotic Spartina alterniflora invasion on sedimentary organic carbon across the coastal areas of the Yellow Sea***

   This case study examined the effects of native and invasive halophytes on sedimentary organic carbon. I compared carbon burial rates in native (*Phragmites* *australis* and *Suaeda japonica*) versus invasive (*Spartina alterniflora*) halophyte habitats. Data on greenhouse gases emissions, the relative contribution of primary diet, sediment erodibility, and carbon burial rates were also used to compare ecological functions between the two halophyte habitats (**Chapter 4**).

4. ***Spatial variation of sedimentary organic carbon in the coastal areas of the Yellow Sea***

   This case study verified organic carbon stocks and sequestration rates of core sediments in the tidal flats of the Yellow Sea. I investigated organic carbon in 19 coastal regions of China and 18 coastal regions of South Korea along the Yellow Sea. I also evaluated environmental parameters affecting organic carbon, and elucidated the sources of organic carbon in tidal flats (**Chapter 5**).

The detailed topics of this dissertation are intended to supplement information on the distribution and fate of sedimentary organic carbon in tidal flat ecosystems that have not been reported previously. To elucidate the fate of organic carbon with its burial in tidal flats, this study explored how the concentrations and origins of organic carbon are affected by biogeochemical properties. Finally, **Chapter 6** provides a summary of the dissertation, environmental implication and limitations, and future research directions.

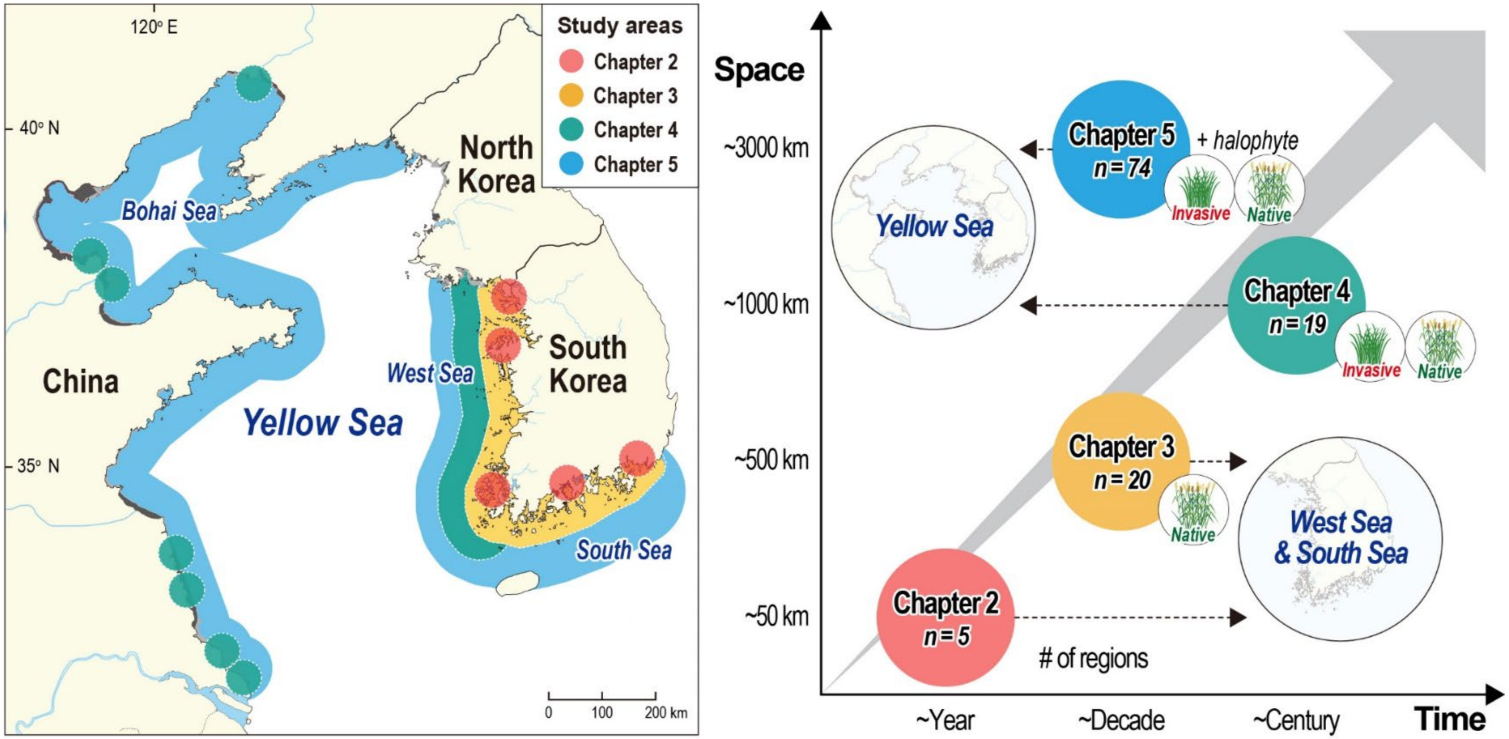

Figure 1.3
Schematic of the present study. Through four case studies, this dissertation addresses the spatiotemporal distribution and fate of sedimentary organic carbon of tidal flat ecosystem in the Yellow Sea.

CHAPTER 2.

NATURAL AND ANTHROPOGENIC SIGNATURES ON SEDIMENTARY ORGANIC MATTERS ACROSS VARYING INTERTIDAL HABITATS IN THE KOREAN WATERS

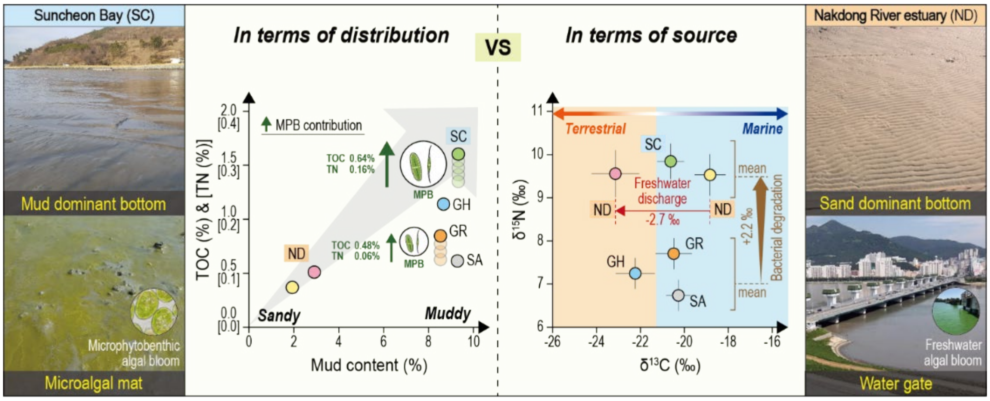

This chapter has been published to Environment International.
Lee, J., Kwon, B-O., Kim, B., Noh, J., Hwang, K., Ryu, J., Park, J., Hong, S., Khim, J.S. Natural and anthropogenic signatures on sedimentary organic matters across varying intertidal habitats in the Korean waters. *Environ. Int.* 2019, **133**, 105166.
https://doi.org/10.1016/j.envint.2019.105166

2.1. Introduction

Coastal sediment has a significant ecological role on the cycling of biogeochemical organic matter locally or globally, because it serves as a large reservoir by accumulating organic carbon in marine environment (Hedges and Keil, 1995; Kubo and Kanda, 2017). Carbon dioxide (CO_2) is one of the crucial greenhouse gases for regulating climate change, and recent reports have highlighted the role that coastal ecosystems play in sequestering CO_2 from the atmosphere (Mcleod et al., 2011). Recently, the carbon captured by several coastal ecosystems such as mangrove, salt marshes, and seagrasses, namely "blue carbon", is increasingly recognized as several studies have confirmed their roles in highly efficient CO2 sinks (Chmura et al., 2003; Duarte et al., 2004; Bouillon et al., 2008; Lo Iacono et al., 2008; Duarte et al., 2010; Kennedy et al., 2010).

Sedimentary organic matter in coastal area is subjected to receive both terrestrial and marine origins, thus its composition would vary and change depending on the sources and fate (Graham et al., 2001; Lamb et al., 2006). Also, the supply of anthropogenic input such as industrial/ municipal sewages and discharges of wastewater-treatment plant contributes to the burial of organic matter in intertidal sediments (Rumolo et al., 2011; Pradhan et al., 2014). Although many studies have been conducted on the very subject, the dynamics of sedimentary organic matters in the lotic system from rivers, estuaries, and to coastal ecosystem is still subject to debate (Krishna et al., 2013).

In particular, about half of the estuaries are artificially separated by the sea-dike in South Korea, namely called "closed estuary", thus distributions and fate of organic matters in this closed system become more complex (Kim et al., 2017; Noh et al., 2019). In fact, the sedimentary organic matter is likely site-specific, either accumulates in natural coastal zone (Hedges and Parker, 1976; Milliman et al., 1984) or could be transported to the open sea (Keil et al., 1998; Galy et al., 2007). Thus, it is necessary to characterize the sources of organic matter by addressing environmental factors influencing its distributions and transport, either under natural or altered environmental condition.

The carbon to nitrogen ratio (C/N) and stable isotope ratios of carbon ($\delta^{13}C$) and nitrogen ($\delta^{15}N$) have been widely utilized to elucidate the distribution, sources, and fate of sedimentary organic matter in aquatic environment (Meyers, 1994; Graham et al., 2001; Lamb et al., 2006; Rumolo et al., 2011; Kubo and Kanda, 2017). When determined the sources of organic matter by using such proxy, the seasonality should be carefully considered as the C/N ratios, along with $\delta^{13}C$ and $\delta^{15}N$ values, in surface sediments might temporally vary due to its association to biogeochemical components (Liu et al., 2006; Kubo and Kanda, 2017). In particular, the influence of algal primary production and/or bacterial degradation would significantly change in the nutrient enriched environments of intertidal zone, estuary, or semi-enclosed bay system (Voβ and Struck, 1997; Liu et al., 2006).

Several earlier studies have reported that the enriched δ13C values were directly influenced by increasing primary production of microphytobenthos (MPBs) in Scheldt estuary (Riera et al., 2000), in Hiroshima Bay (Takai et al., 2004), and in Kwangyang Bay (Kang et al., 2006). In comparison, the $\delta^{15}N$ values of surface sediments were reported to increase with bacterial degradation (Rumolo et al., 2011; Kang et al., 2017). In addition, the $\delta^{13}C$ and $\delta^{15}N$ values revealed significant variations in response to increased discharges of water and suspended sediment from upper Nakdong River through freshwater discharge during the flood season (Liu et al., 2006; Wang et al., 2018).

In general, sediment properties such as mud content and composition are known as important environmental factors to determine the distributions and fate of organic matters in the shallow water system (Serrano et al., 2016). For example, muddy sediment mainly composed of silt and clay retains more organic matter compared to sandy fraction, due to a greater adsorption capacity of fine-grained particles by earning a larger surface area (Keil and Hedges, 1993; Burdige, 2007). Moreover, fine-grained particles enhance the preservation of organic matter through reduced redox potential and/or remineralization rates (Hedges and Keil, 1995; Dauwe et al., 2001; Burdige, 2007). Thus, the critical association of sediment properties to organic matter should be one fundamental question to address its geochemical processes.

The present study aimed to investigate how the various environmental conditions or parameters drive the spatiotemporal variations of sedimentary organic matters in the natural and altered intertidal zones. Field survey was monthly performed to identify and trace organic matters in sediment from the four typical tidal flats and one artificially closed estuary over of one year. The targeted endpoints included total organic carbon (TOC), total nitrogen (TN), water content (WC), mud content (MC), organic content (OC, by loss on ignition), benthic Chlorophyll a (Chl-a), δ^{13}C, and δ^{15}N in the surface sediment. The specific objectives were to: (1) investigate regional and temporal variations of sedimentary organic matter; (2) evaluate relationship between sedimentary organic matter and geochemical properties; (3) determine effects of biological component (e.g., microalgal biomass) on sedimentary organic matter; and finally (4) elucidate sources of sedimentary organic matter, in and cross the natural and altered coastal ecosystems.

2.2. Materials and methods

2.2.1. Study area

Surface sediment samples were monthly collected from the five coastal areas in Korea for the period of one year (in 2018), encompassing 12 consecutive months. To elucidate the sources and fate of organic matter, the target study areas were selected to generally represent the typical and altered tidal flats along the west and south coasts of Korea (Fig. 2.1). Three areas from the west coast (Ganghwa, Garolim Bay, and Sinan) and two from the south coast (Suncheon Bay and Nakdong River estuary) would cover the typical natural intertidal systems and altered closed estuary. In specific, first, the Ganghwa tidal flat (GH1–GH3) is located at the mouth of the Han River in the midwest of the Korean Peninsula, and lies between the Sukmo channel to the west and the Yeomha channel to the east. The huge tidal flats (~240 km2) are developed around the Ganghwa Island, and are affected by freshwater (salinity: 23.1 psu) and tidal currents flowing from the Han River to the main waterways (Choi et al., 2011; Koh and Khim, 2014).

Second, the Garolim Bay (GR1–GR2) encompassing ~90 km2 tidal flats is a semi-enclosed bay surrounded by Seosan and Taean counties. Because there is no large river flowing into the inner bay, freshwater input is quite limited, accordingly salinity is relatively high (31.7 psu) and uniform compared to other study areas.

Third, the Sinan tidal flat (SA1–SA2) is located in southwest Korea, also covering the extended tidal flats of ~343 km2. The Sinan tidal flat is classified as an island tidal flat, as it is surrounded by hundreds of islands and recognized as the Ramsar site because of its outstanding landscape and great marine biodiversity (Choi, 2014; Koh and Khim, 2014).

Fourth, the Suncheon Bay (SC1–SC2) is semi-closed system, on the south coast of Korea, surrounded by Yeosu Peninsula and Goheung Peninsula. The tidal flat is relatively small in size (~24 km2), but extensive reed vegetations are developed with mud-dominated bottom, accordingly recognized as one of representative habitats for the migratory birds (Koh and Khim, 2014). Of note, facilities that discharge pollutants, e.g., sewage treatment plant, in the upstream region would be potential source for organic pollution around the bay.

Finally, the Nakdong River estuary is located on the southeastern part of the Korean peninsula (ND1–ND2), and has a well-developed delta, with ~40 km2 of tidal flats (Joh, 2013), that is protected by sand dunes parallel to the coastline. Nakdong River is the longest river (~525 km) with the largest watersheds (~24,000 km2) in South Korea, encompassing many cities and counties from Taeback County to Busan City. A huge estuarine barrage built in 1987 controls the discharge of freshwater through water gates, thus the estuarine delta has been significantly influenced by both anthropogenic river discharge and natural tidal forcing in morphodynamic manner (Hong et al., 2013; Williams et al., 2013).

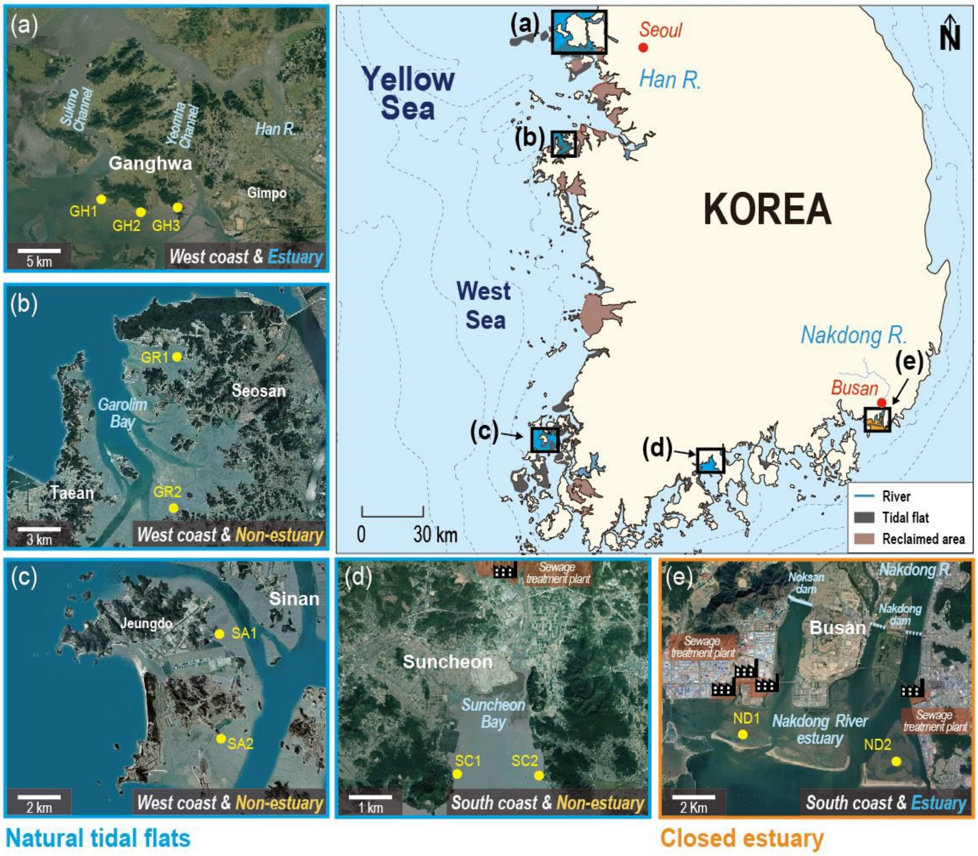

Figure 2.1
Map showing the sampling sites at (a) Ganghwa (GH1-GH3), (b) Garolim Bay (GR1-GR2), (c) Sinan (SA1-SA2), (d) Suncheon Bay (SC1-SC2), and (e) Nakdong River estuary (ND1-ND2), Korea. Surface sediments were collected monthly from January to December in 2018. All satellite images obtained from Google Map. The location of sewage treatment plant given for supplementary information in each study area, if present.

2.2.2. Sampling and laboratory analyses

Surface sediments were collected from a total of 11 locations from January to December 2018, and 2–3 representative locations were selected for the monthly monitoring in each area by considering geographical and oceanographic settings. Surface sediments (0–0.5 cm) were collected in triplicate with a stainless-steel spatula. Seawater was sampled to analyze stable carbon and nitrogen isotopic compositions in particulate organic matter (POM) in water column over two seasons (March and July). All sediments and seawater samples were immediately stored at −25 °C until analysis.

For the further analyses of general sediment parameters, samples were mixed well and stored in airtight plastic bags to prevent evaporation, and were subsequently transferred to the laboratory. WC was obtained by measuring weight loss after drying sediments at 70 °C for 72 h until a constant weight was attained. MC was determined from rapid partial analysis by wet-sieving (Buchanan, 1984). Sediment textural type was classified by mud (silt + clay) content: sand (<5% mud), sandy mud (50–75% mud), slightly sandy mud (75–95% mud), and mud (>95% mud) (Table 2.1). OC was measured by burning sediments to ashes at 550 °C for 4 h (Heiri et al., 2001), to determine weight loss after combustion. Samples for measurement of benthic Chl *a* concentration (indicating *in situ* MPB biomass) were collected by use of the syringe corer. The sediment samples were frozen in the field and brought to the laboratory. Benthic chlorophylls were immediately extracted with acetone (15 mL) for 24 h in the dark at 4 °C. Samples were then centrifuged at 1500 rpm for 5 min, and the supernatant aliquot was measured for Chl *a* by the method described elsewhere (Lorenzen, 1967). The sediment samples for analyses of TOC, TN, $\delta^{13}C$, and $\delta^{15}N$ were freeze-dried, homogenized, and powdered using agate mortar. The sediment was decalcified with 10% HCl, washed twice with deionized water, and freeze-dried for TOC and $\delta^{13}C$ determination. Sediment samples for TOC, TN, $\delta^{13}C$, and $\delta^{15}N$ were measured using an Elemental Analyzer-Isotope Ratio Mass Spectrometer (EA-IRMS) (Elementar, Gmbh, Hanau, Germany). All isotopic compositions were expressed as delta notation (‰) (Eq. 1):

$$\delta^{13}C \text{ or } \delta^{15}N\ (‰) = [R_{sample}/R_{reference} - 1] \times 1000 \qquad (1)$$

where, R_{sample} and $R_{reference}$ are the composition ($^{13}C/^{12}C$ or $^{15}N/^{14}N$) of the sample and reference, respectively. Isotopic compositions were reported relative to conventional reference materials; Vienna Peedee Belemnite (VPDB) for carbon and atmospheric N_2 for nitrogen. IAEA-N-2 (International Atomic Energy Agency (IAEA), Vienna, Austria) and IAEA-CH-3, were used as working standards to calculate the analytical error of carbon and nitrogen, respectively. Measurement precision was approximately 0.04‰ for $\delta^{13}C$ and 0.2‰ for $\delta^{15}N$, respectively.

Table 2.1.

Data on total organic carbon and total nitrogen in surface sediments by sediment textual types.

Sediment textual type[a]	n	Mud contents (%)	Total organic carbon (%)	Total nitrogen (%)
Mud	66	95 <	0.87 ± 0.53	0.11 ± 0.08
Slightly sandy mud	29	75 ~ 95	0.82 ± 0.45	0.10 ± 0.06
Sandy mud	11	50 ~ 75	0.60 ± 0.36	0.06 ± 0.04
Muddy sand	1	25 ~ 50	0.80 ± 0.25	0.09 ± 0.03
Slightly muddy sand	3	5 ~ 25	0.25 ± 0.07	0.03 ± 0.01
Sand	18	< 5	0.15 ± 0.06	0.02 ± 0.01

[a]Sediment textural types were classified by mud (silt + clay) contents: sand (< 5 % mud), slightly muddy sand (5-25 % mud), muddy sand (25-50 % mud), sandy mud (50-75 % mud), slightly sandy mud (75-95 % mud), and mud (> 95 % mud) (Flemming, 2000).

2.2.3. Data analysis

Pearson correlation analysis was performed to test for significant relationships among TOC and MC, TN and MC, Chl-*a* and TOC, Chl-*a* and TN, and Chl-*a* and $\delta^{13}C$. SPSS 23.0 (SPSS INC., Chicago, IL) was used to perform the statistical analysis. TOC and TN contents of sediments were analyzed to test for differences between the textural classes of sediment (mud, slightly sandy mud, sandy mud, and sand) using a T-test and one-way analysis of variance (ANOVA) with Bonferroni post-hoc test. Before the analysis, homogeneity of variance was determined between groups by Levene's homogeneity test, meeting the assumption of homogeneity of variance (p >0.05). The same statistical method was used to test differences in $\delta^{13}C$ and $\delta^{15}N$ of the Nakdong River estuary sediments (ND1 and ND2) in aspect of natural and altered responses. To characterize surface sediment groups in the sampling areas, cluster analysis was performed with PRIMER 6 statistical software (PRIMER-E Ltd., Plymouth, UK). Euclidean distance was calculated, and data were subjected to group average sorting. Principle component analysis (PCA) was performed to explore overall correlations across sedimentary organic matter and environmental parameters.

2.3. Results and discussion

2.3.1. Spatiotemporal distributions of sedimentary organic matter

The data of sedimentary TOC, TN, C/N ratio, $\delta^{13}C$, and $\delta^{15}N$ in the five coastal areas generally indicated their varied distributions spatially and temporally (Figure. 2.2). First, by grouping in cluster analysis, stations were well-grouped according to locality (i.e., Group A (A1 & A2), B, and C at 4 of distance). In particular, geographical difference was playing as a key criterion in a subgrouping among stations such as Group A1 and A2 in west coast and Group B and C in south coast of Korea. Further, by locality, the SC had the greatest TOC (1.27 ± 0.37%) and TN (0.18 ± 0.07%), followed by GH (TOC: 1.09 ± 0.42%; TN: 0.11 ± 0.05%), SA (TOC: 0.44 ± 0.14%; TN: 0.06 ± 0.02%), GR (TOC: 0.36 ± 0.19%; TN: 0.04 ± 0.02%), and ND (TOC: 0.19 ± 0.15%; TN: 0.03 ± 0.02%) (Figure 2.2a, b). Second, the TOC and TN contents of the surface sediment generally showed high monthly fluctuations, particularly at GH, reflecting combined influences of freshwater input from the Han River and tidal circulation (Choi et al., 2011). Further, seasonal variations of TOC and TN in GH indicated the impact of increased freshwater discharge by large amount of precipitation (Figure 2.3). Of note, certain tidal flats showed distinct seasonal variations, i.e., elevated TOC and TN were characteristic at muddy bottom dominated bays of GR and SC during the winter to early spring. This phenomenon could occur as the large amounts of organic matter generated by MPB production might have increased the flux of organic matter to the sediments (Kubo and Kanda, 2017). Whilst, the sand-dominant sediments of ND showed the smallest TOC and TN with weakened seasonal and monthly variabilities, among the five coastal areas.

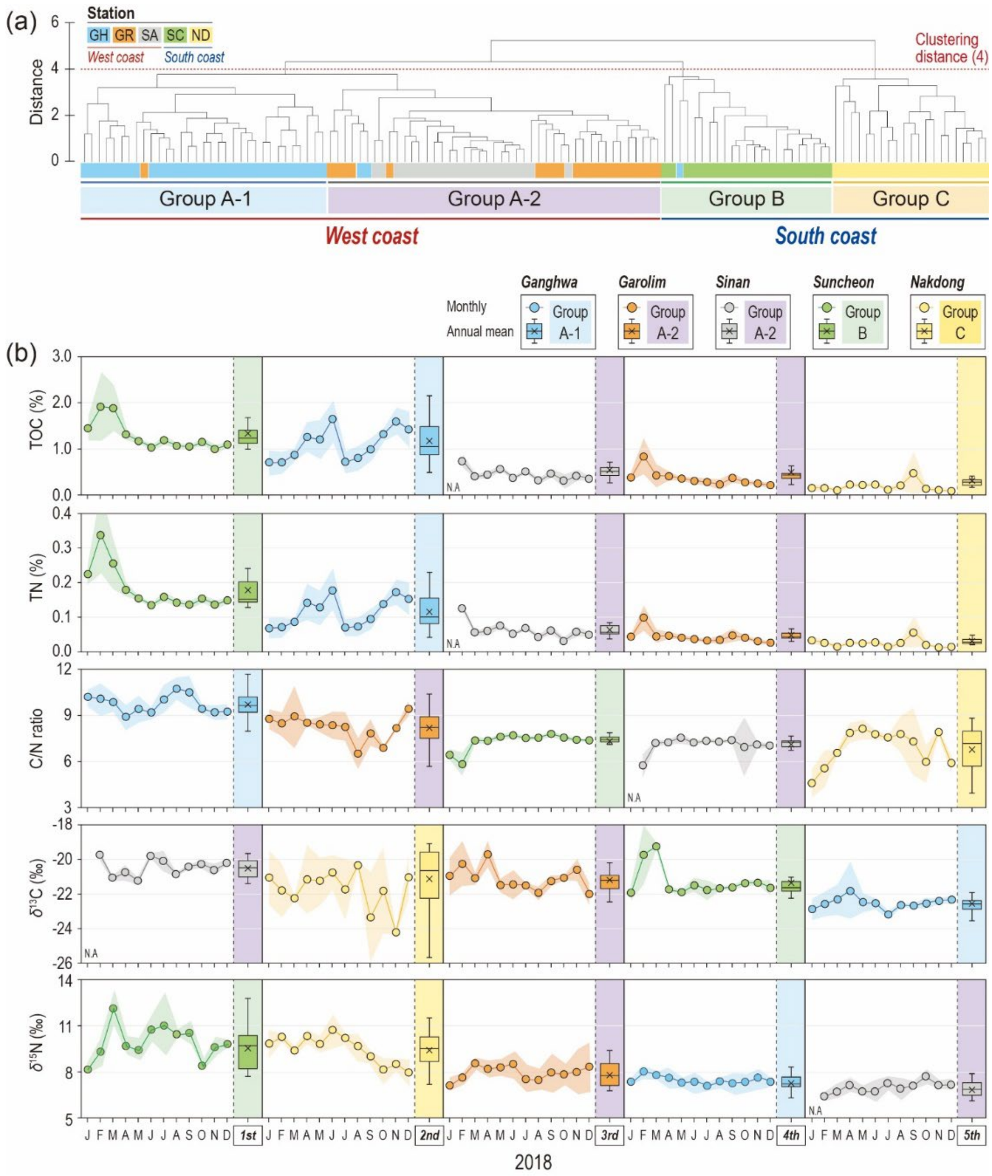

Figure 2.2.

(a) Cluster analysis and (b) monthly variations of TOC (%), TN (%), C/N ratio, δ^{13}C (‰), and δ^{15}N (‰) in surface sediments of five intertidal flats, Korea. Blue, orange, grey, green, and yellow lines denote at Ganghwa, Garolim, Sinan, Suncheon, and Nakdong River estuary, respectively.

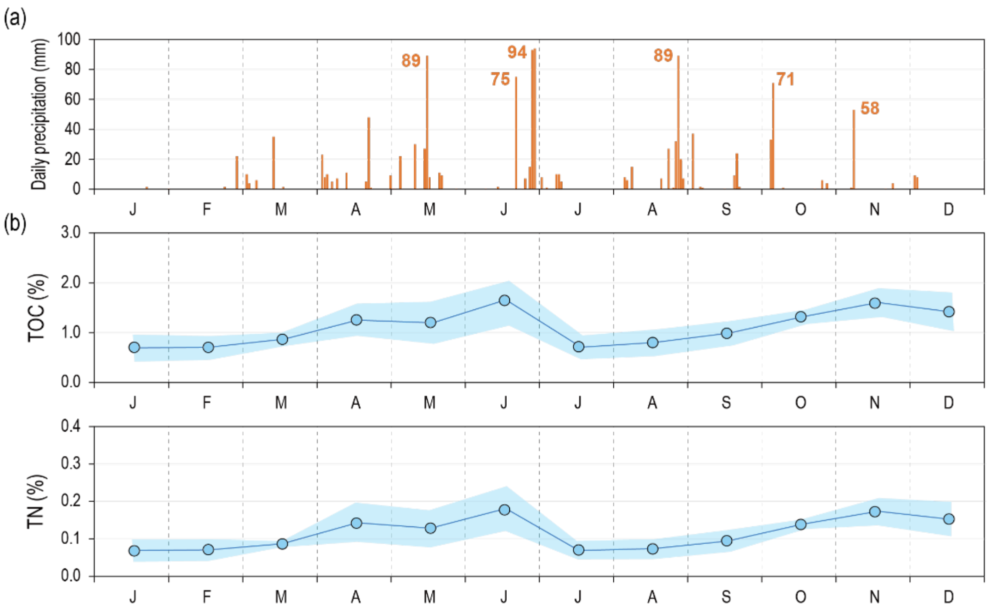

Figure 2.3.
(a) Daily precipitation rate (mm, orange bar) at Ganghwa estuary from January to December in 2018 (The Korea Ministry of Environment, 2019). (b) Total organic carbon (TOC) and total nitrogen (TN) of surface sediments at Ganghwa.

The C/N ratio, a discriminating proxy of terrestrial and marine origin (Rumolo et al., 2011), varied slightly cross the study areas with total mean of 8.0 (3.9–11.7). The monthly variation in C/N ratio was the greatest at ND (3.9–8.8), followed by GR (5.7–10.4), GH (7.9–11.7), SA (5.1–8.3), and SC (5.2–7.9). Considering the mean C/N ratio, only GH sediments (9.7) were found to be dominated by terrestrial organic sources (Hedges et al., 1986). Whilst, all the other coastal areas might have received primarily marine-derived organic matter, considering its reported C/N ratios of 4–9 (Meyers, 1994; Hedges et al., 1997; Kubo and Kanda, 2017). Typical $\delta^{13}C$ and $\delta^{15}N$ values of marine organic matters were reported to range from −22 to −18‰ (Peters et al., 1978; Wada et al., 1987; Middelburg and Nieuwenhuize, 1998) and 3 to 12‰ (Wada et al., 1987; Thornton and McManus, 1994; Lamb et al., 2006), reflecting marine phytoplankton (Yamaguchi et al., 2003). Particularly in Korea, $\delta^{13}C$ of marine organic matters was reported to range from -20.5 to -17.7‰ (mean: -19.0‰) in west coast (Kang et al., 2003; Suh and Shin, 2013; Lee et al., 2017; Park et al., 2019) and -22.9 to -18.20 (mean: -20.3‰) in south coast (Kang et al., 2003; Kang et al., 2007; Park et al., 2015; Park et al., 2019). Whilst, the typical isotope compositions of terrestrial organic matter showed that $\delta^{13}C$ and $\delta^{15}N$ values ranged from −33 to −25‰ (Barth et al., 1998; Middelburg and Nieuwenhuize, 1998) and from 0 to 4‰ (Thornton and McManus, 1994), of which isotopic signatures are indicative of C3 plants. (Maksymowska et al., 2000). Moreover, terrestrial plants that use the C3 photosynthetic pathway constitute about 90% of all plants, and these plants preferentially take up ^{12}C by diffusion resulting in depletion of ^{13}C organic matter compared to marine organic matters (Lamb et al., 2006).

Similar to the results of C/N signatures, the four target areas (GR, SA, SC, and ND; except for ND2) reflected marine dominated signatures, with mean $\delta^{13}C$ values of -20.81‰ (Table 2.2 and Figure 2.4). In contrast, GH sediments exhibited terrestrial origin, with lighter $\delta^{13}C$ values (mean: -22.54‰). In the meantime, the $\delta^{15}N$ values also reflected the site-specific variations of coastal organic matter. For example, GH, GR, and SA showed lesser monthly variations in $\delta^{15}N$, whereas elevated peak of $\delta^{15}N$ at SC was observed in the early spring (February–Marrch) (Figure 2.2). Meantime, the C/N ratio, $\delta^{13}C$ and $\delta^{15}N$ signatures in ND clearly indicated the impact of increased freshwater discharge during the flood season (September–October) (Figure 2.4). The signature of seasonality in $\delta^{13}C$ and $\delta^{15}N$ was consistent to the seasonal pattern in river discharge, with maximum discharge coinciding in the summer monsoon period (Hong et al., 2013). Of note, the western water gate of Nakdong estuarine barrage is only operated during the flood season, while the main watergate is opened daily during the ebb tide (The Korea Ministry of Environment, 2015). Thus, a large amount of suspended particles and organics inside the main Nakdong water gates flow out and affect the distirubtions of mud and organic matter contents in estuarine sediments (Williams et al., 2013). In summary, our results demonstrated that spatiotemporal distributions of sediment organic matter at tidal flats and estuary generally reflected the geographical settings with anthropogenic impacts embedded.

Table 2.2.
Data statistics on the physicochemical parameters of sediment properties, collected from Ganghwa, Garolim, Sinan, Suncheon, and Nakdong River estuary, during the period of 12 months, from January to December in 2018.

	Ganghwa			**Garolim**			**Sinan**[a]			**Suncheon**			**Nakdong River estuary**		
	min	**max**	**mean**	**min**	**max**	**mean**	**min**	**max**	**mean**	**min**	**max**	**mean**	**min**	**max**	**mean**
WC (%)	12.2	58.5	30.1 (±13.0)	30.2	85.9	44.6 (±13.7)	33.2	43.4	39.4 (±2.6)	40.6	82.3	57.9 (±7.2)	17.8	40.9	27.5 (±4.1)
MC (%)	59.0	99.8	87.7 (±13.4)	62.5	99.1	87.2 (±11.4)	91.2	99.6	98.0 (±1.9)	84.9	99.8	96.5 (±4.0)	1.5	36.5	5.8 (±7.3)
OC (%)	3.3	9.7	5.8 (±1.4)	2.4	6.4	4.1 (±0.8)	3.5	10.1	6.2 (±1.7)	7.1	16.9	9.6 (±2.5)	1.3	4.1	2.4 (±0.8)
Chl-*a* (mg m^{-2})	6.7	84.0	31.7 (±21.5)	13.1	107.8	37.7 (±22.5)	4.9	47.9	15.7 (±10.1)	4.2	496.0	43.2 (±100.7)	8.7	119.3	49.2 (±30.3)
TOC (%)	0.39	2.09	1.09 (±0.42)	0.15	1.11	0.36 (±0.19)	0.18	0.82	0.44 (±0.14)	0.93	2.42	1.27 (±0.37)	0.07	0.80	0.19 (±0.15)
TN (%)	0.04	0.23	0.11 (±0.05)	0.02	0.12	0.04 (±0.02)	0.03	0.13	0.06 (±0.02)	0.13	0.46	0.18 (±0.07)	0.01	0.09	0.03 (±0.02)
C/N	7.9	11.7	9.7 (±0.8)	5.7	10.4	8.2 (±1.0)	5.1	8.3	7.1 (±0.7)	5.2	7.9	7.3 (±0.6)	3.9	8.8	6.8 (±1.4)
$\delta^{13}C$ (‰)	-23.5	-19.9	-22.5 (±0.6)	-22.4	-19.2	-21.1 (±0.8)	-21.4	-19.6	-20.5 (±0.5)	-22.2	-18.6	-21.3 (±0.9)	-25.7	-19.0	-21.1 (±1.8)
$\delta^{15}N$ (‰)	6.3	8.3	7.3 (±0.5)	6.7	9.4	7.9 (±0.8)	6.1	7.9	6.9 (±0.5)	7.7	12.9	9.6 (±1.3)	7.2	11.5	9.5 (±1.0)

[a] Samples were collected from Sinan over 11 months (February–December) of 2018.
WC, Water contents; MC, Mud contents; OC, Organic contents; Chl-*a*, Chlorophyll-*a*; TOC, Total organic carbon; TN, Total nitrogen; C/N, Carbon to nitrogen ratio; $\delta^{13}C$, Delta 13-C values; $\delta^{15}N$, Delta 15-N values

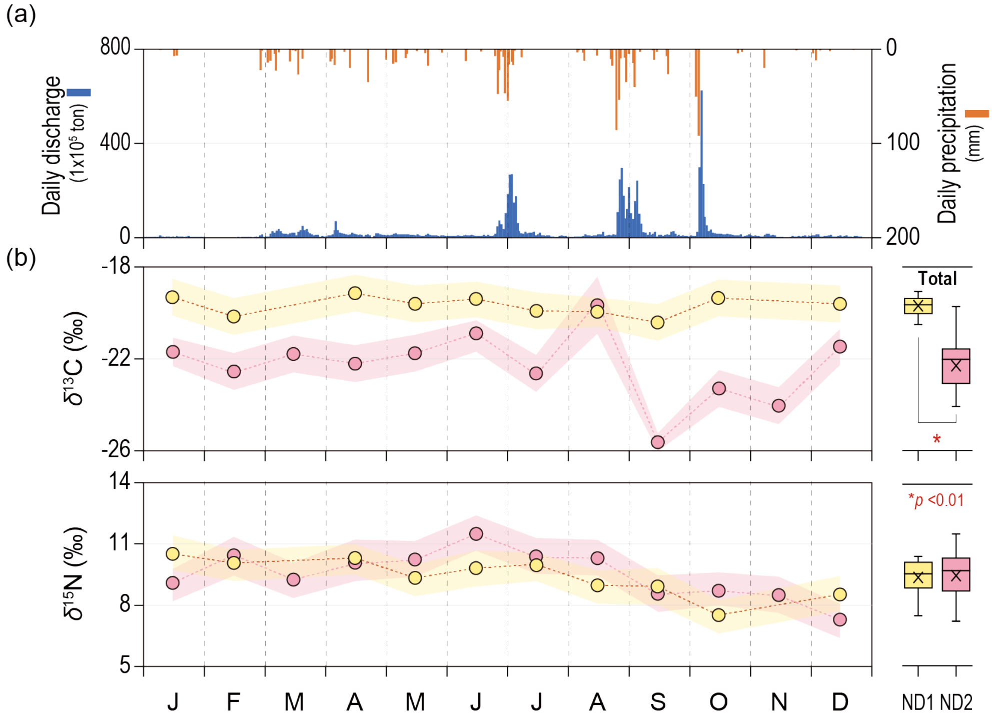

Figure 2.4.

(a) Daily discharge in water mass (1 x 10^5 ton, blue bar) and daily precipitation rate (mm, orange bar) in Nakdong River estuary from January to December in 2018. (b) Stable carbon and nitrogen isotopic ratios ($\delta^{13}C$ and $\delta^{15}N$) of surface sediments in Nakdong River estuary. Surface sediments were collected from two sites including Nakdong River estuary 1 (ND1) and Nakdong River estuary 2 (ND2).

2.3.2. Effects of the mud contents on sedimentary TOC and TN

In general, the coastal sediments collected from the target study areas represented mud dominated bottom fraction, with average of >85% mud content, except for ND. SA had the greatest MC (mean ± SD, 98.0 ± 1.9%), followed by SC (96.5 ± 4.0%), GH (87.7 ± 13.4%), GR (87.2 ± 11.4%), and ND (5.8 ± 7.3%) (Table 2.2). Meantime, not surprisingly, the MC did not show certain seasonal patterns throughout the year, except for flood season at ND. TOC and TN were generally greater in mud-dominant sediments (0.83 ± 0.50% and 0.10 ± 0.07%, respectively) compared to those in sand-dominant ones (0.19 ± 0.15% and 0.03 ± 0.02%). Thus, the relationships between sedimentary organic matter (TOC and TN) and MC (% of particles <63 μm) in different regions were scrutinized (Figure 2.5). The analysis revealed that the MC showed significant positive correlations to TOC (r = 0.66, $p < 0.001$) and TN (r = 0.44, $p < 0.001$), respectively. There was no significant difference in the TOC and TN cross various sediment facies (mud, slightly sandy mud, sandy mud, sand); however, there was a significant difference in TOC (n = 18, F - 20.07, $p < 0.01$) and TN (n = 18, F - 9.99, $p < 0.01$) between sand and non-sand fractions (mud, slightly sandy mud, and sandy mud). MC can be used to predict sediment TOC and TN in bare intertidal sediments, and is used as a cost-effective proxy or indicator of organic matter (Serrano et al., 2016).

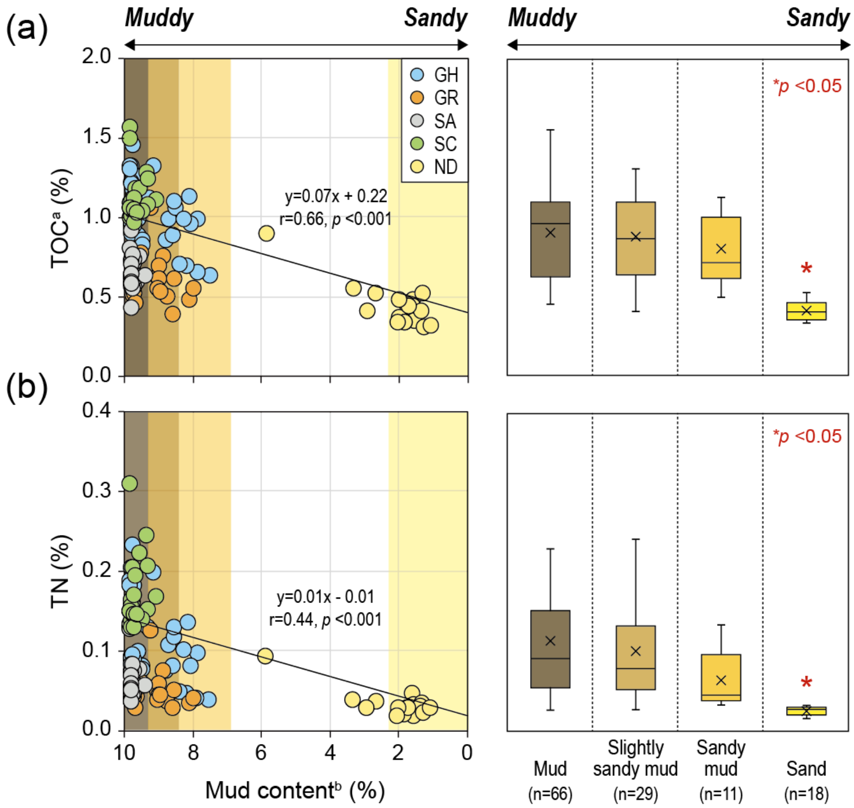

Figure 2.5.
Relationships between mud contents and (a) TOC and (b) TN in surface sediments of five intertidal flats, Korea. [a] TOC and [b] mud contents in the surface sediments were square root transformed for normality. Sediment textural types were classified based on mud (silt + clay) contents: sand (< 5% mud), sandy mud (50–75% mud), slightly sandy mud (75–95% mud), and mud (>95% mud) (Flemming, 2000).

The positive relationship between mud and organic matter found in the present study was consistent to the several previous reports (Keil and Hedges, 1993; Bergamaschi et al., 1997; Flemming and Delafontaine, 2000), generally supporting greater adsorption capacity of fine particles to organics (Mayer, 1994; Burdige, 2007). Because fine-grained sediments (e.g., mud) provide more binding sites for organic matter flocculation by providing larger surface areas than coarse-grained sediments (e.g., sand), cohesive sediments contain greater organic matter in surface sediments (Keil and Hedges, 1993; Mayer, 1994; Burdige, 2007). Meantime, it should be noted that TOC and TN in mud-dominant sediments (>85%) slightly varied (Figure 2.5), possibly indicating prevailing allochthonous sources at some locations (Kennedy et al., 2010; Serrano et al., 2016). In fact, many other factors could control adsorption, affinity, and residence time of particle fractions to organic matter, thus additional aspects such as chemical stabilization (Percival et al., 2000; Galy et al., 2007) and some biological interactions (Sherr, 1982; Danovaro et al., 1994) should also be taken into consideration.

2.3.3. Effects of benthic microalgae on sedimentary TOC and TN

As mentioned earlier, the elevated TOC and TN contents at some tidal flats, particularly in GR and SC, were observed during the periods of MPB winter bloom. Thus, a special caution was given to address the effect of benthic microalgal biomass and distributions on sedimentary TOC and TN. The sediment Chl-*a*, measured as proxy of benthic microalgal biomass, generally indicated high productive intertidal zone across the five study areas (Park et al., 2014). The ND showed the greatest concentrations of Chl-*a* (49.2 ± 30.3 mg Chl-*a* m^{-2}), on average, followed by SC (43.2 ± 101 mg Chl-*a* m^{-2}), GR (37.7 ± 22.5 mg Chl-*a* m^{-2}), GH (31.7 ± 21.5 mg Chl-*a* m^{-2}), and SA (15.7 ± 10.1 mg Chl-*a* m^{-2}) (Table 2.2 and Figure 2.6). It should be noted that some fraction of high concentrations of benthic Chl-*a* in ND included not only MPB but also freshwater-derived microalgae such as cyanobacteria etc. In general, the benthic Chl-*a* in surface sediments found in the present study were comparable to the previously reported values in the Asian tidal flats (Magni and Montani, 1997; Park et al., 2014).

In aspect of seasonal variability of benthic microalgal biomass, the patterns are characterized into three-case groups; 1) distinct seasonal variations with winter algal bloom (GR and SC); 2) relatively constant algal biomass with weak sign of spring bloom (GH and SA); and finally 3) irregular temporal fluctuation with elevated algal biomass during summer flooding time (ND). Thus, relatively great TOC and TN found in the four tidal flat sediments were apparently influenced by the MPB blooms during the corresponding periods; say pattern 1 and 2 above. Of note, the small TOC and TN from ND did not reflect the elevated microalgal biomass, thus large proportion of microalgae did not seem to contribute as sources of organic matter, particularly in sand dominated bottom (Liu et al., 2016).

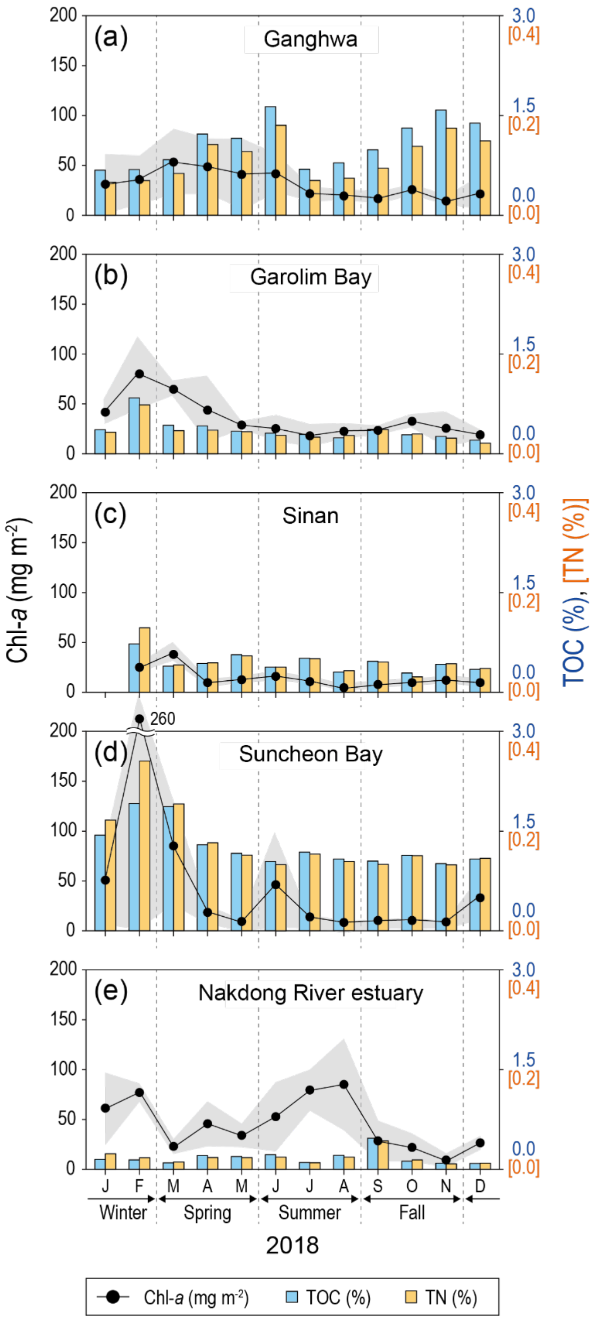

Figure 2.6.
Monthly variations of Chl-*a* (mg m^{-2}) (black lines), TOC (%) (blue bars), and TN (%) (orange bars) in the surface sediments from (a) Ganghwa, (b) Garolim, (c) Sinan, (d) Suncheon, and (e) Nakdong River estuary, Korea.

The relationship between benthic Chl-*a* and the amount of organic matter in each area further explain the direct association between algal biomass and sedimentary organic parameters in site-specific manner. For example, Chl-*a* concentrations were significantly correlated with TOC (r = 0.54, $p < 0.05$ and r = 0.78, $p < 0.01$, respectively), TN (r = 0.55, $p < 0.05$ and r = 0.89, $p < 0.01$), and $\delta^{13}C$ (r = 0.55, $p < 0.05$ and r = 0.74, $p < 0.01$) in GR and SC (Figure 2.7). This result apparently suggested that benthic primary producers significantly contribute to sedimentary organic matter in these natural tidal flats. In contrast, the relationships between benthic Chl-*a* and organic matter parameters were not statistically significant for GH, SA, and ND, which were categorized as pattern 2 and 3 groups above (Figure 2.7). It should be noted that, however, the GH became to show significant association of MPB to organic matters when excluded certain periods; viz., January–March. Altogether, the results of present study generally supported that the greater production in response to winter and/or spring microalgal blooms would have influenced the enriched benthic condition cross the typical soft bottom tidal flats of Korea (Kwon et al. 2018; Montani et al., 2003). Of note, surface sediments from all the natural tidal flats were primarily composed of marine-derived organic matter, suggesting important ecological role of MPB in the given system (Koh and Khim, 2014). Considering the significant CO_2 sink by the microalgal biofilm on surface sediments of the tidal flats (Chen et al. 2019), its ecological role should also be addressed in a holistic view.

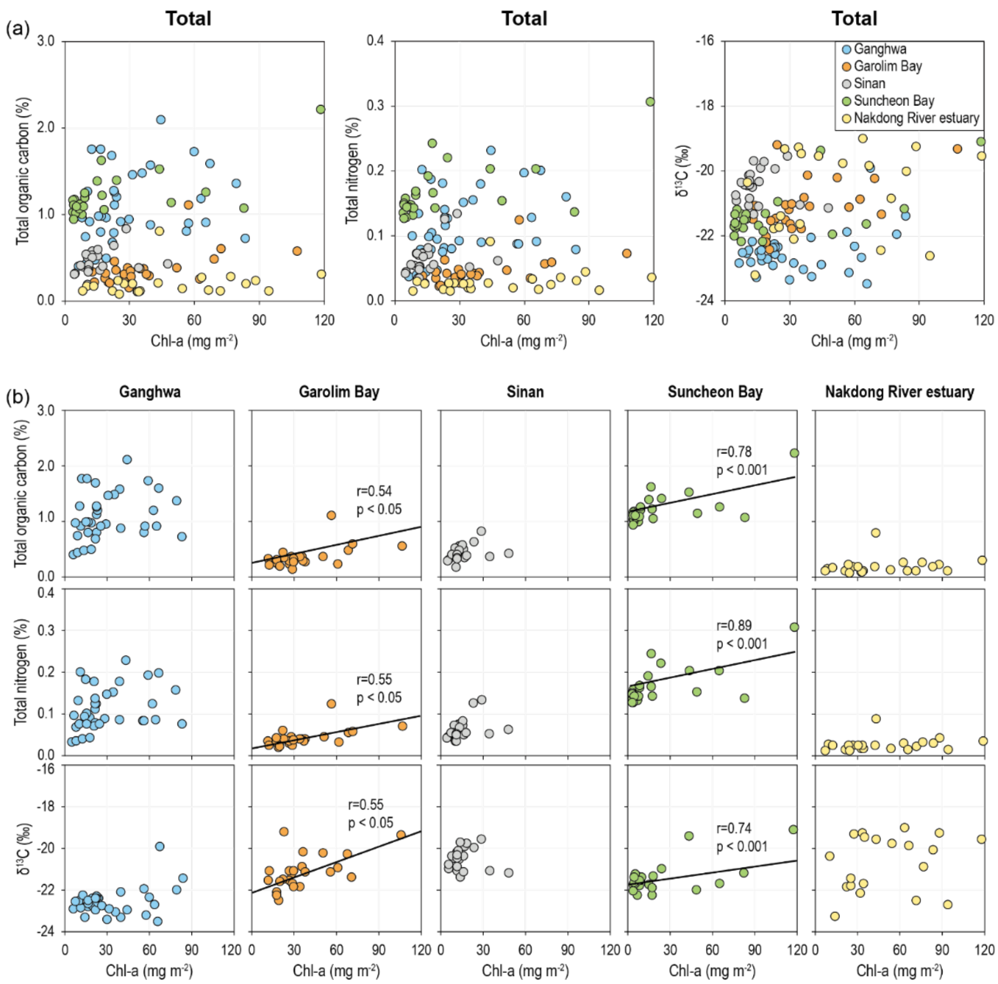

Figure 2.7.
Relationship between Chlorophyll a (Chl-*a*) and Total organic carbon (TOC), Total nitrogen (TN), Carbon stable isotopic ratio ($\delta^{13}C$) at (a) Total, (b) Ganghwa, Garolim Bay, Sinan, Suncheon Bay and Nakdong River estuary

2.3.4. Site-specific variabilities in sources of sedimentary organic matter

GR, SA, SC, and ND1 represented a typical signature of marine-derived organic matters, with $\delta^{13}C$ values ranging from -22.44 to -18.5‰ (mean: -20.81‰) (Figure 2.8). In comparison, GH and ND2 sediments were of terrestrial origin, with $\delta^{13}C$ values of -25.71 to -19.57‰ (mean: -22.47‰). The result indicated that the corresponding sediments were directly affected by freshwater discharges from the Han River and Nakdong River, respectively, through waterways. Meantime, the surface sediments and seawater of ND1 and ND2 contained apparently different organic sources. For example, the $\delta^{13}C$ values measured in ND1 sediment ranged between -20.38 and -19.03‰ (mean: -19.61‰), seawater ranged between -22.37 and -20.64‰ (mean: -21.50‰), indicating signature of marine-derived organic matter (Figure 2.8). This can be simply explained by the limited freshwater discharge from western Nakdong River to estuary via Noksan water gate. Of note, since the construction of Noksan water gate in 1934, the very gate has been operating only for controlling the water level in the freshwater reservoir, accordingly terrestrial influence to the western Nakdong estuary would be negligible. In contrast, the surface sediments and seawater of ND2 indicated a terrestrial source, with $\delta^{13}C$ values ranging from -25.71 to -19.57‰ (mean: -22.28‰) in sediments, -24.12 to -24.00‰ (mean: -24.06‰) in seawater, due to freshwater discharge through the two main Nakdong water gates (Figure 2.1). Altogether, the multiple features of sedimentary organic matter in ND are resulted from the simultaneous operations of Noksan and Nakdong water gates, providing complex dynamics under altered environment of closed Nakdong River estuary.

The potential sources of organic matter in coastal sediments would vary from terrestrial detritus, marine phytoplankton, MPB, and to sewage (Liu et al., 2006). In particular, the $\delta^{15}N$ signature could be potentially useful to determine the sources in respect to pollution, for example, isotopically lighter $\delta^{15}N$ (mean: 3‰) is characteristic for non-treated freshwater input to the coast (Van Dover et al., 1992). Moreover, low $\delta^{15}N$ signatures of organic matters in sediment and POM were reported near the industrial complexes of Sihwa coastal area, in which region was severely contaminated by several classes of persistent toxic substances (PTSs) including PAHs, SOs, and APs (Lee et al., 2017; Hong et al., 2019). The slighted enriched values of δ^{15}N in SC and ND supported the fact that sewage treated freshwater are discharged into the lower reaches for both areas. SC has a sewage treatment plant to purify wastewater from the barn and upstream agricultural area and the ND has a sewage treatment plant to purify wastewater from the surrounding industrial and municipal facilities (Figure 2.1). Of note, anthropogenic nitrogen sources after the sewage treatment are typically more ^{15}N-enriched up to 19‰ (Voss et al., 2000; Bohlin et al., 2006), subsequently sediment δ^{15}N becomes heavier with average of 10‰ (Heaton, 1986; Savage et al., 2004). In addition, the significant difference ($p < 0.01$) between the group of locations near the sewage treatment plants (ND1, ND2, and SC) and the other group of locations (SA, GH, and GR) supported the site-specific distributions of sedimentary organic matter (Figure 2.8). The δ^{15}N of the other regions (GH, GR, and SA) was of marine origin, ranging from 6.08 to 9.41‰.

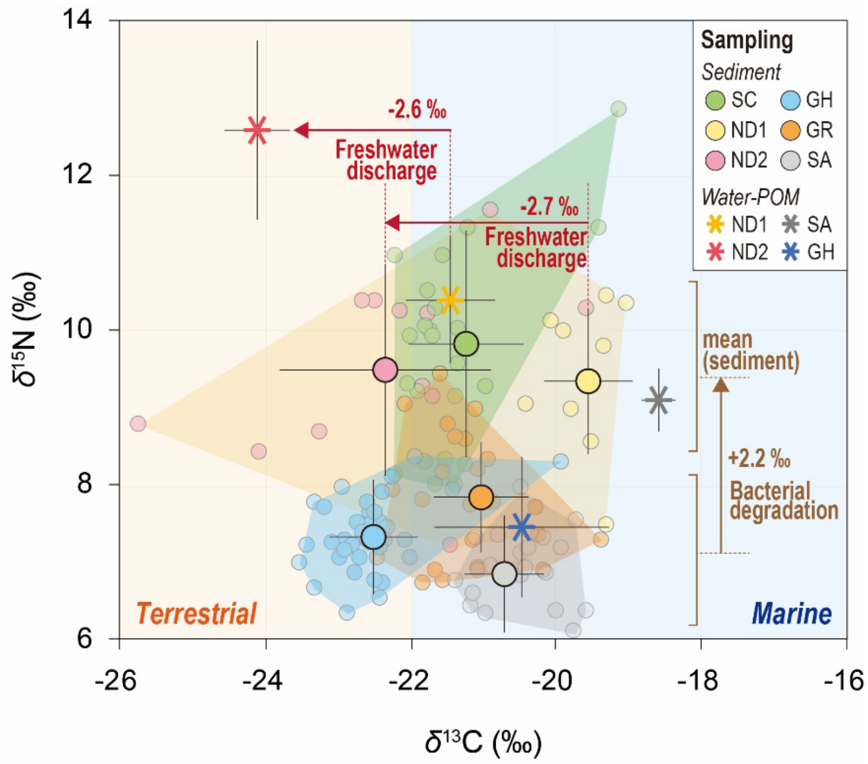

Figure 2.8.
Scatter plots of stable carbon and nitrogen isotopic composition (δ^{13}C and δ^{15}N) of the surface sediments and particulate organic matter (POM) collected from five intertidal flats, Korea. Mean values of sediment and water samples are presented as total mean with standard deviation (black line).

2.3.5. Factors affecting complex dynamics of sedimentary organic matter

Table 2.3 shows the result of the Pearson correlations between sedimentary organic matter and general sediment properties. The result showed that TOC and TN were significantly, positively correlated with WC, MC, OC, and Chl-*a* ($p < 0.05$). A significant positive relationship was found for Chl-*a* with TOC and TN ($p < 0.05$) in GR and SC (Figure 2.6). The relationships of TOC and TN with selected sediment parameters at these sampling locations are summarized in a PCA biplot for the sampling period (Figure 2.9). The first two axes of the PCA explained a high proportion of variance (i.e., 39.2% and 21.4% for axes 1 and 2, respectively). The results revealed the relationship between the sampling sites, which were clustered into four groups on the PCA diagram. Group A1 had $\delta^{13}C$ and C/N ratios of terrestrial origin, and mostly included muddy tidal flat of GH, which showed prevailed input of terrestrial organic matter from the Han River. Group A2 was located in GR and SA, and had mud-dominant samples, representing marine derived $\delta^{13}C$ and $\delta^{15}N$. Group B identified samples with the greatest TOC, TN, and MC, and was localized in SC. The $\delta^{13}C$ of sediments was of marine origin, while the sediments had greater $\delta^{15}N$, due to a sewage treatment plant located in the upstream region. Finally, Group C locations showed the smallest TOC and TN values in the dataset, which were characterized by sand-dominant intertidal flats in ND. The area was also characteristic with relatively great $\delta^{15}N$ signature, due to sewage treatment plant, industrial, and municipal facilities. In summary, the clusters of clearly identified groups cross varying locality and habitats successfully demonstrated the complex (in)direct association between sediment properties and isotopic signatures of organic matter.

Table 2.3.

Pearson correlation analysis of the sedimentary organic matter and sediment environmental parameters. Values in bold indicate that the correlation was significant at $p < 0.01$ (matched with ++).

	TOC	**TN**	**C/N**	**δ^{13}C**	**δ^{15}N**	**WC**	**MC**	**OC**	**Chl-*a***
TOC		++	++	+		++	++	++	++
TN	.953					++	++	++	++
C/N	**.243**	.016		++	++	+	++		
δ^{13}C	-.225	-.049	**-.556**			++			++
δ^{15}N	.060	.129	**-.260**	.161		++	++		
WC	**.307**	**.434**	-.220	**.270**	**.240**		++	++	+
MC	**.508**	**.469**	**.261**	-.106	**-.353**	**.422**		++	
OC	**.637**	**.695**	-.007	.017	.073	**.540**	**.636**		
Chl-*a*	**.255**	**.413**	-.162	.294	.144	.207	-.103	.153	

++ Significantly correlated at $p < 0.01$ level (2-tailed).

+ Significantly correlated at $p < 0.05$ level (2-tailed).

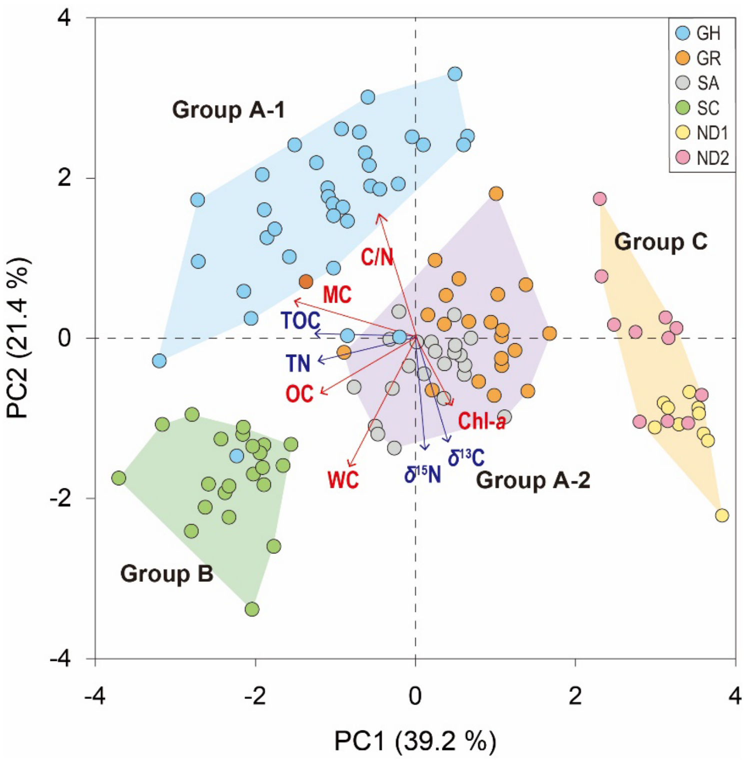

Figure 2.9.

Principal component analysis (PCA) ordination showing the first and second axes, indicating the relationship between sedimentary organic matters and sediment properties. Partial correlations of the significant environmental variables are superimposed on the ordination as vectors; blue arrows represent sedimentary organic matter and red arrows refer to the influencing factors. The length and direction of sediment property vectors indicate the strength and direction of the relationship to sedimentary organic matter. Cluster analysis was overlaid on the PCA plot.

CHAPTER 3.

THE FIRST NATIONAL SCALE EVALUATION OF ORGANIC CARBON STOCKS AND SEQUESTRATION RATES OF COASTAL SEDIMENTS ALONG THE WEST SEA, SOUTH SEA, AND EAST SEA OF SOUTH KOREA

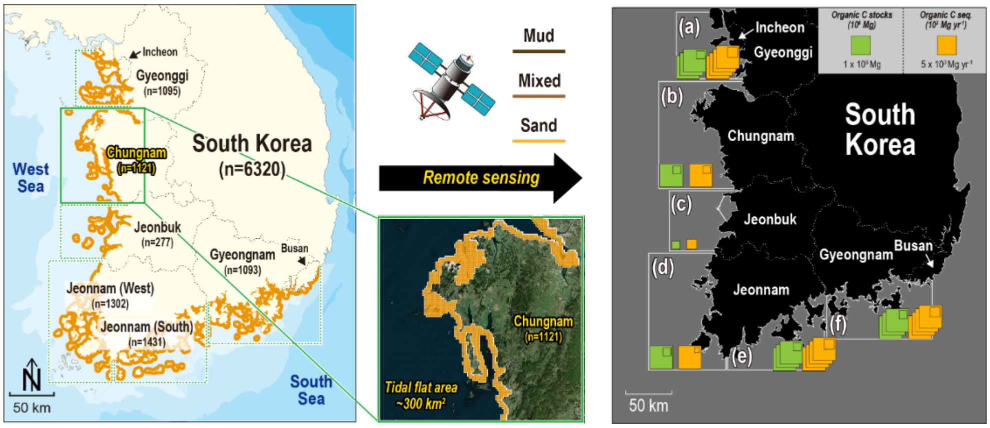

This chapter has been published to Science of the Total Environment.
Lee, J., Kim, B., Noh, J., Lee, C., Kwon, I., Kwon, B-O., Ryu, J., Park, J., Hong, S., Lee, S., Kim, S-G., Son, S., Yoon, H.J., Yim, J., Nam, J., Choi, K., Khim, J.S. The first national scale evaluation of organic carbon stocks and sequestration rates of coastal sediments along the West Sea, South. *Sci. Total Environ*. 2021, **793**, 148568
https://doi.org/10.1016/j.scitotenv.2021.148568

3.1. Introduction

Recently, researchers have highlighted the role of coastal ecosystems under global warming, with respect to coastal protection and buffering and for regulating "Blue Carbon" services (Mcleod et al., 2011). Coastal sediment represents a dominant reservoir of sequestered organic carbon in marine environments, and have an important ecological role in global biogeochemical carbon cycling (Hedges et al., 1997; Kubo and Kanda, 2017). Salt marshes and other coastal ecosystems (mangroves and seagrasses) are representative blue carbon habitats, due to their serving as highly efficient CO_2 sinks (Chmura et al.,2003; Mcleod et al., 2011; Kelleway et al., 2016). For example, coastal vegetated ecosystems, such as salt marshes, contribute to almost 50% of carbon sequestration in marine sediments, despite occupying only 0.2% of the ocean surface (Chmura et al., 2003; Mcleod et al., 2011; Duarte et al., 2013; Kelleway et al., 2016). Recently, several studies have demonstrated that global blue carbon habitats store up to 1.02 Pg CO_2 yr^{-1}, which is equivalent to 3–19% total carbon emission by deforestation, globally (Pendleton et al., 2012; Macreadie et al., 2019). This phenomenon exists because salt marshes are highly productive ecosystems that convert plant biomass carbon from CO_2 through primary production, and deposit biomass carbon in sediments over long-periods (Duarte et al., 2013; Spivak et al., 2019).

Sedimentary organic carbon in coastal areas originates from both terrestrial and marine sources, with quantities varying depending on the source (Graham et al., 2001; Lamb et al., 2006; Kubo and Kanda, 2017). Anthropogenic inputs (e.g., industrial, aquacultural, and municipal sewages) from terrestrial areas also contribute to the burial of organic carbon in coastal sediments (Rumolo et al., 2011; Pradhan et al., 2014). While this phenomenon is widely reported, organic carbon dynamics from rivers to the coastal ecosystem remain subject to debate (Krishna et al., 2013).

Sediment characteristics, such as mud content (silt + clay), represent typical environmental factors that influence the distribution of organic carbon in the marine ecosystem (Burdige, 2007; Serrano et al., 2016). For instance, mud-dominated sediment is mainly composed of silt and clay, which traps more organic particles compared to sand-dominated sediment, due to the presence of a larger surface area with higher adsorption capacity (Keil and Hedges, 1993; Burdige, 2007). Thus, the existence of a significant relationship between mud and organic contents means that mud content could be used as a reliable proxy of organic carbon, facilitating the low-cost assessment of blue carbon stock (Serrano et al., 2016).

For example, an equation showing the relationship between organic carbon in bare sediment and mud content was proposed ($R^2 = 0.78$, $p < 0.001$): Organic carbon content (%) = 0.06 × Mud content (%) – 0.03 (Serrano et al., 2016). Therefore, the strong association of sediment characteristics with organic carbon should be explored to examine carbon geochemical processes.

Remote sensing technologies and geographical information systems are being increasingly used to obtain reliable estimates of sedimentary organic carbon stock and sequestration rates (Mohamed et al., 2019). In particular, remote sensing technologies provide useful information to estimate organic carbon stock from tidal flat delineation data (Yim et al., 2018). Indeed, the remote sensing technology could be used to overcome the limitation of field surveys and laboratory analyses, particularly for large scale estimations.

South Korea is located in the eastern part of the East Asia between China and Japan. The Korean Peninsula has three main coastlines (east-, west-, and south-facing) abutting the East Sea, West Sea, and South Sea, respectively. The region extending from western coast to the southern coast of Korea is connected geographically to the eastern part of the Yellow Sea. This region has a shallow shelf (< 200 m of water depth) and an archipelago with strong macrotidal conditions (4–9 m) (NGII, 2016). As a result, there are extensive tidal flats (~2,487 km^2), along the western and southern coasts of Korea (Figure 3.1). Such environmental conditions potentially favor the burial and/or sequestration of organic matter; however, there have been no studies on this phenomenon at a national scale in Korea.

The present study investigated how various parameters drive spatiotemporal variation in the organic carbon stock of coastal sediments along the West, South, and East Sea of Korea. The targeted endpoints included total organic carbon, organic carbon stock, organic carbon sequestration rate, mud content in the tidal flat areas of Korea. The specific objectives were to: (1) investigate regional and temporal variations of organic carbon stock per unit area; (2) elucidate environmental factors affecting sedimentary organic carbon; (3) evaluate the relationship between biogeochemical properties (e.g., sediment mud content and vegetation) and sedimentary organic carbon; (4) determine the accuracy of remote sensing classification for sediment textual types compared to experimental (field-based) classification; and (5) identify sedimentary organic carbon stocks and sequestration rates in South Korea. Overall, the present study aimed to present a national-scale evaluation of organic carbon stocks and sequestration rates in the tidal flats of Korea.

3.2. Materials and methods

3.2.1. Study area

Core sediment samples were collected in 2018 and 2019 from 21 regions across provinces (Gyeonggi, Chungnam, Jeonbuk, Jeonnam, Gyeongnam, and Gyeongbuk) of South Korea (Table 3.1). To identify the quantity and geographic distribution of carbon in tidal flats, 21 regions were selected to represent tidal flats along the west, south, and east coasts (Figure 3.1). To observe the annual temporal variation of organic carbon stocks from 2017 to 2020, we selected five target regions (Ganghwa, Garolim Bay, Sinan, Suncheon, and Nakdong River estuary). Target regions were selected for the following reasons; 1) representing the mean values of carbon stocks of each province, and 2) including various environmental conditions (e.g., Geography, morphology, sediment type) (Figure 3.2).

Gyeonggi tidal flats cover ~876 km^2 (Ganghwa, Youngjong, Siheung, Daebu, and Hwaseong), and are located near the Han River, which is the largest river in South Korea. The Han River estuary is located on the border between South Korea and North Korea. It discharges about 19–25 × 10^9 m^3 yr^{-1}, and flows through the center of Seoul. Chungnam tidal flats cover ~357 km^2 (Garolim Bay, Geungheung, Ocheon, and Biin), and are located on the western part of the Korean peninsula. Jeonbuk tidal flats (Seonyudo and Gomso Bay) encompass 118 km^2, and are located on southwestern part of Korea. Jeonnam tidal flats (Hampyeong, Sinan, Aphaedo, Gangjin Bay, Deukryang Bay, Suncheon Bay, and Yeoza Bay) encompass 41.7% (~1044 km^2) of the remaining tidal flats in Korea (Choi, 2014a). Finally, Gyeongnam tidal flats (Jinhae Bay and Nakdong River estuary) are relatively small in size (~92 km^2), and are located on the southeastern part of the Korean peninsula.

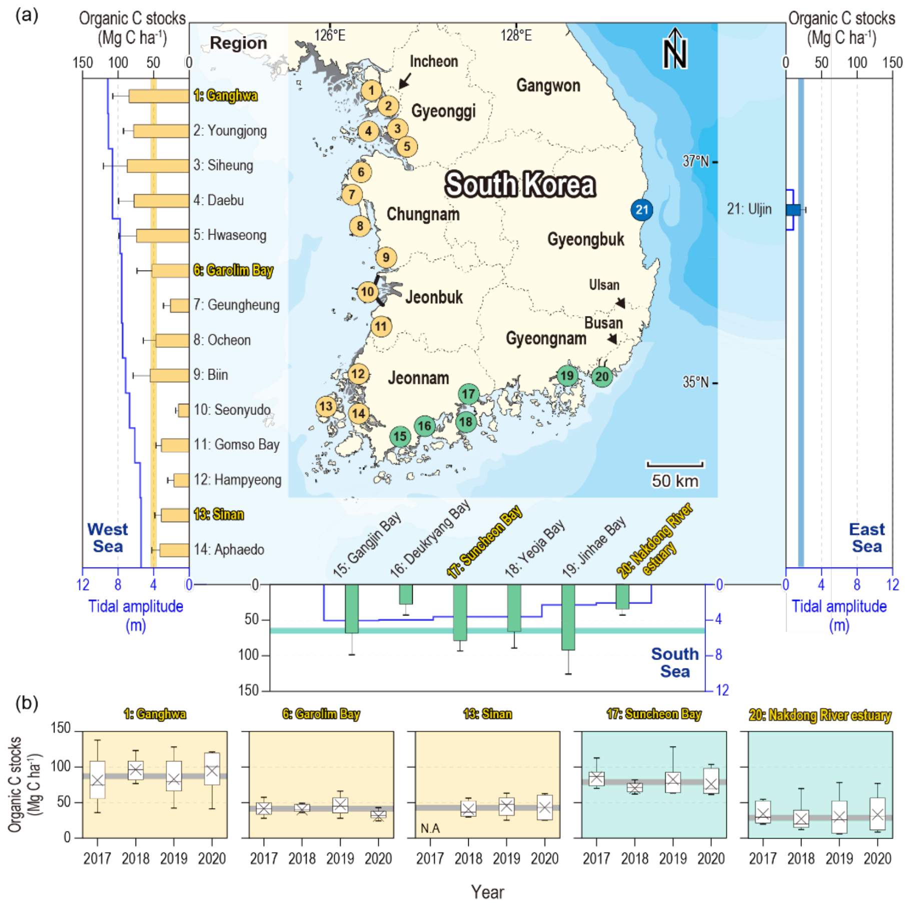

Figure 3.1.

Map showing the sampling sites along thewest, south, and east coasts of South Korea. (a) Spatial distribution of organic carbon stocks in the core sediments of 21 regions of South Korea. Core sediments were collected from Ganghwa (n = 44), Youngjong (n = 4), Siheung (n = 8), Daebu (n = 8), Hwaseong (n = 8), Garolim Bay (n=36), Geungheung (n =8), Ocheon (n=8), Biin (n=10), Seonyudo (n=8), Gomso Bay (n=4), Hampyeong (n=10), Sinan (n=25), Aphaedo (n=5), Gangjin Bay (n=12),Deukyang Bay (n=6), Suncheon Bay (n=32), Yeoza Bay (n=12), Jinhae Bay (n=10), Nakdong River estuary (n=33), and Uljin (n=12). Yellow, green, and navy shading denotes sedimentary organic carbon stocks along thewest, south, and east coasts, respectively. Mean values of organic carbon stocks forwest, south, and east coasts represent yellow, green, and navy lines. Blue lines denote the tidal amplitude in the West, South, and East Sea. (b) Temporal distribution (2017–2020) of organic stock in five regions (Ganghwa, Garolim Bay, Sinan, Suncheon Bay, and Nakdong River estuary). Grey lines denotemean values of organic carbon stocks over four years.

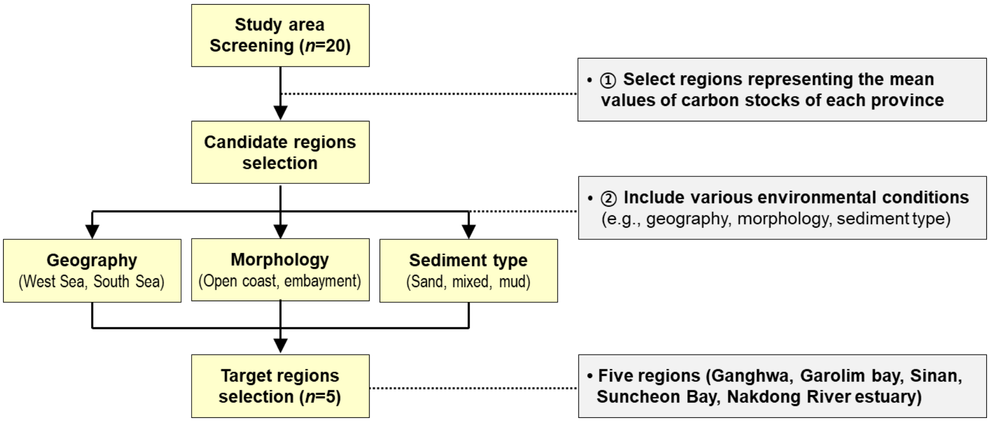

Figure 3.2.
Flowchart for selecting five target regions for observing annual temporal variation from 2017 to 2020.

Table 3.1.
Organic carbon content measured in the coastal sediments (salt marshes and bare tidal flats) of South Korea.

Location	Sampling year	Latitude	Longitude	Habitat[a]	Dominant halophyte	Core type[b]	Core depth (cm)	Organic carbon stock[c] (Mg C ha^{-1})	Ref
Ganghwa, Incheon	2017	37°36'29"N	126°23'03"E	SM	*Phragmites* sp.	M	60	**92**	**This study**
	2017			SM	*Phragmites* sp.	M	75	**80**	
	2017			SM	*Phragmites* sp.	M	80	**78**	
	2017			SM	*Phragmites* sp.	M	100	**65**	
	2017			SM	*Phragmites* sp.	M	90	**64**	
	2018			SM	*Phragmites* sp.	M	100	**96**	
	2019			SM	*Phragmites* sp.	A	70	**117**	
	2019			SM	*Phragmites* sp.	A	70	**85**	
	2020			SM	*Phragmites* sp.	A	70	**107**	
	2017	37˚36'24"N	126˚23'07"E	B	Bare	M	85	**44**	
	2017			B	Bare	M	50	**40**	
	2017			B	Bare	M	90	**43**	
	2018			B	Bare	M	100	**100**	
	2019			B	Bare	A	70	**97**	
	2019			B	Bare	A	70	**74**	
	2020			B	Bare	A	70	**88**	
	2017	37˚35'42"N	126˚27'48"E	SM	*Spartina* sp.	M	100	**62**	
	2018			SM	*Spartina* sp.	M	100	**83**	
	2019			SM	*Spartina* sp.	A	70	**77**	
	2019			SM	*Spartina* sp.	A	70	**59**	
	2020			SM	*Spartina* sp.	A	70	**100**	
	2017	37˚35'39"N	126˚27'52"E	B	Bare	M	60	**52**	
	2017			B	Bare	M	95	**31**	
	2018			B	Bare	M	100	**77**	
	2019			B	Bare	A	70	**46**	
	2019			B	Bare	A	70	**40**	
	2019			B	Bare	A	60	**61**	
	2020			B	Bare	A	70	**45**	
	2017	37°35'17"N	126°30'07"E	SM	*Suaeda* sp.	M	100	**161**	
	2017			SM	*Phragmites* sp.	M	70	**115**	
	2018			SM	*Suaeda* sp.	M	95	**93**	
	2019			SM	*Suaeda* sp.	A	70	**96**	
	2019			SM	*Suaeda* sp.	A	70	**68**	

Table 3.1. (continued).

Location	Sampling year	Latitude	Longitude	Habitat[a]	Dominant halophyte	Core type[b]	Core depth (cm)	Organic carbon stock[C] (Mg C ha^{-1})	Ref
Ganghwa, Incheon	2020	37°35'17"N	126°30'07"E	SM	*Suaeda* sp.	A	70	**94**	**This study**
	2017	37°35'21"N	126°30'12"E	B	Bare	M	100	**111**	
	2017			B	Bare	M	90	**104**	
	2017			B	Bare	M	100	**90**	
	2017			B	Bare	M	90	**82**	
	2017			B	Bare	M	100	**72**	
	2018			B	Bare	M	100	**121**	
	2019			B	Bare	A	60	**63**	
	2019			B	Bare	A	60	**67**	
	2019			B	Bare	A	60	**80**	
	2020			B	Bare	A	70	**78**	
Youngjong, Incheon	2018	37°31'50"N	126°30'13"E	SM	*Suaeda* sp.	M	100	**81**	
	2019			SM	*Suaeda* sp.	A	70	**55**	
	2018			B	Bare	M	100	**84**	
	2019			B	Bare	A	70	**82**	
Siheung, Gyeonggi	2018	37°23'40"N	126°46'16"E	SM	*Phragmites* sp.	M	100	**73**	
	2019			SM	*Phragmites* sp.	A	70	**65**	
	2018			SM	*Phragmites* sp.	M	100	**109**	
	2019			SM	*Phragmites* sp.	A	70	**58**	
	2018			B	Bare	M	100	**56**	
	2019			B	Bare	A	70	**100**	
	2018			B	Bare	M	100	**145**	
	2019			B	Bare	A	70	**56**	
Daebu, Gyeonggi	2018	37°12'49"N	126°35'21"E	SM	*Suaeda* sp.	M	100	**52**	
	2019			SM	*Suaeda* sp.	A	70	**77**	
	2018	37°15'59"N	126°33'24"E	B	Bare	M	95	**51**	
	2019			B	Bare	A	60	**65**	
	2018	37°13'02"N	126°34'34"E	SM	*Phragmites* sp.	M	95	**56**	
	2019			SM	*Phragmites* sp.	A	70	**56**	
	2018	37°16'57"N	126°34'04"E	B	Bare	M	100	**60**	
	2019			B	Bare	A	65	**95**	
Hwaseong, Gyeonggi	2018	37°03'13"N	126°45'15"E	SM	*Suaeda* sp.	M	95	**59**	
	2019			SM	*Suaeda* sp.	A	70	**77**	
	2018	37°04'19"N	126°43'48"E	B	Bare	M	100	**56**	
	2019			B	Bare	A	70	**125**	

Table 3.1. (continued).

Location	Sampling year	Latitude	Longitude	Habitat[a]	Dominant halophyte	Core type[b]	Core depth (cm)	Organic carbon stock[C] (Mg C ha^{-1})	Ref
Hwaseong, Gyeonggi	2018	37°09'02"N	126°41'48"E	SM	*Suaeda* sp.	M	85	**80**	**This study**
	2019			SM	*Suaeda* sp.	A	60	**52**	
	2018	37°07'03"N	126°40'57"E	B	Bare	M	85	**35**	
	2019			B	Bare	A	70	**53**	
Garolim Bay, Chungnam	2017	36°54'57"N	126°18'49"E	SM	*Suaeda* sp.	M	80	**44**	
	2017			B	Bare	M	100	**33**	
	2018			B	Bare	M	100	**36**	
	2019			SM	*Suaeda* sp.	A	60	**26**	
	2019			SM	*Suaeda* sp.	A	60	**26**	
	2019			SM	*Suaeda* sp.	A	60	**40**	
	2019			SM	*Suaeda* sp.	A	60	**37**	
	2019			B	Bare	A	60	**30**	
	2019			B	Bare	A	60	**26**	
	2019			B	Bare	A	60	**32**	
	2019			B	Bare	A	60	**14**	
	2020			SM	*Suaeda* sp.	A	45	**23**	
	2020			B	Bare	A	60	**31**	
	2017	36°52'37"N	126°21'41"E	SM	*Suaeda* sp.	M	85	**38**	
	2017			B	Bare	M	65	**28**	
	2018			B	Bare	M	100	**42**	
	2019			B	Bare	A	60	**36**	
	2020			B	Bare	A	60	**21**	
	2017	36°55'23"N	126°25'02"E	SM	*Suaeda* sp.	M	85	**25**	
	2017			B	Bare	M	100	**41**	
	2018			B	Bare	M	100	**36**	
	2019			SM	*Suaeda* sp.	A	60	**64**	
	2019			SM	*Suaeda* sp.	A	60	**39**	
	2019			SM	*Suaeda* sp.	A	60	**38**	
	2019			SM	*Suaeda* sp.	A	60	**32**	
	2019			B	Bare	A	60	**56**	
	2019			B	Bare	A	60	**57**	
	2019			B	Bare	A	60	**22**	
	2019			B	Bare	A	60	**21**	
	2020			SM	*Suaeda* sp.	A	60	**24**	
	2020			B	Bare	A	60	**22**	

Table 3.1. (continued).

Location	Sampling year	Latitude	Longitude	Habitat[a]	Dominant halophyte	Core type[b]	Core depth (cm)	Organic carbon stock[C] (Mg C ha^{-1})	Ref
Garolim Bay, Chungnam	2017	36°58'25"N	126°23'04"E	B	Bare	M	100	**42**	**This study**
	2017			SM	*Suaeda* sp.	M	100	**32**	
	2018			B	Bare	M	100	**39**	
	2019			B	Bare	A	60	**58**	
	2020			B	Bare	A	60	**28**	
Geunheung, Chungnam	2018	36°43'02"N	126°16'23"E	B	Bare	M	75	**22**	
	2019			B	Bare	A	60	**20**	
	2018	36°43'05"N	126°14'27"E	B	Bare	M	70	**21**	
	2019			SM	*Phragmites* sp.	A	60	**20**	
	2018	36°43'47"N	126°11'55"E	B	Bare	M	80	**47**	
	2019			B	Bare	A	60	**11**	
	2018	36°44'51"N	126°11'10"E	B	Bare	M	80	**31**	
	2019			B	Bare	A	50	**8**	
Ocheon, Chungnam	2018	36°20'43"N	126°35'09"E	B	Bare	M	70	**75**	
	2019			SM	*Phragmites* sp.	A	60	**51**	
	2018	36°26'23"N	126°31'50"E	B	Bare	M	85	**36**	
	2019			B	Bare	A	60	**18**	
	2018	36°33'07"N	126°27'51"E	B	Bare	M	75	**48**	
	2019			B	Bare	A	60	**46**	
	2018	36°34'50"N	126°27'21"E	B	Bare	M	75	**33**	
	2019			B	Bare	A	60	**26**	
Biin, Chungnam	2018	36°08'21"N	126°34'17"E	SM	*Phragmites* sp.	M	60	**20**	
	2019			SM	*Phragmites* sp.	A	60	**13**	
	2018	36°08'59"N	126°30'25"E	B	Bare	M	100	**70**	
	2019			B	Bare	A	60	**51**	
	2018	36°08'00"N	126°33'49"E	B	Bare	M	100	**45**	
	2019			B	Bare	A	60	**58**	
	2018	36°04'33"N	126°37'51"E	B	Bare	M	100	**32**	
	2019			B	Bare	A	60	**69**	
	2018	36°02'24"N	126°39'29"E	SM	*Phragmites* sp.	M	85	**63**	
	2019			SM	*Phragmites* sp.	A	60	**35**	
Seonyudo, Jeonbuk	2018	35°49'04"N	126°24'47"E	SM	*Suaeda* sp.	M	85	**16**	
	2019			SM	*Suaeda* sp.	A	60	**7**	
	2018	35°49'24"N	126°24'45"E	B	Bare	M	80	**13**	
	2019			B	Bare	A	60	**1**	

Table 3.1. (continued).

Location	Sampling year	Latitude	Longitude	Habitat[a]	Dominant halophyte	Core type[b]	Core depth (cm)	Organic carbon stock[C] (Mg C ha^{-1})	Ref
Seonyudo, Jeonbuk	2018	35°48'53"N	126°24'43"E	SM	*Suaeda* sp.	M	100	**19**	**This study**
	2019			SM	*Suaeda* sp.	A	60	**4**	
	2018	35°49'12"N	126°24'58"E	B	Bare	M	95	**33**	
	2019			B	Bare	A	60	**11**	
Gomso Bay, Jeonbuk	2018	35°32'14"N	126°35'47"E	SM	*Suaeda* sp.	M	100	**41**	
	2018	35°31'58"N	126°30'56"E	B	Bare	M	100	**25**	
	2018	35°32'51"N	126°40'33"E	SM	*Phragmites* sp.	M	100	**45**	
	2018	35°34'40"N	126°39'47"E	B	Bare	M	100	**41**	
Hampyeong, Jeonnam	2018	35°07'51"N	126°20'29"E	SM	*Phragmites* sp.	M	60	**33**	
	2019			SM	*Phragmites* sp.	A	70	**24**	
	2018	35°06'19"N	126°26'37"E	B	Bare	M	80	**8**	
	2019			SM	*Phragmites* sp.	A	70	**14**	
	2018	35°05'13"N	126°26'23"E	B	Bare	M	90	**7**	
	2019			B	Bare	A	60	**17**	
	2018	35°05'05"N	126°09'55"E	B	Bare	M	90	**14**	
	2019			B	Bare	A	70	**21**	
	2018	35°06'12"N	126°20'06"E	SM	*Phragmites* sp.	M	100	**32**	
	2019			SM	*Phragmites* sp.	A	70	**10**	
Sinan, Jeonnam	2018	34°58'06"N	126°10'01"E	SM	*Phragmites* sp.	M	100	**34**	
	2019			SM	*Phragmites* sp.	A	70	**46**	
	2019			SM	*Phragmites* sp.	A	70	**38**	
	2019			SM	*Phragmites* sp.	A	70	**37**	
	2019			SM	*Phragmites* sp.	A	70	**32**	
	2019			SM	*Phragmites* sp.	A	65	**24**	
	2019			SM	*Phragmites* sp.	A	65	**21**	
	2019			B	Bare	A	70	**53**	
	2019			B	Bare	A	70	**52**	
	2019			B	Bare	A	70	**47**	
	2019			B	Bare	A	70	**44**	
	2019			B	Bare	A	70	**36**	
	2019			B	Bare	A	70	**32**	
	2020			SM	*Phragmites* sp.	A	70	**54**	
	2018	34°58'06"N	126°10'01"E	B	Bare	M	100	**31**	
	2019			B	Bare	A	70	**30**	
	2020			B	Bare	A	70	**29**	

Table 3.1. (continued).

Location	Sampling year	Latitude	Longitude	Habitat[a]	Dominant halophyte	Core type[b]	Core depth (cm)	Organic carbon stock[C] (Mg C ha^{-1})	Ref
Sinan, Jeonnam	2018	35°00'14"N	126°09'56"E	SM	*Suaeda* sp.	M	85	**52**	**This study**
	2018			B	Bare	M	100	**45**	
	2019			SM	*Suaeda* sp.	A	70	**60**	
	2019			B	Bare	A	70	**47**	
	2020			SM	*Suaeda* sp.	A	70	**47**	
	2018	34°59'18"N	126°08'26"E	B	Bare	M	100	**27**	
	2019			B	Bare	A	70	**30**	
	2020			B	Bare	A	70	**25**	
Aphaedo, Jeonnam	2019	34°50'29"N	126°15'56"E	SM	*Phragmites* sp.	A	70	**53**	
	2019	34°50'02"N	126°20'40"E	SM	*Suaeda* sp.	A	70	**42**	
	2019	34°53'23"N	126°19'40"E	SM	*Phragmites* sp.	A	60	**31**	
	2019	34°53'08"N	126°16'46"E	B	Bare	A	70	**43**	
	2019	34°50'45"N	126°18'57"E	B	Bare	A	70	**21**	
Gangjin Bay, Jeonnam	2018	34°29'28"N	126°45'04"E	SM	*Phragmites* sp.	M	100	**67**	
	2018			B	Bare	M	100	**41**	
	2019			SM	*Phragmites* sp.	A	60	**119**	
	2019			B	Bare	A	60	**79**	
	2018	34°32'58"N	126°47'58"E	SM	*Phragmites* sp.	M	60	**98**	
	2019			SM	*Suaeda* sp.	A	60	**70**	
	2018	34°29'45"N	126°47'32"E	B	Bare	M	60	**51**	
	2019			B	Bare	A	60	**31**	
	2018	34°37'20"N	126°46'53"E	SM	*Phragmites* sp.	M	60	**91**	
	2019			SM	*Phragmites* sp.	A	60	**107**	
	2018	34°32'25"N	126°45'58"E	B	Bare	M	100	**51**	
	2019			B	Bare	A	60	**26**	
Deukryang Bay, Jeonnam	2019	34°44'32"N	127°17'48"E	SM	*Phragmites* sp.	A	60	**36**	
	2019			SM	*Phragmites* sp.	A	60	**25**	
	2019	34°40'12"N	127°17'06"E	SM	*Phragmites* sp.	A	60	**20**	
	2019	34°34'19"N	126°58'48"E	B	Bare	A	60	**40**	
	2019	34°40'51"N	127°14'07"E	B	Bare	A	60	**12**	
	2019	34°35'27"N	127°09'58"E	B	Bare	A	60	**6**	
Suncheon Bay, Jeonnam	2017	34°52'28"N	127°30'12"E	SM	*Phragmites* sp.	M	100	**80**	
	2017			SM	*Phragmites* sp.	M	60	**86**	
	2017			SM	*Phragmites* sp.	M	100	**69**	
	2018			SM	*Phragmites* sp.	M	100	**73**	

Table 3.1. (continued).

Location	Sampling year	Latitude	Longitude	Habitat[a]	Dominant halophyte	Core type[b]	Core depth (cm)	Organic carbon stock[C] (Mg C ha^{-1})	Ref
Suncheon Bay, Jeonnam	2019	34°52'28"N	127°30'12"E	SM	*Phragmites* sp.	A	60	**116**	**This study**
	2019			SM	*Phragmites* sp.	A	60	**122**	
	2019			SM	*Phragmites* sp.	A	60	**92**	
	2019			SM	*Phragmites* sp.	A	60	**82**	
	2019			B	Bare	A	60	**99**	
	2019			B	Bare	A	60	**89**	
	2019			B	Bare	A	60	**79**	
	2019			B	Bare	A	60	**71**	
	2020			SM	*Phragmites* sp.	A	60	**116**	
	2017	34°52'05"N	127°31'05"E	SM	*Phragmites* sp.	M	100	**106**	
	2018			SM	*Phragmites* sp.	M	85	**60**	
	2019			SM	*Phragmites* sp.	A	60	**57**	
	2019			SM	*Phragmites* sp.	A	60	**69**	
	2019			SM	*Phragmites* sp.	A	60	**87**	
	2019			SM	*Phragmites* sp.	A	60	**80**	
	2019			B	Bare	A	60	**49**	
	2019			B	Bare	A	60	**74**	
	2019			B	Bare	A	60	**64**	
	2019			B	Bare	A	60	**58**	
	2020			SM	*Phragmites* sp.	A	60	**76**	
	2017	34°50'48"N	127°29'36"E	B	Bare	M	100	**82**	
	2018			B	Bare	M	100	**70**	
	2019			B	Bare	A	60	**76**	
	2020			B	Bare	A	60	**90**	
	2017	34°51'12"N	127°31'23"E	B	Bare	M	100	**61**	
	2018			B	Bare	M	90	**61**	
	2019			B	Bare	A	60	**56**	
	2020			B	Bare	A	60	**79**	
Yeoza Bay, Jeonnam	2018	34°46'05"N	127°34'29"E	B	Bare	M	90	**72**	
	2019			B	Bare	A	60	**40**	
	2018	34°47'10"N	127°23'22"E	SM	*Phragmites* sp.	M	85	**86**	
	2019			SM	*Phragmites* sp.	A	50	**33**	
	2018	34°50'19"N	127°27'01"E	SM	*Phragmites* sp.	M	90	**72**	
	2019			SM	*Phragmites* sp.	A	60	**50**	
	2018	34°44'26"N	127°35'03"E	B	Bare	M	100	**76**	

Table 3.1. (continued).

Location	Sampling year	Latitude	Longitude	Habitat[a]	Dominant halophyte	Core type[b]	Core depth (cm)	Organic carbon stock[C] (Mg C ha^{-1})	Ref
Yeoza Bay, Jeonnam	2019	34°44'26"N	127°35'03"E	B	Bare	A	60	**41**	**This study**
	2018	34°50'31"N	127°32'22"E	SM	*Phragmites* sp.	M	100	**74**	
	2019			SM	*Phragmites* sp.	A	60	**95**	
	2018	34°42'20"N	127°24'10"E	B	Bare	M	60	**60**	
	2019			B	Bare	A	60	**36**	
Jinhae Bay, Gyeongnam	2018	35°02'59"N	128°22'30"E	B	Bare	M	100	**83**	
	2019			B	Bare	A	50	**25**	
	2018	35°08'50"N	128°41'26"E	B	Bare	M	40	**103**	
	2019			B	Bare	A	60	**144**	
	2018	35°05'53"N	128°26'49"E	SM	*Phragmites* sp.	M	60	**120**	
	2019			SM	*Phragmites* sp.	A	60	**139**	
	2018	35°07'11"N	128°32'14"E	B	Bare	M	60	**106**	
	2018	35°05'13"N	128°34'52"E	B	Bare	M	80	**81**	
	2019			B	Bare	A	60	**25**	
	2019	35°12'59"N	128°37'26"E	B	Bare	A	60	**101**	
Nakdong River estuary, Gyeongnam	2017	35°04'19"N	128°56'41"E	B	Bare	M	60	**17**	
	2017	35°03'37"N	128°54'41"E	B	Bare	M	100	**11**	
	2017	35°03'34"N	128°53'50"E	B	Bare	M	90	**10**	
	2017	35°03'27"N	128°56'24"E	SM	*Phragmites* sp.	M	100	**26**	
	2018			SM	*Phragmites* sp.	M	100	**26**	
	2018			B	Bare	M	100	**14**	
	2019			SM	*Phragmites* sp.	A	60	**42**	
	2019			SM	*Phragmites* sp.	A	60	**14**	
	2019			B	Bare	A	60	**53**	
	2019			B	Bare	A	60	**24**	
	2019			B	Bare	A	60	**23**	
	2019			B	Bare	A	60	**21**	
	2019			B	Bare	A	60	**29**	
	2019			B	Bare	A	60	**16**	
	2020			SM	*Phragmites* sp.	A	60	**79**	
	2020			B	Bare	A	60	**61**	
	2017	35°04'42"N	128°55'49"E	SM	*Phragmites* sp.	M	100	**49**	
	2018			SM	*Phragmites* sp.	M	100	**65**	
	2019			SM	*Phragmites* sp.	A	60	**50**	
	2020			SM	*Phragmites* sp.	A	60	**83**	

Table 3.1. (continued).

Location	Sampling year	Latitude	Longitude	Habitat[a]	Dominant halophyte	Core type[b]	Core depth (cm)	Organic carbon stock[C] (Mg C ha^{-1})	Ref
Nakdong River estuary, Gyeongnam	2017	35°04'06"N	128°52'22"E	SM	*Phragmites* sp.	M	90	**19**	**This study**
	2018			SM	*Phragmites* sp.	M	65	**11**	
	2018			B	Bare	M	100	**22**	
	2019			SM	*Phragmites* sp.	A	60	**39**	
	2019			SM	*Phragmites* sp.	A	60	**36**	
	2019			B	Bare	A	60	**7**	
	2019			B	Bare	A	60	**7**	
	2019			B	Bare	A	60	**5**	
	2019			B	Bare	A	60	**6**	
	2019			B	Bare	A	60	**5**	
	2019			B	Bare	A	60	**4**	
	2020			SM	*Phragmites* sp.	A	60	**38**	
	2020			B	Bare	A	60	**23**	
Uljin, Gyeongbuk	2018	36°53'03"N	129°24'58"E	B	Bare	M	60	**15**	
	2018			B	Bare	M	60	**11**	
	2018			B	Bare	M	60	**15**	
	2018	36°50'31"N	129°26'04"E	SM	*Carex* sp.	M	60	**17**	
	2018			SM	*Carex* sp.	M	60	**17**	
	2018			SM	*Carex* sp.	M	60	**16**	
	2018	36°47'03"N	129°27'56"E	B	Bare	M	60	**24**	
	2018			B	Bare	M	60	**20**	
	2018			B	Bare	M	60	**16**	
	2018	36°41'06"N	129°27'53"E	SM	*Carex* sp.	M	60	**25**	
	2018			SM	*Carex* sp.	M	60	**20**	
	2018			SM	*Carex* sp.	M	60	**19**	

3.2.2. Tidal flat delineation using remote sensing

The tidal flats along the West, South, and East Sea of South Korea were delineated with intertidal polygon data maps using the QGIS program (https://www.qgis.org/en/site/). QGIS is a Geographic Information System (GIS) analysis tool that provides spatial analysis of geographic information, such as vector and raster images, based on a Graphic User Interface (GUI). The study area consisted of 11,905 grid zones (grid size: 0.9×0.9 km^2) of an intertidal cover map. The tidal flat area delineated in each grid zone was calculated by an intersection algorithm, which is a spatial processing algorithm generated by overlaying vector layers. The procedure is presented in Figure 3.3. First, the intertidal polygon and grid zones were overlaid using QGIS. Second, the intertidal polygons in each grid zone were divided by intersection algorithms based on the cross points. Finally, the intersected area of each grid zone was delineated, and entered on the database following grid IDs. The tidal flat area delineated in each grid zone was calculated by an intersection algorithm, which is a spatial processing algorithm generated by overlaying vector layers. This algorithm divides the intersected area by calculating the cross points between the input layer and intersection layer. Overall, tidal flat areas in South Korea were calculated by summing the intersected area of 11,905 grid zones.

To delineate tidal flats along the west and south coast, we used intertidal polygon data maps provided by the Ministry of Oceans and Fisheries (MOF) (Data of 2018). The MOF provides intertidal polygon data maps and statistical databases (Source: https://kosis.kr/eng/) on tidal flats once every five years through a national investigation. However, intertidal polygon data were not available for the east coast, because of limited data. Thus, we extracted the East Sea intertidal polygon data maps using Electronic Navigational Chart (ENC) provided by Korea Hydrographic and Oceanographic Agency (KHOA). The procedure involved, first, extracting map data at low-tide and high-tide along the east coasts using ENC. Second, closed curve data were constructed by modifying topological errors in ENC data. Finally, we transformed closed curve data to intertidal polygon data maps to delineate the east coast.

The similarity of ENC data to MOF data is debatable, due to possible errors in the analysis process. Thus, the similarity of tidal flat delineation results for the West and South Sea based on ENC data was evaluated in the present study. The delineation results using ENC were quantitatively compared with the official MOF data. Specifically, we calculated Mean Bias Error (MBE) and Root Mean Square Error (RMSE) between the two datasets for 2,252 grid zones selected from tidal flats along the west and south coasts (Table 3.2).

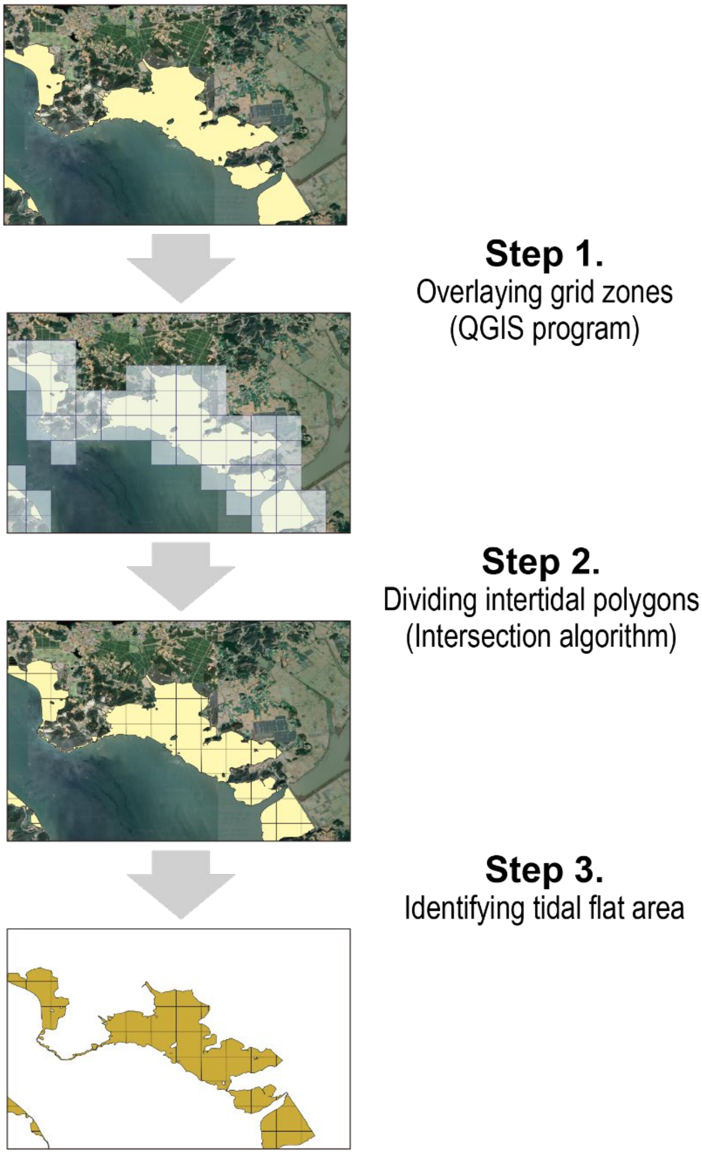

Figure 3.3.
The procedure of delineation of the tidal flats, performed through the QGIS analysis tool using a spatial processing algorithm.

Table 3.2.
Mean Bias Error (MBE) and Root Mean Square Error (RMSE) of the delineation results for tidal flats between the Electronic Navigational Chart (ENC) and the Ministry of Oceans and Fisheries (MOF) (Data of 2018). To evaluate the delineation results for tidal flats, 2,252 grid zones of tidal flats were selected along the west and south coasts.

	Absolute value (m^2)	**Compared to area of each grid zone (%)**	**Compared to mean area of 2,252 grid zones (%)**
Mean Bias Error	8,690	1.2	2.8
Root Mean Square Error	56,125	7.9	18.0
Area of each grid zone	810,000	-	-
Mean area of grid zones (MOF)	307,068	-	-
Mean area of grid zones (ENC)	315,759	-	-

3.2.3. Validation of sediment textural types using remote sensing

The textural type of sediment in the tidal flats of each grid zone was classified as sand, mixed, and mud based on the judgment of morphology, sedimentology, and stratigraphy by an expert marine geologist for South Korea (coauthor: Choi, K.,; for details, see in Choi, 2014b). We verified this approach by comparing the remote sensing derived data with experimental classification data (over 2,500 samples were analyzed for mud contents, covering the 74-unit grid area of 0.9×0.9 km^2) obtained from the *in situ*, with the two being statistically significant ($p < 0.01$; Table 3.1).

3.2.4. Sampling and laboratory analyses

To sample core sediments, we used both a cylindrical multisampler core (diameter = 5 cm) and a semi-cylindrical gouge (diameter = 3 cm) depending on whether the substrate was slack (low cohesion) or compact (high cohesion), respectively (Table 3.3). Core sediments (60–100 cm; subsamples at 5 cm intervals) from 21 regions along the western, southern, and eastern coasts of South Korea were sampled in salt marshes and bare tidal flats from 2018 to 2019, respectively (Table 3.1). To monitor the annual variation in organic carbon stocks, five regions (Ganghwa, Garolim Bay, Sinan, Suncheon Bay, and Nakdong River estuary) were selected as representing typical tidal flats along the west and south coasts of South Korea. In addition, core sediments in five target regions were sampled over four years (2017 to 2020; Table 3.4).

To analyze general sediment parameters, samples were stored in airtight plastic bags to prevent evaporation, and were subsequently transferred to the laboratory. Mud content was measured by rapid partial analysis through wet-sieving (Buchnan, 1984). Three sediment textural type was classified by mud (silt + clay) content; 1) sand (sand + slightly muddy sand, 0–25% mud content), 2) mixed (muddy sand + sandy mud, 25–75 %), and 3) mud (slightly sandy mud + mud, 75–100%) (Flemming, 2000). Sediment samples for analyzing total organic carbon were freeze-dried, homogenized, and powdered using agate mortar. To determine TOC, the sediment was decalcified with 10% HCl, washed twice with deionized water, and freeze-dried. TOC was measured using an Elemental Analyzer-Isotope Ratio Mass Spectrometer (EA-IRMS) (Elementar, Gmbh, Hanau, Germany). The age of core sediments was calculated using a constant rate of supply (CRS) model for the vertical profiles of excess ^{210}Pb activity (Appleby and Oldfield, 1983) (Table 3.5). Excess ^{210}Pb activity was calculated from the differences between the activity of supported and unsupported ^{210}Pb. Supported and unsupported ^{210}Pb activity was measured using gamma spectroscopy attached to a low background HPGe detector of the Korea Basic Science Institute (KBSI). All ^{210}Pb dating models used excess ^{210}Pb (Krishnaswamy et al., 1971; Sanchez-Cabeza and Ruiz-Fernández, 2012), in which (Eq. 1):

Unsupported $^{210}Pb = {}^{210}Pb$ (1)

Supported $^{210}Pb = {}^{226}Ra$

Excess $^{210}Pb = {}^{210}Pb - {}^{226}Ra$

The relationship between excess ^{210}Pb in sediment and age was expressed with the following equation (Eq. 2):

$$t = \frac{1}{\lambda} \ln \frac{C_0}{C_i} \quad (2)$$

where t is layer age (yr); C_0 is the cumulative activity of all excess ^{210}Pb from the water-sediment interface to the background; C_i is the cumulative inventory of ^{210}Pb at depth i (cm); and λ is the radioactive decay constant of $^{210}Pb_{ex}$ (0.03114 yr^{-1}). Both C_0 and C_i were be obtained by integrating excess ^{210}Pb activity at corresponding intervals in core sediments. The sedimentation rate was estimated using the following equation (Appleby, 2001) (Eq. 3):

$$r = \frac{m}{t} \quad (3)$$

where r is the sedimentation rate (cm yr^{-1}); m is the depth of the core sediment (cm); and t is layer age (yr). The sedimentation rate of core sediments at the sampling sites is shown in Figure 3.4.

Table 3.3.

The two types of coring equipment used in this study.

Coring equipment 1	Coring equipment 2
 **Multisampler core (Eijelkamp)** (Source: https://en.eijkelkamp.com)	 **Gouge auger core (Van Walt)** (Source: https://www.vanwalt.com)
Advantage • Suitable for muddy sediments • Less disturbance on bulk density of core • Less sediment compaction during sampling	**Advantage** • Suitable for sandy sediments • Demand untrained/inexperienced manpower • Specialized at coring rooted sediments
Disadvantage • Unsuitable for sandy sediments • Demand trained/skilled manpower	**Disadvantage** • Unsuitable for muddy sediments • More disturbance on bulk density of core

Table 3.4.
Organic carbon stock and sequestration rate in five target regions (Ganghwa, Garolim Bay, Sinan, Suncheon Bay, and Nakdong River estuary) over four years (2017 to 2020).

Location	Organic carbon stock (Mg C ha^{-1})				Organic carbon sequestration rate (Mg C ha^{-1} yr^{-1})			
	2017	2018	2019	2020	2017	2018	2019	2020
Ganghwa	77 (±8) (n = 18)	89 (±6) (n = 6)	74 (±6) (n = 14)	85 (±9) (n = 6)	0.53 (±0.05) (n = 18)	0.62 (±0.04) (n = 6)	0.51 (±0.04) (n = 14)	0.59 (±0.06) (n = 6)
Garolim Bay	35 (±2) (n = 8)	38 (±2) (n = 4)	36 (±3) (n = 18)	25 (±2) (n = 6)	0.14 (±0.01) (n = 8)	0.16 (±0.01) (n = 4)	0.15 (±0.01) (n = 18)	0.10 (±0.01) (n = 6)
Sinan[a]	-	38 (±5) (n = 5)	39 (±3) (n = 16)	39 (±7) (n = 4)		0.16 (±0.02) (n = 5)	0.16 (±0.01) (n = 16)	0.16 (±0.03) (n = 4)
Suncheon Bay	81 (±6) (n = 6)	66 (±3) (n = 4)	79 (±5) (n = 18)	84 (±4) (n = 4)	0.31 (±0.02) (n = 6)	0.25 (±0.01) (n = 4)	0.30 (±0.02) (n = 18)	0.31 (±0.01) (n = 4)
Nakdong River estuary	22 (±6) (n = 6)	28 (±8) (n = 5)	22 (±4) (n = 17)	37 (±4) (n = 5)	0.07 (±0.02) (n = 6)	0.08 (±0.03) (n = 5)	0.07 (±0.01) (n = 17)	0.09 (±0.01) (n = 5)

[a]Samples were collected from Sinan over three years (2018–2020).

Table 3.5.
Description of methods used to measure sedimentation rate in coastal wetlands, along with depth and time scale, strength, and weakness of each method. Methods were referenced from previous study (Breithaupt et al., 2018).

Method	Depth & Time scale	Strength	Weakness
Surface marker horizons (e.g., Feldspar, brick dust)	• Depth: 0–10 cm • Time: 0–10 yr	• Capable of quantifying erosion • Time-series analysis with fine scale resolution	• Limited timescale along durability of marker • Confusion of time scale using wrong marker
Surface elevation tables (e.g., Vertical pipe)	• Depth: 0–10 cm • Time: 0–10 yr	• Capable of quantifying surface elevation change • Time-series analysis with regular sampling	• Limited comparison between sites for some of stations with inconsistent reference depths
^{137}Cs (e.g., Chernobyl (1986) or Fukushima (2011) explosion)	• Depth: 0–100 cm • Time: 0–40 yr	• Capable of quantifying multi-decadal resolution • Straightforward age dating calculations	• Limitation of peak detection in Southern Hemisphere due to atmospheric fallout/washout • ^{137}Cs can be mobilized in saline sediments
^{210}Pb (e.g., Half-life of ^{210}Pb; 22.3 years)	• Depth: 0–100 cm • Time: 0–150 yr	• Capable of quantifying sub-decadal resolution • Long-term record including onset of sea level rise	• Limitation of peak detection in arid climate sediments due to atmospheric fallout/washout
Historic event horizons (e.g., Volcanic eruption)	• Depth: 0–150 cm • Time: 10–1,000 yr	• Capable of quantifying from sub-decadal to millennial resolution	• Limited to only opportunistically available
^{14}C (e.g., Half-life of ^{14}C; 5,700 years)	• Depth: 10–10,000 cm • Time: 100–100,000 yr	• Capable of quantifying from centennial to millennial resolution • Capable for identification of variable rates when multiple macrofossils and depths are dated	• Limitation of age dating of plant roots which grow to various depth • Limitation of age dating of mollusks which capable of mobility

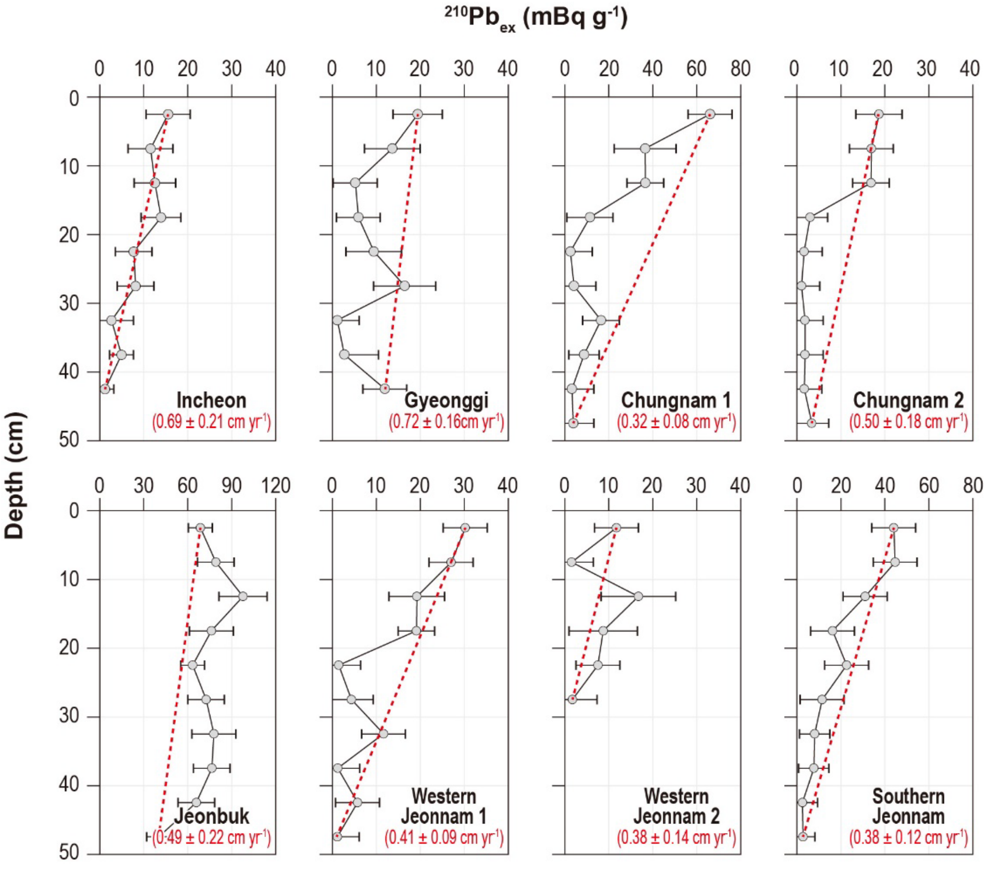

Figure 3.4.

Depth profiles of unsupported ^{210}Pb ($^{210}Pb_{ex}$) and sedimentation rate of core sediments at Incheon, Gyeonggi, Chungnam, Jeonbuk, Jeonnam (West), and Jeonnam (South).

3.2.5. Calculation of organic carbon stock

To estimate organic carbon stock per unit area in core sediments, we followed the standard method of Howard et al. (2014) (Eq. 4–7).

$$\text{Bulk density (g cm}^{-3}) = \frac{\text{Mass of dry sediment (g)}}{\text{Original volume sampled (cm}^{3})} \quad (4)$$

Amount carbon in core section (g cm^{-3}) (5)

$$= \text{Bulk density (g cm}^{-3}) \times \frac{\text{Organic carbon (\%)}}{100} \times \text{Sediment thichness interval (cm)}$$

The bulk density data of core sediments in the study areas are shown in Table 3.6.

Core #1 summed (g cm^{-2}) (6)

= Amount carbon in core section A (g cm^{-3}) + Amount carbon in core section B (g cm^{-3}) + Amount carbon in core section C (g cm^{-3}) + ····· All the samples from a single core

Sediment organic carbon stock in each core section per sediment core was calculated and summed to the entire 1 m depth.

Organic carbon stock per unit area (Mg C ha^{-1}) (7)

= Summed core carbon (g cm^{-2}) × 0.01

where 0.01 is the conversion factor from Eq. 6 to units commonly used in organic carbon stock assessments (Mg C ha^{-1}) (1 Mg = 1,000,000 g, 1 ha = 100,000,000 cm^2). We also normalized the organic carbon stock of core sediments for which core depth was <100 cm (Figure 3.5). Under this normalization method, we assumed that organic carbon content (%) at 60–100 cm depth was same as that at 60 cm.

To determine the total amount of organic carbon stock (Mg C) in the ecosystem, we multiplied the organic carbon stocks per unit area (Mg C ha^{-1}) for each core obtained in Eq. 7 by the tidal flat area (km^2) (Mg C) (Eq. 8).

Organic carbon stocks (Mg C) (8)

$$= \text{Organic carbon stock per unit area } (\text{Mg C ha}^{-1}) \times \text{Tidal flat area } (\text{km}^2) \times \frac{100 \text{ ha}}{1 \text{ km}^2}$$

Organic carbon stock (Mg C) was calculated using unit conversion factors (1 km^2 = 100 ha) of tidal flat area (km^2).

As part of the analysis, we obtained organic carbon stocks in the coastal zones of Ganghwa, Youngjong, Siheung, Daebu, Hwaseong, Garolim Bay, Geunheung, Ocheon, Biin, Seonyu, Gomso Bay, Hampyeong, Sinan, Aphaedo, Gangjin Bay, Deukryang Bay, Suncheon Bay, Yeoza Bay, Jinhae Bay, Nakdong River estuary, and Uljin. Overall, 303 sediment core samples (50–100 cm; subsamples at 5 cm intervals) were collected from salt marshes and bare tidal flats, respectively. The mean organic carbon stocks from 10 to 20 subsamples were utilized to normalize organic carbon stock values for 1 m depth values in each zone.

Table 3.6.
Bulk density (g cm^{-3}) of core sediments in the west, south, and east coasts of South Korea.

Sea	Region	Bulk density (g cm^{-3})		
		Sand	Mixed	Mud
West Sea	Gyeonggi (including Incheon)	1.55 (±0.03)	1.59 (±0.13)	1.25 (±0.16)
	Chungnam	1.34 (±0.16)	1.38 (±0.12)	1.28 (±0.16)
	Jeonbuk	1.53 (±0.13)	1.49 (±0.04)	1.37 (±0.08)
	Jeonnam	1.39 (±0.24)	1.30 (±0.10)	1.12 (±0.08)
South Sea	Jeonnam	1.05 (±0.07)	1.31 (±0.32)	0.86 (±0.14)
	Gyeongnam (including Busan)	1.36 (±0.06)	1.27 (±0.11)	1.00 (±0.30)
East Sea	Gyeongbuk	3.46 (±0.40)	-	-

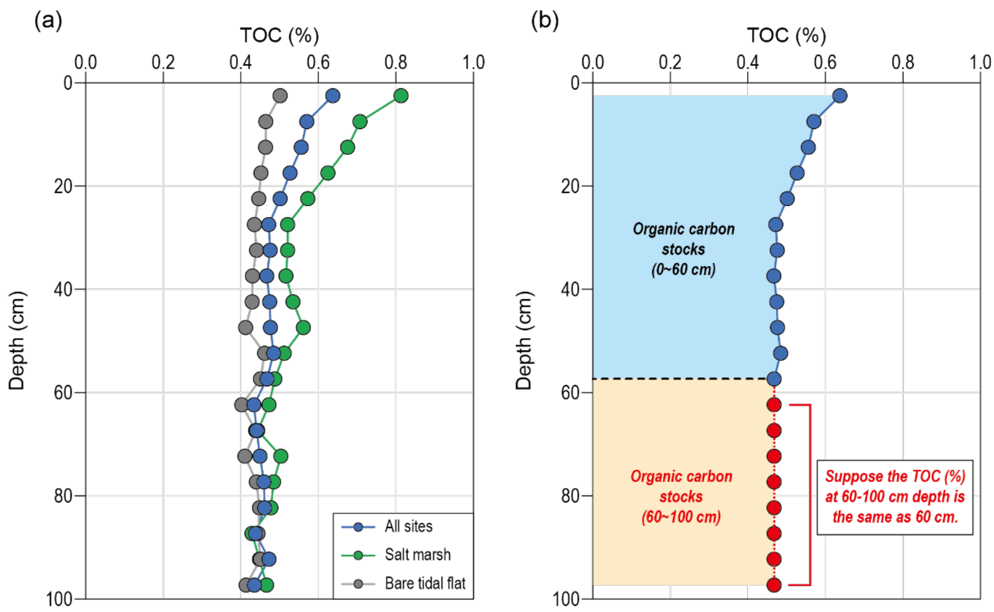

Figure 3.5.
(a) Mean vertical distribution of organic carbon in the core sediments at all sites, salt marshes, and bare tidal flats. (b) Normalizing method of organic carbon stock in core sediments for which core depth was <100 cm.

3.2.6. Calculation of organic carbon sequestration rate

The organic carbon sequestration rate was estimated using the following equation (Xiaonan et al., 2008; EI-Hussieny and Ismail, 2015) (Eq. 9).

$$\text{Organic carbon sequestration rate per unit area (g C m}^{-2}\text{ yr}^{-1}) \quad (9)$$
$$= \text{Bulk density (g cm}^{-3}) \times \text{organic carbon (g kg}^{-1}) \times \text{sedimentation rate (mm yr}^{-1})$$

Where bulk density (g cm^{-3}) and organic carbon (g kg^{-1}) are average values in the sediment core profile. We then converted Eq. 9 to commonly used units by implementing a 0.01 conversion factor (Mg C ha^{-1} yr^{-1}) (1 Mg = 1,000,000 g, 1 ha = 100,000,000 cm^2). To estimate overall organic carbon sequestration rates, we multiplied the organic carbon sequestration rate per unit area (Mg C ha^{-1} yr^{-1}) for each core obtained in Eq. 10 by the tidal flat area (km^2) to determine the organic carbon sequestration rate (Mg C yr^{-1}) (Eq. 11).

$$\text{Organic carbon sequestration rate per unit area (Mg C ha}^{-1}\text{ yr}^{-1}) \quad (10)$$
$$= \text{Organic carbon sequestration rate per unit area (g cm}^{-2}\text{ yr}^{-1}) \times 0.01$$

$$\text{Organic carbon sequestration rate (Mg C yr}^{-1}) \quad (11)$$
$$= \text{Organic carbon sequestration rate per unit area (Mg C ha}^{-1}\text{ yr}^{-1}) \times \text{Tidal flat area (km}^2) \times \frac{100\text{ ha}}{1\text{ km}^2}$$

3.2.7. Statistical analyses

SPSS 23.0 (SPSS Inc., Chicago, IL) was used to perform the statistical analyses. Organic carbon stocks of core sediments were analyzed to test for differences between the four survey years (2017, 2018, 2019, and 2020) across five regions (Ganghwa, Garolim Bay, Sinan, Suncheon Bay, and Nakdong River estuary) using one-way analysis of variance (ANOVA) with Scheffe's post-hoc test. Before the analysis, homogeneity of variance was determined between groups with Levene's homogeneity test, meeting the assumption of homogeneity of variance ($p > 0.05$). To estimate variation in geography, morphology, salinity, land-use, and vegetation, we performed t-test. Pearson correlation analysis was used to test for significant relationships with: 1) organic carbon stocks and human population, 2) organic carbon stocks and tidal amplitude, 3) organic carbon stocks and mud content, 4) organic carbon content and mud content, and 5) remote sensing classification and mud content.

3.3. Results and discussion

3.3.1. Spatiotemporal distribution of organic carbon stocks per unit area

The data on sedimentary organic carbon stock per unit in the 21 coastal regions generally indicated varied spatial and temporal distributions (Figure 3.1). The topographical characteristics (e.g., coastline, tidal flat area, and salt marsh area) of the stations in the tidal flats of the West, South, and East Sea of South Korea differed (Table 3.7). By province, Gyeonggi (including Incheon) had the greatest organic carbon stock per unit area (81.0 ± 3.3 Mg C ha^{-1}), followed by Southern Jeonnam (77.0 ± 3.2 Mg C ha^{-1}), Gyeongnam (including Busan) (68.3 ± 3.4 Mg C ha^{-1}), Chungnam (35.6 ± 1.9 Mg C ha^{-1}), Western Jeonnam (33.6 ± 2.2 Mg C ha^{-1}), Jeonbuk (21.3 ± 4.4 Mg C ha^{-1}), and Gyeongbuk (18.1 ± 1.2 Mg C ha^{-1}) (Figure 3.1a). Furthermore, the tidal flats along the south coast had slightly higher sedimentary organic carbon stock (58.1 ± 3.3 Mg C ha^{-1}) compared to those of the west coast (50.3 ± 2.2 Mg C ha^{-1}). Because most of the tidal flats along the South Sea are semi-enclosed embayments compared to those of the West Sea (Koh and Khim, 2014), larger quantities of organic carbon likely accumulate from terrestrial sources (e.g., freshwater algae, plants, and human activities) (Wang et al., 2018).

In general, the concentration of sedimentary organic carbon showed local fluctuations in relation to potential anthropogenic- and natural sources (Lee et al., 2019). Sources tend to be a mixture of different contributions of both marine and terrestrial origin, indicating the importance of local environments (Graham et al., 2001; Lamb et al., 2006). In the present study, Gyeonggi and Gyeongnam provinces had the highest organic carbon stocks of the west and south coasts, respectively (Figure 3.1a). Both provinces are strongly influenced by terrestrial inputs through freshwater discharge (Choi et al., 2011; Koh and Khim, 2014; Lee et al., 2018; Lee et al., 2019). Furthermore, riverine inputs of anthropogenic organic matter (such as municipal sewage and discharge) possibly contribute to the burial of organic carbon in sediments (Bae et al., 2017; Lee et al., 2019). For example, high organic carbon stocks in Jinhae Bay reflect exposure to point-sources of coastal pollutions from industry, aquaculture, and municipal sewage discharge since the 1970s (Lim et al., 2006; Seo et al., 2014). Overall, terrestrial input considerably influenced the dynamics of sedimentary organic matter in this province, with a strong direct effect from freshwater discharge.

Furthermore, we investigated temporal variation in the organic carbon stock of core sediments from the five target regions (Ganghwa, Garolim Bay, Sinan, Suncheon Bay, and Nakdong River estuary) between 2017 and 2020 (Figure 3.1b; Table 3.4). Temporal variability of organic carbon stock was generally stable across the five regions over the four-year period. There was no significant difference in the organic carbon stocks of core sediments over the monitoring period in the target regions. Such stable storage of organic carbon (viz., refractory carbon) could be generated through a decrease in microbial activity. This phenomenon occurs in the anaerobic conditions of core sediments, resulting in it contributing to the "Blue Carbon" of tidal flats (Macreadie et al., 2019).

Table 3.7.

Coastline, tidal flat area, and salt marsh area in the West, South, and East Sea of South Korea.

Sea	Region	Coastline[a] (km)	Tidal flat area (km^2)	Salt marsh area[b] (km^2)	Ratio of salt marsh in tidal flat (%)
West Sea	Gyeonggi (including Incheon)	1,339	920	0.005	0.001
	Chungnam	1,242	378	0.007	0.002
	Jeonbuk	549	12	0.011	0.089
	Jeonnam	3,562	595	0.004	0.001
	Subtotal	**6,692**	**1,905**	**0.027**	**0.001**
South Sea	Jeonnam	3,181	281	0.031	0.011
	Gyeongnam (including Busan)	2,893	296	0.013	0.004
	Subtotal	**6,074**	**577**	**0.043**	**0.008**
East Sea	Gyeongbuk (including Ulsan)	704	6	0.007	0.110
	Gangwon	402	2	0.002	0.120
	Subtotal	**1,106**	**8**	**0.009**	**0.113**
	Total	**13,871**	**2,490**	**0.080**	**0.003**

[a]Coastline of South Korea was investigated by The Ministry of Oceans and Fisheries, 2020

[b]Lee et al. (2019)

3.3.2. Environmental factors affecting the complex dynamics of sedimentary organic carbon stocks

Organic carbon stocks of intertidal sediments along the west, south, and east coast significantly different with respect to their environmental conditions, including geography, salinity, land-use type, vegetation, and mud content (Figure 3.6). Although there was no statistically significant difference in organic carbon stocks with morphology, embayments had relatively higher values compared to open coasts. Higher organic carbon stocks of brackish water stations seemed to reflect the large quantities of anthropogenic inputs from industrial and/or municipal sources. In addition, the organic carbon stock of salt marshes significantly differed to that of bare tidal flats, indicating organic carbon residues originated from halophytes. Human population density, linked to nutrient inputs from industrial and/or municipal sources (e.g., sewage) (Caccia and Boyer, 2007), showed no statistical correlation with organic carbon stocks. For example, low organic carbon stocks of the Nakdong River estuary, which are sand-dominant intertidal flats with the highest population, did not reflect the elevated nutrient loading. Thus, the large quantity of anthropogenic inputs did not seem to contribute as sources of organic carbon, particularly in sand-dominated bottoms (Liu et al., 2016; Lee et al., 2019).

Interestingly, organic carbon stocks were significantly related to tidal amplitude in certain regions (Figure 3.7). For example, the organic carbon stocks in West Sea and open coasts were positively correlated with tidal amplitude ($r = 0.67$, $p < 0.01$ and $r = 0.53$, $p < 0.01$, respectively), but there were no significant relationships for the samples collected in the South Sea and embayment regions. This result suggested that tidal energy under varied topographical and morphological settings could be a key factor to increase not only supply of waterborne sediment particles but also organic carbon burial in the intertidal sediments (Collins et al., 2017). In the same context, we found a positive relationship between mud contents and organic carbon stocks ($r = 0.60$, $p < 0.01$). In other words, the larger surface areas of more muddy sediment particles provide a better capture capacity compared to sandy sediments (Keil and Hedges, 1993; Mayer, 1994; Burdige, 2007; Serrano et al., 2016).

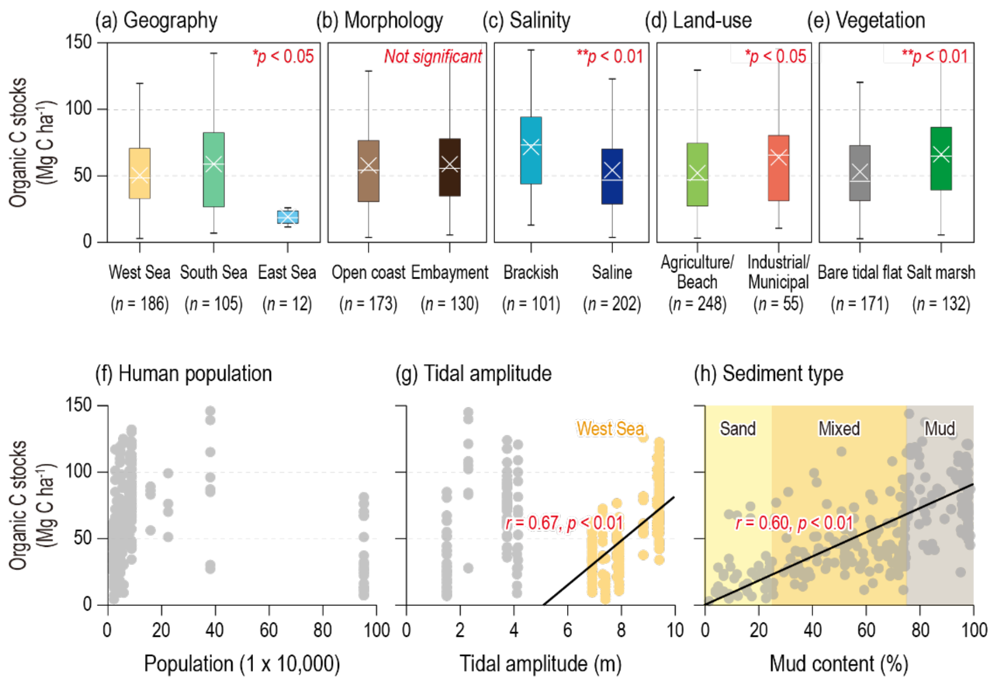

Figure 3.6.
Distribution of organic carbon stocks in core sediments with respect to (a) geography, (b) morphology, (c) salinity, (d) land-use. Panels: (a)West Sea (n= 186), South Sea (n= 105), and East Sea (n=12). (b) Open coast (n=173) and Embayment (n=130). (c) Brackish (n=101) and Saline (n=202). (d) Agriculture/Beach (n=248) and Industrial/Municipal (n=55). (e) Bare tidal flat (n=171) and Salt marsh (n=132). Relationships between organic carbon stocks and (f) human population (1 × 10,000), (g) tidal amplitude, and (h)mud content of 303 core sediments of South Korea.

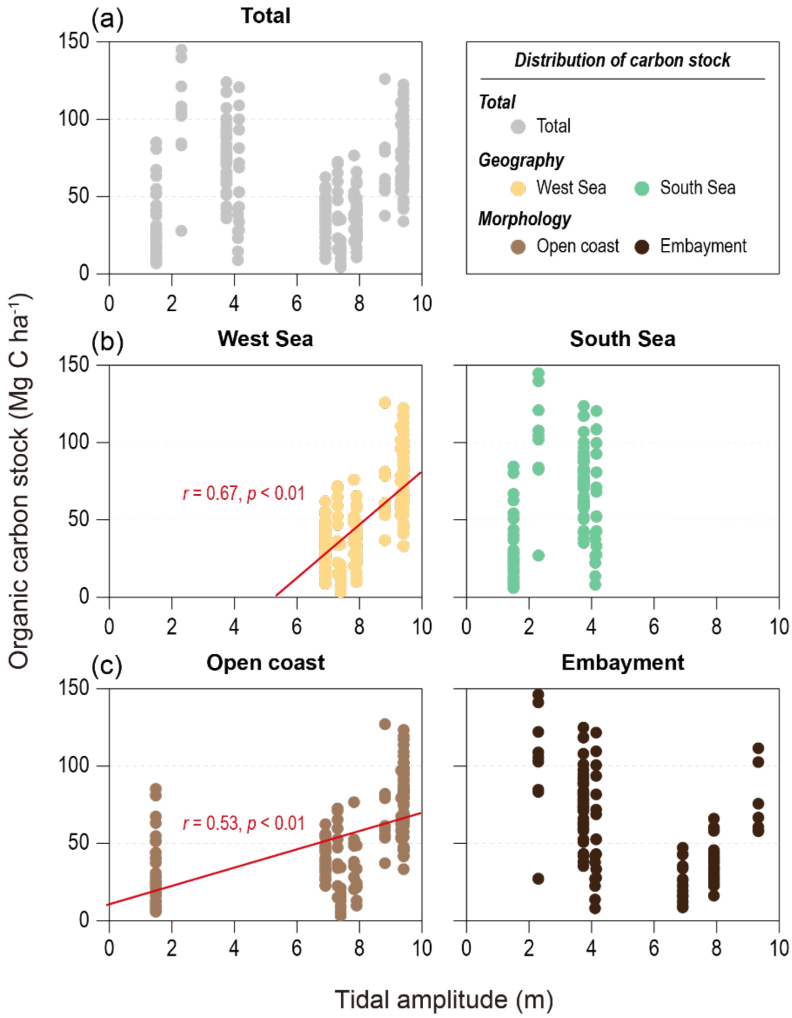

Figure 3.7.
Relationship between tidal amplitude and organic carbon stock in core sediments with respect to (a) total, (b) geography, and (c) morphology.

3.3.3. Effects of mud content and vegetation on sedimentary TOC

Total organic carbon content and mud content in sediments varied in the bare tidal flats and salt marshes of the West, South, and East Sea. We classified sediment textural type based on mud (silt + clay) content; namely, sand (< 25%), mixed (25–75%), and mud (> 95% mud). The intertidal sediments collected in our study areas contained both mixed and mud bottom fractions, with >25% mud content on average, except for Nakdong River estuary and Uljin (Figure 3.8). Gyeonggi had the highest mud content (mean ± SD, 80.2 ± 21.1%), followed by Southern Jeonnam (79.4 ± 27.3%), Chungnam (66.3 ± 27.2%), Western Jeonnam (61.0 ± 33.7%), Jeonbuk (51.0 ± 34.1%), Gyeongnam (26.3 ± 24.8%), and Gyeongbuk (0.6 ± 0.5%) (Figure 3.9). In South Korea, tidal flats are typically characterized by mud-dominated sediments in the upper intertidal flats and sand-dominated sediments in the lower intertidal flats (Choi, 2014b). Moreover, textural trends in tidal flat sediments are caused by differences to critical shear stress for deposition and erosion (Dalrymple and Choi, 2003; Choi, 2014b)

As expected, organic carbon content was greater in mud-dominated sediment (0.58 ± 0.24%) compared to mixed sediment (0.48 ± 0.28%) and sand-dominated sediment (0.23 ± 0.05). The relationships between sedimentary organic carbon and mud content (% particles <63 μm) of bare tidal flats and salt marshes in different provinces were evaluated (Figure 3.9). The analysis revealed that mud content had a significantly positive correlation with organic carbon in bare tidal flats ($r = 0.59$, $p < 0.01$) and salt marshes ($r = 0.30$, $p < 0.01$) in all provinces (Figure 3.10). The positive relationship between mud and organic carbon content has been repeatedly documented (Keil and Hedges, 1993; Mayer, 1994; Bergamaschi et al., 1997; Flemming and Delafontaine, 2000; Burdige, 2007; Serrano et al., 2016). This relationship is attributed to the larger surface area of fine-grained sediments (e.g., mud) compared to coarse-grained sediments (e.g., sand), providing more binding sites for sedimentary organic carbon (Keil and Hedges, 1993; Mayer, 1994; Burdige, 2007; Serrano et al., 2016). Therefore, mud content could be used as a universal proxy for estimating sedimentary organic carbon by applying each relationship equation of bare tidal flats and salt marshes in different provinces of

South Korea.

Interestingly, significant differences in organic carbon content between bare tidal flats and salt marshes were detected in South Korea ($p < 0.01$) (Figure 3.10). Salt marshes serve as highly efficient CO_2 sinks through primary production and the trapping of sediments, resulting in their accreting higher sedimentary organic carbon compared to bare tidal flats (Duarte et al., 2013; Spivak et al., 2019). Salt marshes capture CO_2 gas from the atmosphere, and then sequester carbon in organic forms within underlying sediments, living biomass aboveground (leaves, stems) and belowground (roots), and non-living biomass (litter) (Mcleod et al., 2011). The structural complexity of vegetated coastal ecosystems (root systems and dense vegetation) allows salt marshes to be highly efficient in trapping sediment and associated organic carbon originating from autochthonous and allochthonous sources. Overall, higher sedimentary organic carbon content in salt marshes primarily results from higher carbon input through plant litter and roots, and their being located in more saturated and, presumably, more anaerobic environments (Yuan et al., 2015; Spivak et al., 2019).

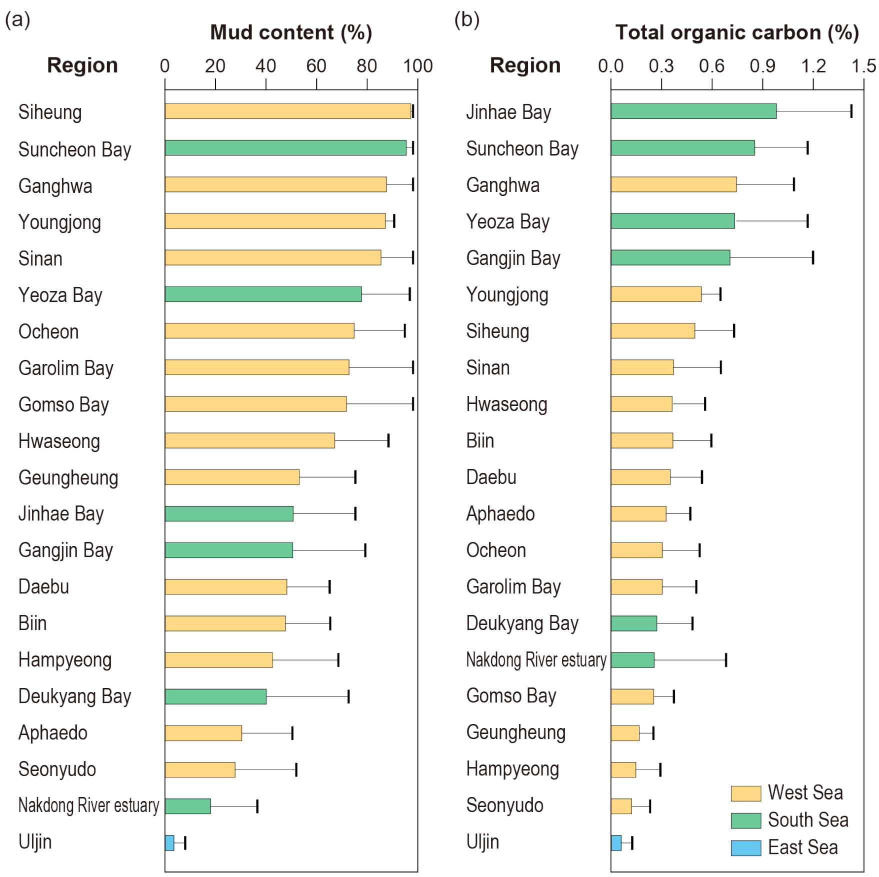

Figure 3.8.
Spatial distribution of (a) mud content (%) and (b) total organic carbon (%) of core sediments in 21 intertidal flats. Yellow, green, and blue bars denote at West Sea, South Sea, and East Sea, respectively.

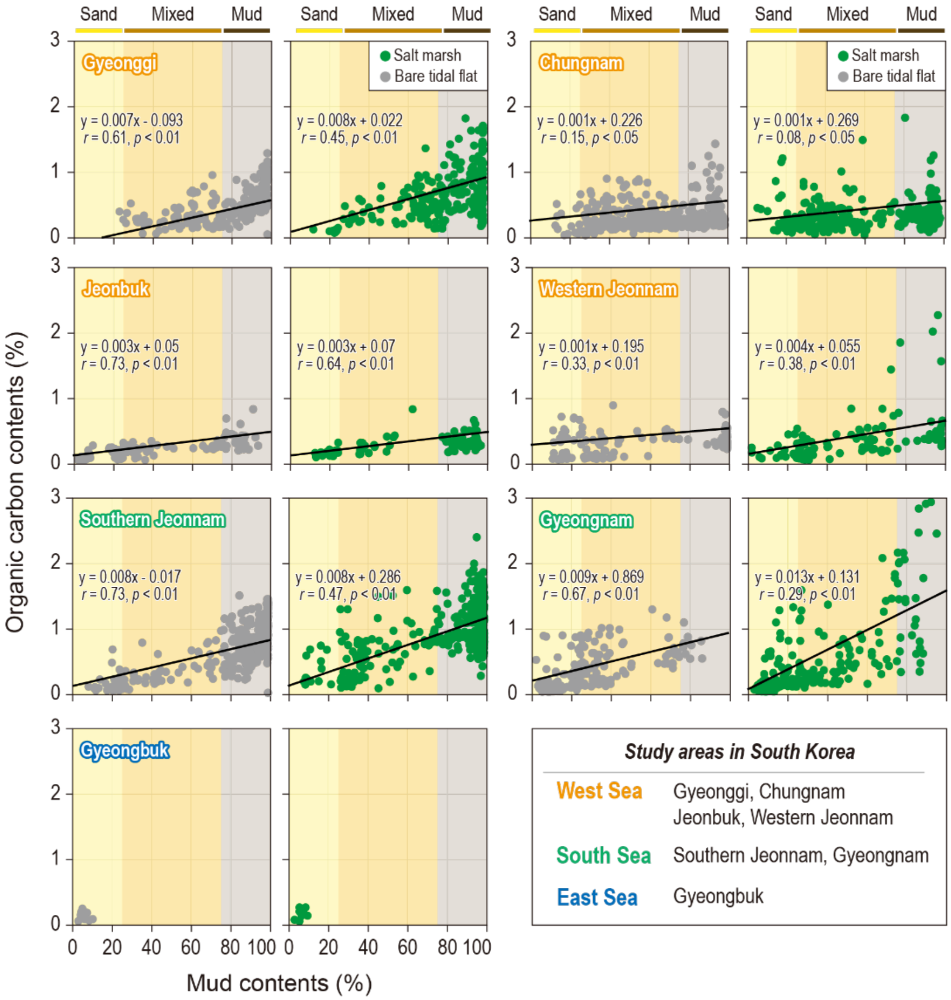

Figure 3.9.

Relationships between mud content and organic carbon content in the sediments of bare tidal flats and salt marshes in the provinces of Gyeonggi, Chungnam, Jeonbuk,Western Jeonnam, Southern Jeonnam, Gyeongnam, and Gyeongbuk, South Korea. The textural type of sediment was classified into 3 types based on mud (silt + clay) contents: followed by sand (<25% mud), mixed (25–75% mud), and mud (>75% mud) (Flemming, 2000).

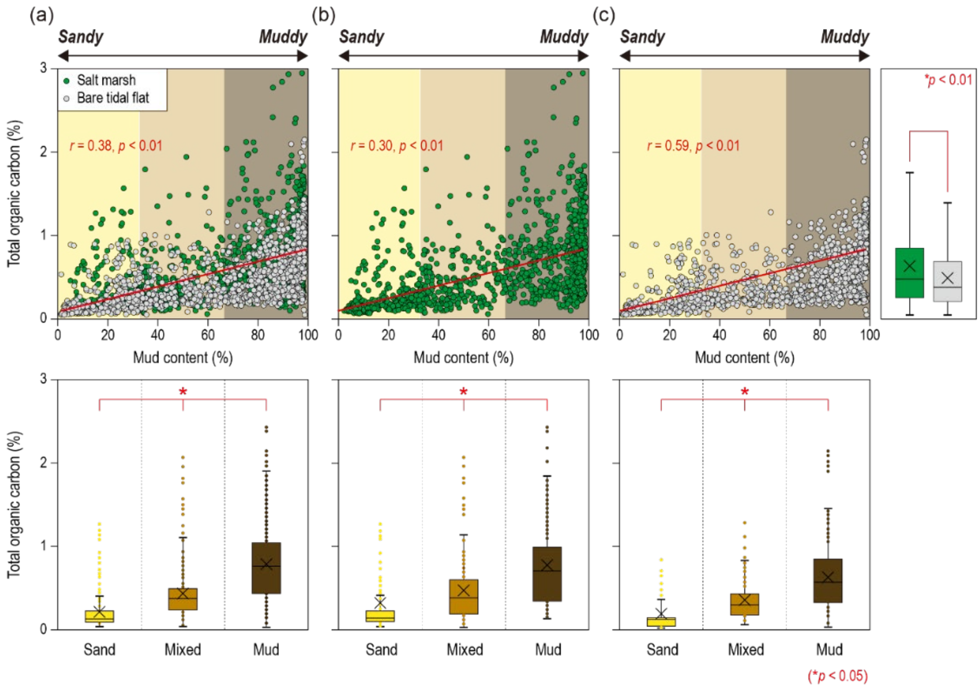

Figure 3.10.
Relationship between mud content and total organic carbon in core sediments of (a) total, (b) salt marshes, and (c) bare tidal flats.

3.3.4. Validation of tidal flat areas and sediment textural types using remote sensing classification

The intertidal flats of the West, South, and East Sea were divided into 11,905 grid zones, with the tidal flat area being delineated using QGIS (Figure 3.11). The analysis showed that Incheon had the greatest tidal flat area (742 km^2), followed by Western Jeonnam (595 km^2), Chungnam (378 km^2), Southern Jeonnam (281 km^2), Gyeongnam (265 km^2), Gyeonggi (178 km^2), Busan (31 km^2), Jeonbuk (12 km^2), Gyeongbuk (4 km^2), Gangwon (2 km^2), and Ulsan (2 km^2) (Table 3.8).

The textural type of sediments in all grid zones was classified by remotely sensed imagery as sand, mixed, and mud. Remote sensing and experimental data classifications were generally well matched. A significant positive relationship was obtained for remote sensing classification and measured mud content ($r = 0.40$, $p < 0.01$) (Figure 3.11b; c). In parallel to determining sediment textural type, we delineated each tidal flat area as sand, mixed, and mud-dominated sediments in all grid zones (Table 3.9). Through these comprehensive analyses, the current study reported tidal flat areas per sediment textural type along the entire coast of the West, South, and East Sea of South Korea. The remote sensing results delineated three types of tidal flat areas based on sediment mud content: 1) mixed (mud dominant) tidal flats (Gyeonggi, Chungnam, Western Jeonnam, Western Jeonnam, Southern Jeonnam, Gyeongnam); 2) mixed (sand dominant) tidal flats (Incheon, Jeonbuk); and 3) sandy tidal flats (Gyeongbuk, Ulsan, Gangwon). As a result, mixed tidal flats had the greatest areas in the southwestern coast of Korea. However, the classification of sediment textural types based on expert judgment still has limitations with uncertainty and limited information. Therefore, it should be necessary to develop classification methods using state-of-art techniques, including machine learning.

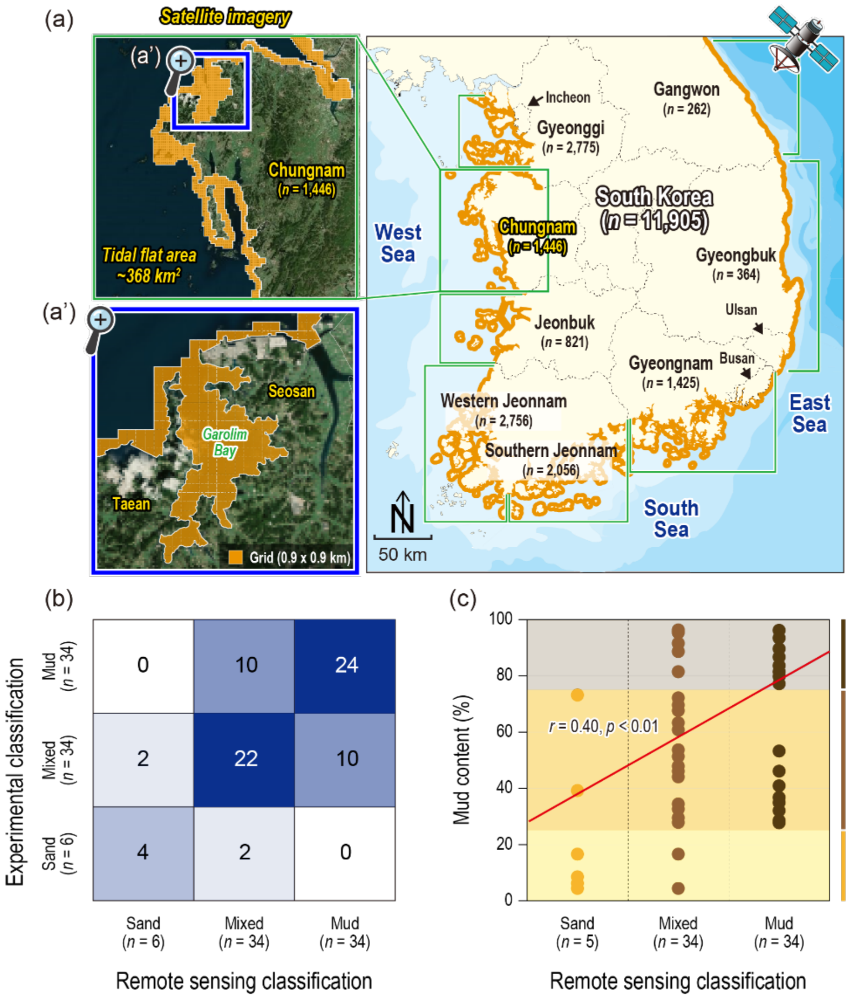

Figure 3.11.
Relationship between mud content and total organic carbon in core sediments of (a) total, (b) salt marshes, and (c) bare tidal flats.

Table 3.8.
Organic carbon stocks (Mg C) and organic carbon sequestration rate (Mg C yr^{-1}) in the coastal regions along the west, south, and east coast of South Korea (1 Mg = 10^6 g).

Sea	Region	Tidal flat area (km^2)	Sedimentation rate ($cm\ yr^{-1}$)		Oraganic carbon stocks (Mg C)	Organic carbon sequestration rate (Mg C yr^{-1})
			This study	Reference		
West Sea	Incheon	742	0.69		4,923,784	34,425
	Gyeonggi	178	0.72		1,243,775	9,048
	Chungnam	378	0.41		1,274,415	5,240
	Jeonbuk	12	0.49		20,211	100
	Jeonnam	595	0.40		1,952,907	7,886
	Subtotal	**1,906**			**9,415,091**	**56,698**
South Sea	Jeonnam	281	0.38		1,621,985	6,198
	Gyeongnam	265		0.41[b]	1,939,344	7,979
	Busan	31		0.30[c]	149,935	451
	Subtotal	**577**			**3,711,264**	**14,629**
East Sea	Gangwon	2[a]		0.33[d]	4,361	14
	Gyeongbuk	4[a]		0.27[e]	8,009	22
	Ulsan	2[a]		0.60[f]	3,424	21
	Subtotal	**9**[a]			**15,794**	**57**
	Total	**2,491**			**13,142,149**	**71,383**

[a]Tidal flat areas were delineated using Electronic Navigational Chart (ENC) data.
[b]Park and Lee (1996); Woo et al. (2003); Jeong et al. (2006); Lim et al. (2012).
[c]Cho et al. (2000)
[d]Song et al. (2019)
[e]Park et al. (1999)
[f]Cha et al. (2005)

Table 3.9.
Mapped tidal flat area (km^2) by remote sensing classification in the West, South, and East Sea, South Korea.

Sea	Region	Tidal flat area (km^2)			
		Sand	Mixed	Mud	Total
West Sea	Incheon	404	202	136	742
	Gyeonggi	50	69	60	178
	Chungnam	157	143	77	378
	Jeonbuk	9	2	2	12
	Jeonnam	157	241	198	595
	Subtotal	**777**	**657**	**472**	**1,906**
South Sea	Jeonnam	31	181	68	281
	Gyeongnam	36	161	68	265
	Busan	15	15	1	31
	Subtotal	**82**	**357**	**138**	**577**
East Sea	Gangwon	2	-	-	2
	Gyeongbuk	4	-	-	4
	Ulsan	2	-	-	2
	Subtotal	**9**	-	-	**9**
	Total	**868**	**1,014**	**610**	**2,491**

3.3.5. Estimation of organic carbon stocks and sequestration rates in South Korea

Through integrating sedimentary organic carbon stock per unit with tidal flat type, we estimated the organic carbon stocks (Table 3.10) and sequestration rates (Table 3.11) in sand, mixed, and mud-dominated sediments. For tidal flats delineated by remote sensing, Gyeonggi (including Incheon) had the highest organic carbon stocks (6,167,559 Mg C), followed by Gyeongnam (including Busan) (2,089,279 Mg C), Western Jeonnam (1,952,907 Mg C), Southern Jeonnam (1,621,985 Mg C), Chungnam (1,274,415 Mg C), Jeonbuk (20,211 Mg C), Gyeongbuk (including Ulsan) (11,433 Mg C), and Gangwon (4,361 Mg C) (Table 3.8; Figure 3.12). The organic carbon sequestration rate of all provinces in South Korea was also estimated from sedimentation rates. The results provided baseline values for organic carbon stocks (Total: 13,142,149 Mg C; 13 Tg C) and sequestration rates (71,383 Mg C yr^{-1}; 0.07 Tg C yr^{-1}) in the tidal flats of Korea. Total organic carbon content was positively correlated with mud content; thus, organic carbon stock was also higher in mud-dominated sediments (Table 3.12). However, current estimates of organic carbon stock and sequestration rates was based on tidal flat delineated data, with no separation of bare tidal flats or salt marshes in the study area. Thus, further study is required.

We conducted an extensive literature review of data on carbon that were available for salt marshes and bare tidal flats in the Yellow Sea of China (Table 3.13). Organic carbon stocks in the sediments of China's coastal areas were available from the published literature, encompassing typical bare intertidal flats and salt marsh zones along the Yellow Sea, including the Liaohe Delta, Liadong, Dongying Port, Shandong, Yellow River Estuary, Yancheng Jiangsu, Sheyang, Jiangsu, Wanggang River estuary, Jiangsu, Chongming Island, and Shanghai. Sediment depth for the reported organic carbon stocks ranged from 10 to 100 cm across studies; thus, organic carbon stocks were normalized to the amount within 1 m depth for all subsequent calculations. The results showed that, for China, organic carbon stocks ranged from 3 to 116 Mg C ha^{-1} in bare tidal flats and 4 to 170 Mg C ha^{-1} in salt marshes (Table 3.13). For South Korea, organic carbon stocks ranged from 1 to 145 Mg C ha^{-1} in bare tidal flats and 4 to 161 Mg C ha^{-1} in salt marshes. Among the two countries, Chinese salt marshes generally had higher organic carbon stocks than Korean salt marshes. Thus, the different rates of increase for organic carbon stocks in the sediment of halophyte habitats in China and Korea were evaluated cautiously. In China, three species of halophytes (*Phragmites* sp., *Spartina* sp., and *Suaeda* sp.) dominate the vegetation in intertidal flats. In comparison, *Phragmites* sp. and *Suaeda* sp. are the dominant halophytes in most coastal areas of South Korea, while *Spartina* sp. habitats are only found in Ganghwa of Gyeonggi (Table 3.1). Yuan et al. (2015) reported that sedimentary organic carbon sequestration rates in *S. alterniflora* marshes were 2.63 to 8.78 times higher compared to those of native halophyte marshes (e.g., *Phragmites australis* and *Suaeda salsa*) in Yancheng National Nature Reserve, China. Therefore, the species composition of halophytes contributes to different burial rates of organic carbon in intertidal flats.

Only a small number of studies exist on organic carbon stocks and sequestration rates in bare tidal flats areas (Chen et al., 2020). Bare tidal flats have relatively small amounts of organic carbon stocks, due to their having low net primary production (NPP) compared to salt marshes, seagrasses, and mangroves (Table 3.14). Nevertheless, given extensive areal coverage and microphytobenthos, bare tidal flats could be an important carbon sink (Chen et al., 2020; Lin et al., 2020), and also a terminal reservoir of detrital organic matter from adjacent “Green Carbon” ecosystems.

Table 3.10.
Organic carbon stock (Mg C) using mapped tidal flat area based on remote sensing classification in the West, South, and East Sea of South Korea.

Sea	Region	Organic carbon stock (Mg C)			
		Sand	Mixed	Mud	Total
West Sea	Incheon	2,479,324	1,362,680	1,081,781	**4,923,784**
	Gyeonggi	307,182	461,533	475,061	**1,243,775**
	Chungnam	463,978	509,401	301,036	**1,274,415**
	Jeonbuk	8,980	3,709	7,522	**20,211**
	Jeonnam	404,613	796,276	752,018	**1,952,907**
	Subtotal	**3,664,076**	**3,133,598**	**2,617,417**	**9,415,091**
South Sea	Jeonnam	57,540	1,049,983	514,461	**1,621,985**
	Gyeongnam	92,502	1,056,771	790,072	**1,939,344**
	Busan	39,450	99,965	10,519	**149,935**
	Subtotal	**189,492**	**2,206,720**	**1,315,052**	**3,711,264**
East Sea	Gangwon	4,361	-	-	**4,361**
	Gyeongbuk	8,009	-	-	**8,009**
	Ulsan	3,424	-	-	**3,424**
	Subtotal	**15,794**	-	-	**15,794**
	Total	**3,869,362**	**5,340,318**	**3,932,469**	**13,142,149**

Table 3.11.
Organic carbon sequestration rate (Mg C yr^{-1}) using mapped tidal flats area by remote sensing classification in the West, South, and East Sea, South Korea.

Sea	Region	Organic carbon sequestration rate (Mg C yr^{-1})			
		Sand	Mixed	Mud	Total
West Sea	Incheon	17,423	9,497	7,505	**34,425**
	Gyeonggi	2,253	3,357	3,439	**9,048**
	Chungnam	1,906	2,099	1,234	**5,240**
	Jeonbuk	44	18	37	**100**
	Jeonnam	1,619	3,215	3,052	**7,886**
	Subtotal	**23,245**	**18,186**	**15,267**	**56,698**
South Sea	Jeonnam	219	4,016	1,963	**6,198**
	Gyeongnam	380	4,344	3,255	**7,979**
	Busan	119	301	32	**451**
	Subtotal	**717**	**8,661**	**5,250**	**14,629**
East Sea	Gangwon	14	-	-	**14**
	Gyeongbuk	22	-	-	**22**
	Ulsan	21	-	-	**21**
	Subtotal	**57**	-	-	**57**
	Total	**23,963**	**26,847**	**20,517**	**71,383**

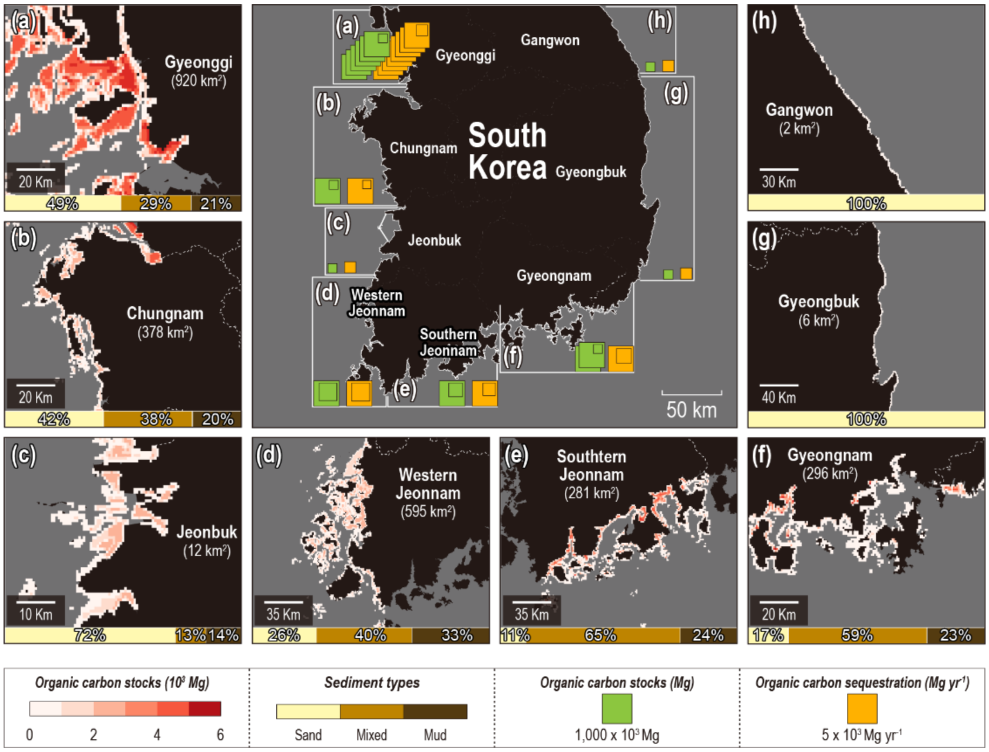

Figure 3.12.
Organic carbon stocks, organic carbon sequestration rates, and sediment textural types (sand, mixed, mud) at the provinces of: (a) Gyeonggi, (b) Chungnam, (c) Jeonbuk, (d)Western Jeonnam, (e) Southern Jeonnam, (f) Gyeongnam, (g) Gyeongbuk, and (h) Gangwon, South Korea.

Table 3.12.
Organic carbon stock (Mg C ha^{-1}) per unit of core sediments in the West, South, and East Sea, South Korea.

Sea	Region	Organic carbon stock (Mg C ha^{-1})		
		Sand	Mixed	Mud
West Sea	Gyeonggi (including Incheon)	61.4 (±12.4)	67.3 (±25.5)	79.7 (±27.4)
	Chungnam	29.5 (±11.6)	35.5 (±16.7)	39.0 (±15.0)
	Jeonbuk	10.0 (±7.0)	22.8 (±10.9)	42.2 (±2.5)
	Jeonnam	25.8 (±17.6)	33.1 (±14.0)	38.0 (±11.7)
South Sea	Jeonnam	18.6 (±11.6)	57.9 (±30.3)	75.4 (±20.4)
	Gyeongnam (including Busan)	25.6 (±23.1)	65.8 (±34.8)	115.5 (±17.6)
East Sea	Gyeongbuk	18.1 (±4.0)	-	-

Table 3.13.

Organic carbon content reported in the coastal sediments (salt marshes and bare tidal flats) of China.

Location	Sampling year	Latitude	Longitude	[a]Habitat	Dominant halophyte	Core depth (cm)	Organic carbon stock (Mg C ha^{-1})	[b]Organic carbon stock (Mg C ha^{-1})	Reference
Liaohe Delta, Liadong	2011	40°45'N	121°30'E	SM	*Suaeda* sp.	30	42	140	Mao et al. (2018)
	2011			SM		30	30	101	
	2011			B	Bare	30	35	116	
Dongying port, Shandong	2013	37°54'N	118°54'E	SM	*Phragmites* sp.	30	16	54	Zhao et al. (2017)
	2013			SM	*Suaeda* sp.	30	19	63	
	2013			B	Bare	30	16	55	
Yellow River Estuary, Shandong	2015	37°48'N	119°06'E	SM	*Suaeda* sp.	50	36	73	Zhao et al. (2018)
	2015			B	Bare	50	24	49	
	2014	37°47'N	119°11'E	SM	*Phragmites* sp.	10	12	116	Lu et al. (2018)
	2014			SM	*Suaeda* sp.	10	16	164	
	2014			B	Bare	10	6	61	
	2009	37°46'N	119°09'E	SM	*Suaeda* sp.	60	39	66	Mou et al. (2012)
	2009			SM	*Suaeda* sp.	60	36	60	
	2012	37°45'N	119°11'E	SM	*Phragmites* sp.	50	43	87	Wang et al. (2016)
	2012			SM	*Phragmites* sp.	50	41	83	
	2016	37°45'N	118°58'E	SM	*Phragmites* sp.	20	23	115	Tao et al. (2018)
	2008	37°42'N	119°15'E	SM	*Phragmites* sp.	40	21	52	Zhao et al. (2016)
	2008			SM	*Phragmites* sp.	40	20	49	
	2008			SM	*Phragmites* sp.	40	18	45	
	2008			SM	*Phragmites* sp.	40	16	41	
	2008			B	Bare	40	21	52	
Yancheng, Jiangsu	2011	32°36'N	119°51'E	SM	*Spartina* sp.	30	29	96	Yang et al. (2013)
	2011			SM	*Suaeda* sp.	30	16	54	
	2011			SM	*Phragmites* sp.	30	14	46	
	2011			B	Bare	30	9	30	
	2012			SM	*Spartina* sp.	30	32	108	Yang et al. (2015)
	2012			SM	*Phragmites* sp.	30	17	48	
	2012			SM	*Suaeda* sp.	30	14	56	
	2012			B	Bare	30	3	8	
	2012			SM	*Spartina* sp.	30	38	126	Yang et al. (2016)
	2012			SM	*Phragmites* sp.	30	20	56	
	2012			SM	*Suaeda* sp.	30	17	68	
	2012			B	Bare	30	4	15	
	2012			SM	*Spartina* sp.	30	38	126	Yang et al. (2017)
	2012			SM	*Spartina* sp.	30	51	170	

Table 3.13. (continued).

Location	Sampling year	Latitude	Longitude	[a]Habitat	Dominant halophyte	Core depth (cm)	Organic carbon stock (Mg C ha^{-1})	[b]Organic carbon stock (Mg C ha^{-1})	Reference
Yancheng, Jiangsu	2012	32°36'N	119°51'E	SM	*Spartina* sp.	30	43	143	Yang et al. (2017)
	2012			SM	*Spartina* sp.	30	33	109	
	2012			B	Bare	30	4	15	
	2011	33°35'N	120°30'E	SM	*Spartina* sp.	20	22	109	Wang et al. (2013)
	2011			SM	*Spartina* sp.	20	20	102	
	2011			SM	*Spartina* sp.	20	5	25	
	2011			SM	*Spartina* sp.	20	4	19	
	2011			B	Bare	20	4	21	
	2012	32°34'N	119°48'E	SM	*Spartina* sp.	100	35	35	Liu et al. (2017)
	2012			SM	*Suaeda* sp.	100	21	21	
	2012			B	Bare	100	24	24	
	2005	32°20'N	119°29'E	SM	*Spartina* sp.	30	16	53	Zhou et al. (2015)
	2005			SM	*Phragmites* sp.	30	13	50	
	2005			SM	*Suaeda* sp.	30	15	42	
	2005			B	Bare	30	6	21	
Sheyang, Jiangsu	2011	33°30'N	120°38'E	SM	*Spartina* sp.	30	39	130	Xiang et al. (2015)
	2011			SM	*Spartina* sp.	30	29	98	
	2011			SM	*Spartina* sp.	30	25	82	
	2011			B	Bare	30	15	50	
Wanggang River Estuary, Jiangsu	2002	33°19'N	120°44'E	SM	*Spartina* sp.	20	15	77	Liu et al. (2007)
	2002	33°18'N	120°43'E	SM	*Spartina* sp.	20	11	55	
	2002	32°35'N	120°59'E	B	Bare	20	12	60	
	2002	32°36'N	120°59'E	SM	*Spartina* sp.	20	7	37	Zhou et al. (2008)
	2002			B	Bare	20	9	43	
Chongming Island, Shanghai	2013	31°30'N	121°57'E	SM	*Spartina* sp.	50	30	45	Zhang et al. (2017)
	2013			SM	*Phragmites* sp.	50	23	61	
	2013			B	Bare	50	3	5	
	2015	31°27'N	122°00'E	SM	*Spartina* sp.	50	9	18	Chen et al. (2017)
	2007	31°00'N	121°55'E	SM	*Phragmites* sp.	100	54	54	Bu et al. (2015)

[a]SM: Salt marsh, B: Bare tidal flat
[b]Organic carbon stock normalized to the amount for 1 m depth

Table 3.14.
Results of the review on net primary production (NPP) on salt marshes, mangroves, seagrasses, and bare tidal flats of coastal ecosystems.

Habitat	Location	Net Primary Production ($g\ C\ m^{-2}\ yr^{-1}$)	Global area (km^2)	Global NPP ($Tg\ C\ yr^{-1}$)	Reference
Salt marshes	Global	1,100	22,000–400,000	20–440	Duarte et al. (2013)
	Global	1,585	300,000	475	Algoni (2014)
Mangroves	Global	1,000	137,760–152,361	140-150	Duarte et al. (2013)
	Global	652	140,000	90	Algoni (2014)
Seagrasses	Global	817	177,000–600,000	140-490	Duarte et al. (2013)
	Global	1,211	400,000	533	Algoni (2014)
Bare tidal flats	Global		128,000	11	Lin et al. (2020)
	Global		124,286–131,821		Murray et al. (2019)
	South Korea	217			Kwon et al. (2020)
	South Korea	312			Kwon et al. (2018)

CHAPTER 4.

THE EFFECT OF EXOTIC *S. ALTERNIFLORA* INVASION ON BENTHIC ENVIRONMENTS ACROSS THE COASTAL AREAS OF THE YELLOW SEA

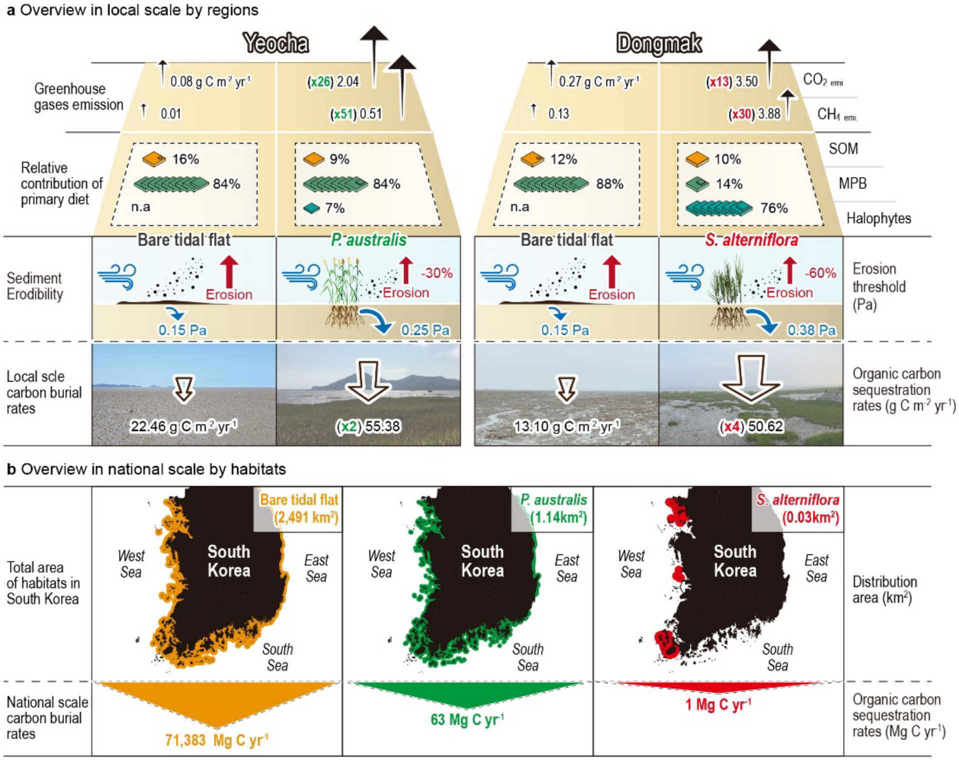

This chapter is in preparation.

4.1. Introduction

The introduction of exotic plants to salt marshes in coastal ecosystems alters the structure of the vegetation community and biotic interactions (Yang et al., 2017). In 1979, *Spartina alterniflora* was first introduced from North America to coastal areas in the Yellow Sea for ecological engineering purposes (e.g., control of coastal erosion and stabilization of sediments) (Wan et al., 2009; Qiu, 2013). Over the last four decades, the coastal area supporting *S. alterniflora* habitats in the Yellow Sea has continuously expanded, and now covers over 54,000 ha (Figure 4.1). Due to its high primary production, propagation capability, and resistance to extreme tidal condition, the invasion of *S. alterniflora* has had both positive (e.g., CO_2 fixation, nutrient absorption, and coastal erosion control) and negative (e.g., native species niche occupation, biodiversity diminishment, and aquaculture damage) effects on the coastal ecosystem (Wan et al., 2009; Rout and Callaway, 2009).

As exotic *S. alterniflora* habitats expanded, it replaced native C_3 halophyte (*Phragmites australis*, *Suaeda glauca* and *Scirpus planiculmis*) habitats and bare tidal flats in the Yellow Sea (Liu et al., 2018). This phenomenon could be related to elevated temperature in coastal regions along the Yellow Sea. For instance, the photosynthesis efficiency of C_3 plants declines with increasing temperature; however, this phenomenon does not apply to C_4 plants (Hovenden and Newton, 2018). This is because C_4 plants (unlike C_3 plants) are already adapted to relatively high temperatures, and are more tolerant of heat stress (Sage and Kubien, 2003). Consequently, C_4 plants respond to warming in a way that promotes faster canopy growth and root proliferation compared to C_3 plants (Chuine et al., 2012). Thus, it is necessary to identify the elevated temperature which contributes to the rapid spread of *S. alterniflora* through long-term temperature monitoring in the Yellow Sea.

Although plant invasion enhances carbon accumulation in sediments, due to higher net photosynthetic rates and longer growing seasons, the effects of such invasions on the dynamics of sedimentary carbon are subject to debate (Liao et al., 2008). For instance, several studies indicated that the introduction of exotic *S. alterniflora* increases organic carbon sequestration in invaded ecosystems in the

Yellow Sea (Yang et al., 2013; Yang et al., 2017). Yet, *S. alterniflora* invasion also enhances methane (CH_4) emission, one of the main greenhouse gases, because it contributes more to methylotrophic methanogenesis (Yuan et al., 2015; 2019; Kim et al., 2020). Therefore, it is important to quantify how *S. alterniflora* invasion affects sedimentary carbon dynamics to predict coastal carbon cycling under climate change.

In 2016, the Korea Ministry of Oceans and Fisheries (MOF) listed *S. alterniflora* as harmful invasive species (MOF and KOEM, 2019), because it was reported to cause unexpected side effects such as diminishing biodiversity and displacing native halophytes (Wang et al., 2006; Wan et al., 2009). Consequently, an eradication program was initiated in 2017 to reduce *S. alterniflora* habitats and prevent their further spread in Ganghwa, South Korea (MOF and KOEM, 2019). However, the rapid eradication of invasive *S. alterniflora* leads to negative impacts on ecosystems if native organisms use these invaders as a resource (Buckley and Han, 2014). For instance, after *S. alterniflora* eradication in San Francisco Bay (USA), the number of endangered California clapper rail (*Rallus longirostris obsoletus*) declined, along with the slow recovery of native plants (*Spartina foliosa*) (Buckley and Han, 2014; Lampert et 2014). Therefore, it is important to understand how *S. alterniflora* invasion affects coastal ecosystems from multiple perspectives.

Here, we first assessed the effects of *S. alterniflora* invasion using multi-perspective approaches in the Yellow Sea. Specifically, we: (1) verified that the temperature of coastal areas in the Yellow Sea has risen; (2) investigated the effect of *S. alterniflora* invasion on sedimentary organic carbon; (3) elucidated the effect of *S. alterniflora* eradication on communities of *S. alterniflora* and macrobenthos; and (4) compared ecological functions among bare tidal flats, native *P. australis* habitats, and invasive *S. alterniflora* habitats.

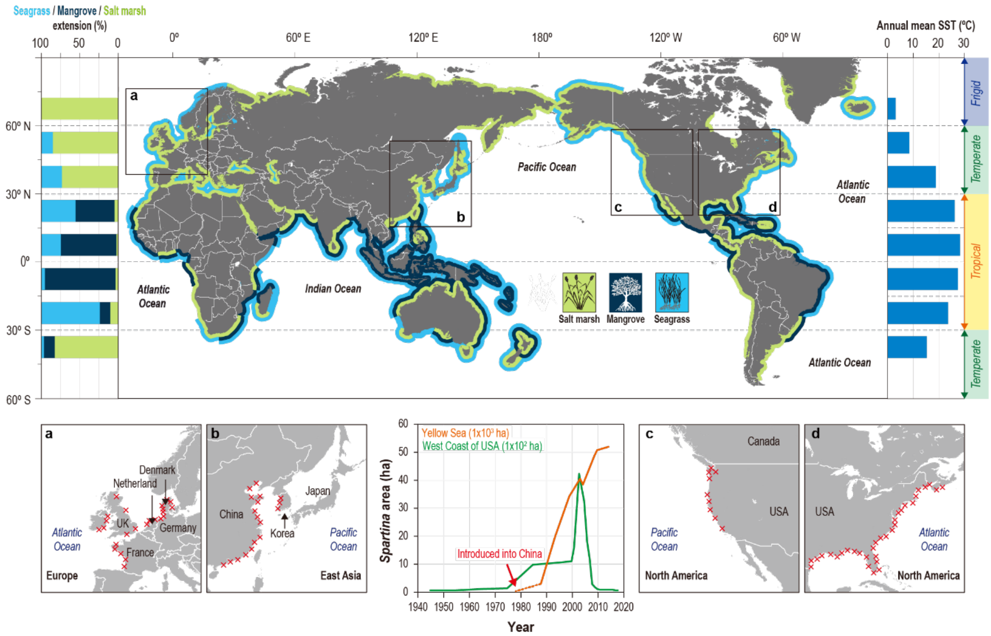

Figure 4.1.
Global-scale distribution of salt marshes, mangroves, seagrasses, and *Spartina alterniflora* along the coastal areas. Bottom insets (a-d), *Spartina alterniflora* distribution in the four representative sub-regions; (a) western Europe, (b) East Asia, (c) western North America, and (d) eastern North America. Middle of bottom, temporal variation of *Spartina* spp. area (ha) in Yellow Sea (1 x 10^3 ha, red line) and West Coast of USA (1 x 10^2 ha, green line), respectively.

4.2. Materials and methods

4.2.1. Data packages

This study assessed the effect of exotic *S. alterniflora* invasion on benthic environments across the coastal areas of the Yellow Sea. Six data sets (Data sets I, II, III, IV, V, and VI) were used to evaluate certain parameters (Table 4.1). The distribution of temperature anomalies in the coastal regions of the Yellow Sea were examined using the first data package (Data set I). As part of the study, sedimentary organic carbon was investigated at Ganghwa, South Korea (Data set II). Communities of *S. alterniflora* and macrobenthos were investigated to assess the effect of eradicating *S. alterniflora* at Ganghwa (Data set III). Finally, meta-datasets (Data Set II, III, IV, V, and VI) were obtained to comparatively evaluate ecological functions in bare tidal flats, native *P. australis* marshes, and invasive *S. alterniflora* marshes.

Table 4.1.
Overview of the study design for this study, summarized by data packages with specifics progressive purposes from Data sets.

	Data Set I	Data Set II	Data Set III	Data Set IV	Data Set V	Data Set VI
Main subject with specific purposes	**Spatiotemporal comparison of air temperature anomaly**	**Spatial comparison of organic C stocks and sequestration rates**	**Charaterization of the effect of eradication on *S. alterniflora* and macrobenthos community**	**Comparison of CO_2 and CH_4 emission**	**Comparison of Relative contribution of primary diet**	**Comparison of Sediment erodibility**
Study area	**S-KOR** (3 regions) **CHN** (5 regions)	**S-KOR** (12 regions) **CHN** (9 regions)	**S-KOR** (1 region; Ganghwa)	**S-KOR** (1 region; Ganghwa)	**S-KOR** (1 region; Ganghwa)	**S-KOR** (1 region; Ganghwa)
Investigation period	**1980–2020**	**2017–2019**	**2017–2018**	**2018–2019**	**2018–2019**	**2018–2019**
Key parameters	**Temperature anomaly** (Air)	**TOC** (Sediment) **C/N ratio** (Sediment) **$\delta^{13}C$** (Sediment) **Organic C stocks** (Sediment) **Organic C sequestration rates** (Sediment)	**Stem length** (*S. alterniflora*) **Number of species** (Macrofauna) **Density** (*S. alterniflora* & Macrofauna) **Biomass** (*S. alterniflora* & Macrofauna)	**CO_2 emission** (Sediment) **CH_4 emission** (Sediment)	**$\delta^{13}C$** (Macrofauna, MPB, POM, SOM) **$\delta^{15}N$** (Macrofauna, MPB, POM, SOM)	**Erosion threshold** (Sediment)
Data presented	**Figure 4.2.**	**Figures. 4.2., 4.4. and 4.6.**	**Figure 4.5. and 4.6.**	**Figure 4.6.**	**Figure 4.6.**	**Figure 4.6.**
Reference	**This study**	**This study**	**This study**	**This study**	**This study**	**Ha et al. (2018); Seo et al. (2021)**

4.2.2. Air temperature anomaly

The instrumental data used in the study are Yellow Sea annually temperature anomalies starting from 1980 to 2020. This gridded data set with a horizontal resolution of 1° (in longitudinal direction) x 1° (in latitudinal direction) was developed and updated by the European Centre for Medium-Range Weather Forecasts based on ERA5 (Copernicus Climate Change Service C3S, 2020).

4.2.3. Sedimentary organic carbon stocks per unit area

Study areas included salt marshes and bare tidal flats of South Korea and China, from 2017–2018. To elucidate the quantity and geographic distribution of sedimentary organic carbon stocks in coastal regions, 12 and 8 regions were selected from South Korea and China, respectively. To compare organic carbon sequestration rates and carbon sources between native C_3 plant marshes (*P. australis* and S. *japonica*) and invasive C_4 plant marshes (*S. alterniflora*), we investigated tidal flats of Ganghwa, South Korea. To sample core sediments, both a cylindrical multisampler core (diameter = 5 cm) and a semi-cylindrical gouge auger core (diameter = 3 cm) were used depending on sediment substrates (e.g., mud and sand). Detailed information of organic carbon stocks of Koean coastal areas was presented in Table 3.1 (see Chapter 3).

We also conducted an extensive literature review of data on carbon that were available for salt marshes and bare tidal flats in the Yellow Sea of China. Sedimentary organic carbon stocks of China's coastal area were available from the published literature, encompassing bare tidal flats and salt marshes along the Yellow Sea, including the Liaohe Delta, Dongying port, Yellow River Estuary, Yancheng, Sheyang, Wanggang River Estuary, Chongming Island. Sediment depth for the reported organic carbon stocks ranged from 10 to 100 cm across studies; thus, organic carbon stocks were normalized to the amount within 1 m depth for all subsequent calculations. Detailed information of organic carbon stocks of Chinese coastal areas was presented in Table 3.13 (see Chapter 3).

All sediment samples were stored in plastic bags, and were subsequently transferred to the laboratory. Samples for TOC, TN, $\delta^{13}C$ and $\delta^{15}N$ analyses were freeze-dried, homogenized, and powdered using agate mortar. Sediments were decalcified with 10% HCl, washed twice with deionized water, and free dried for TOC and $\delta^{13}C$ determination. The TOC, TN, $\delta^{13}C$, and $\delta^{15}N$ were measured using an Elemental Analyzer-Isotope Ratio Mass Spectrometer (EA-IRMS) (Elementar, Gmbh, Hanau, Germany). All isotopic compositions were expressed as delta notation (‰) (Eq. 1):

$\delta^{13}C$ or $\delta^{15}N$ (‰) = [$R_{sample}/R_{reference} - 1$] × 1000

(1)

Where, R_{sample} and $R_{reference}$ are the composition ($^{13}C/^{12}C$) of the sample and reference, respectively. Isotopic compositions were reported relative to conventional reference materials; Vienna Peedee Belemnite (VPDB) for carbon and atmospheric N_2 for nitrogen. IAEA-N-2 (International Atomic Energy Agency (IAEA), Vienna, Austria) and IAEA-CH-3, were used as working standards to calculate the analytical error of carbon. Measurement precision was approximately 0.04‰ for $\delta^{13}C$ and 0.2‰ for $\delta^{15}N$. Calculation of age and sedimentation rates of core sediments were used constant rate of supply (CRS) model for the vertical profiles of excess ^{210}Pb activity (Appleby and Oldfieldz, 1983; Appleby, 2001; Sanchez-Cabeza and Ruiz- Fernández, 2012). Excess ^{210}Pb activity was calculated from the differences between the activity of supported and unsupported ^{210}Pb. Supported and unsupported ^{210}Pb activity was measured using gamma spectroscopy attached to a low background HPGe detector of the Korea Basic Science Institute (KBSI).

To calculate organic carbon stock per unit area in core sediment, we followed the standard method (Howard et al., 2014) (Eq. 2–3).

$$\text{Bulk density (g cm}^{-3}) = \frac{\text{Mass of dry sediment (g)}}{\text{Original volume sampled (cm}^{3})} \qquad (2)$$

$$\text{Organic carbon stocks (Mg C ha}^{-1}) \qquad (3)$$
$$= \text{Organic carbon content (g C g}^{-1}) \times \text{Bulk density (g cm}^{-3})$$
$$\times \text{ Sediment thickness interval (cm)} \times 0.01$$

Where 0.01 is the conversion factor (1 ha = 100,000,000 cm^2, 1 Mg = 1,000,000 g) to express unit (Mg C ha^{-1}), that commonly used in organic carbon stock assessment. The organic carbon sequestration rate was estimated using the following equation (Xiaonan et al., 2008; EI-Hussieny and Ismail, 2015) (Eq. 4).

Organic carbon sequestration rates (Mg C ha^{-1} yr^{-1}) (4)

$$= \text{Organic carbon content } (\text{g C g}^{-1}) \times \text{ Bulk density } (\text{g cm}^{-3}) \times \text{ sedimentation rate } (\text{cm yr}^{-1}) \times 0.01$$

Where organic carbon content (g C g^{-1}) and bulk density (g cm^{-3}) are average values in the core sediment profile. Also, we used a 0.01 conversion factor (1 ha = 100,000,000 cm^2) as commonly used unit (Mg C ha^{-1} yr^{-1}).

4.2.4. Benthic community after *S. alterniflora* eradication

To evaluate how *S. alterniflora* eradication affects the communities of *S. alterniflora* and macrobenthos, this experiment was conducted in *S. alterniflora* habitats in Ganghwa marsh. Three eradication methods were implemented, including mowing (Treatment 1), mowing plus tilling (Treatment 2), combined mowing and tilling together with the biological substitution of a native species *S. japonica* (Treatment 3). Adjacent bare tidal flats were also monitored as a control. All of the eradication treatments were implemented during November 2017. Observations of *S. alterniflora* growth and the sampling of the macrobenthos community were carried out once a month from April 2018 to December 2018. To determine the stem length of *S. alterniflora*, plant stems were measured from the base part of the stem to the top. To estimate the density and biomass of *S. alterniflora* habitats, plant stems were counted using 0.25 m^{-2} quadrats in each experimental site. To analyze macrofaunal assemblages, sediment samples were taken from the top 30 cm using a 154 cm^2 acrylic corer for each sampling interval at each experimental site. Sediment samples collected using an acrylic corer were sieved on site using a 1 mm mesh size. The sorted macrofauna samples were then fixed in 4% buffered formalin solution and preserved in 70% ethanol for species identification and counting. Taxa were identified to the species level using a dissecting microscope and an optical microscope, where necessary.

4.2.5. CO_2 and CH_4 emissions

To determine the annual emissions of CO_2 and CH_4 gases, year-round seasonal sampling was implemented from March 2018 to February 2019 in Ganghwa. We used the static chamber method and gas chromatography (CP-3800 Varian, USA) with a flame ionization detector (FID). PVC static chambers (diameter 30 cm, height 30 cm) were installed on the marsh surface and were allowed to stabilize for 1-h. Then, the chambers were closed, and gas samples were collected with a syringe. After the chambers were closed, 5mL gas vials were inserted at 0, 10, 20, and 30 min. CO_2 and CH_4 emissions were calculated from changes to gas concentration over time using the following equation;

$$\text{Gas emissions} = \frac{\text{dGas}}{\text{dt}} \times \frac{\text{V}}{\text{A}} \times \frac{273.15°\text{C} + \text{T}}{298.15°\text{C}}$$

where, dGas/dt is the concentration gradient of CO_2 or CH_4 over time (mg Gas m^{-3} hr^{-1}), V is the volume of the chamber (m^3), A is the bottom surface area of the chamber (m^2), and T is the temperature inside the chamber (°C).

4.2.6. Relatively contribution of primary diet

To estimate the influence of *S. alterniflora* invasion on ecosystem function, year-round seasonal sampling was conducted to analyze $\delta^{13}C$ and $\delta^{15}N$ (March 2018 to February 2019). Potential food sources and benthic consumers were collected from bare tidal flats, *P. australis* habitats, and *S. alterniflora* habitats at Ganghwa marsh. Pre-filtered particulate organic matter (POM) with a 100-μm mesh net was used to remove zooplankton, and was re-filtered with a pre-combusted (450 °C, 4 h) Whatman GF/F glass fiber filter. Microphytobenthos (MPB) mat and sedimentary organic matter (SOM) were collected from the surface sediment (0.5 cm), and were directly transferred to the laboratory to extract MPB following a previously described method (Couch, 1989). The collected leaves of *P. australis* and *S. alterniflora* were transferred to the laboratory and scraped with a razor blade to remove epibionts, and were rinsed with distilled water. A fine powder of POM, SOM, MPB, and halophytes was decalcified using HCl (24 h), and was freeze-dried to determine stable carbon isotope values. The muscle tissues of organisms were lyophilized, homogenized, and ground to a fine powder with a mortar and a pestle. The lipid was subsequently removed from samples using 10 *ml* dichloromethane/methanol (2:1, v/v). The mixture was sonicated (10 min) and centrifuged (2,000 rpm, 15 min) to discard the organic solvent three to five times, depending on lipid content. Lipid-free samples were placed under a stream of nitrogen gas until dry. All samples were weighed in a tin capsule and packed for further stable isotopic analysis.

4.2.7. Statistical analysis

Statistical analyses were performed using SPSS 23.0 (SPSS INC., Chicago, IL, USA), PRIMER 6 statistical software (PRIMER-E Ltd., Plymouth, UK). Pearson correlation analysis was used to test for significant relationships for: 1) temperature anomaly and year, and 2) organic carbon content and *S. alterniflora* invasion time. The organic carbon content of core sediments in Ganghwa were analyzed to test for differences between bare tidal flats and salt marshes (*P. australis*, *S. alterniflora*, and *S. japonica*) using a *t*-test. Stem length, density, and biomass of the *S. alterniflora* community were analyzed to test for differences among the three eradication treatments (T1, T2, and T3) using one-way analysis of variance (ANOVA) with Scheffe's post-hoc test. The same statistical method was used to test for differences in the number of species, density, and biomass of the macrobenthos community for T1, T2, T3, and bare tidal flats. Before the analysis, homogeneity of variance was determined between groups with Levene's homogeneity test, meeting the assumption of homogeneity of variance ($p < 0.05$). To characterize macrobenthos groups in the sampling areas, cluster analysis was performed with Bray-Curtis similarity. Non-metric multidimensional scaling (NMDS) was also used, based on the similarity matrix used for cluster analysis.

4.3. Results and discussion

4.3.1. Elevated temperature affecting the spread of *Spartina alterniflora* in the Yellow Sea

Annual and seasonal mean air temperature anomalies from 1980 to 2020 of eight coastal regions along the Yellow Sea were analyzed using the European Centre for Medium Range Weather Forecasts data (Figure 4.2a). The analysis revealed that the annual temperature anomaly had a significantly positive correlation with time in three regions (viz., Weifang, Cangzhou, and Jinzhou) in China ($p < 0.01$) and three regions (viz., Ganghwa, Jindo, and Jeju) in South Korea ($p < 0.01$), respectively. These results confirmed that annual air temperature increased between 1980 and 2020 due to global warming in the Yellow Sea. After *S. alterniflora* was first introduced 40 years ago, its coverage increased by over 54,000 in China (Figure 4.1). Higher temperatures could be correlated to the rapid spread of *S. alterniflora*, because C_4 halophytes (e.g., *S. alterniflora*) have relatively higher propagation ability and photosynthesis efficiency compared to C_3 halophytes (e.g., *P. australis*, *Suaeda japonica*) under warm conditions (Hovenden and Newton, 2018). C_4 halophytes respond to higher temperatures by promoting rapid canopy growth, root proliferation, and colonization of disturbed patches (Chuine et al., 2012).

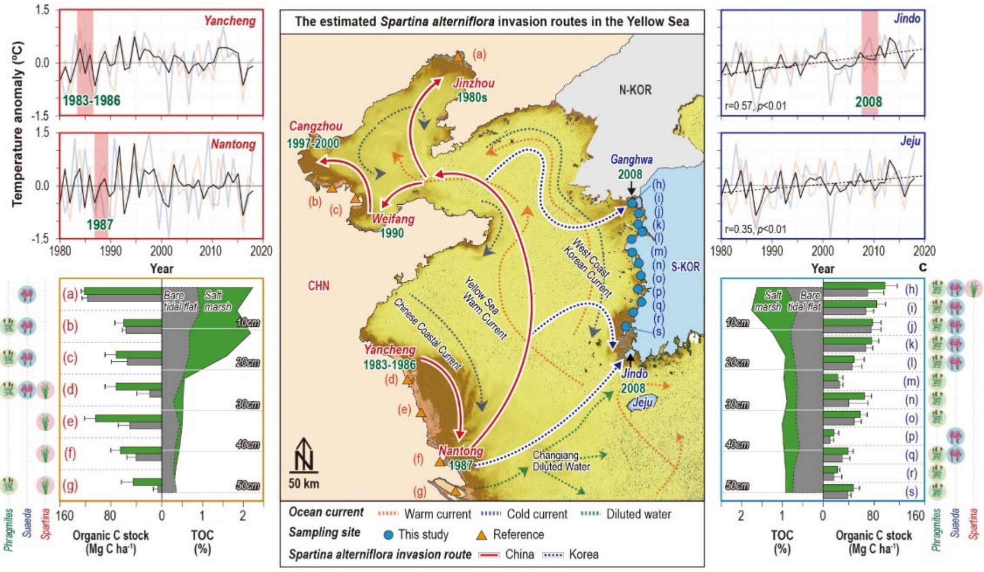

Figure 4.2.
Spatial distribution of temperature anomaly and sedimentary organic carbon stocks in the Yellow Sea. Map showing possible *S. alterniflora* invasion routes along the coasts of the Yellow Sea. (a) Temperature anomaly during 1980–2020 and year of *S. alterniflora* introduction in eight coastal regions of the Yellow Sea; China (n = 5) and South Korea (n = 3). The year of *S. alterniflora* introduction to China and South Korea was derived from previous studies (MOF and KOEM, 2019; Zhang et al., 2017). (b, c) Organic carbon stocks (Mg C ha^{-1}) (left in Figure 4.2b and right in Figure 4.2c) and vertical distribution of TOC (%) (right in Figure 4.2b and left in Figure 4.2c) in the core sediments (0–50 cm) of salt marshes and bare tidal flats along the coast of the Yellow Sea; China (n = 7) and South Korea (n = 12). Green and gray bars denote salt marsh and bare tidal flat, respectively.

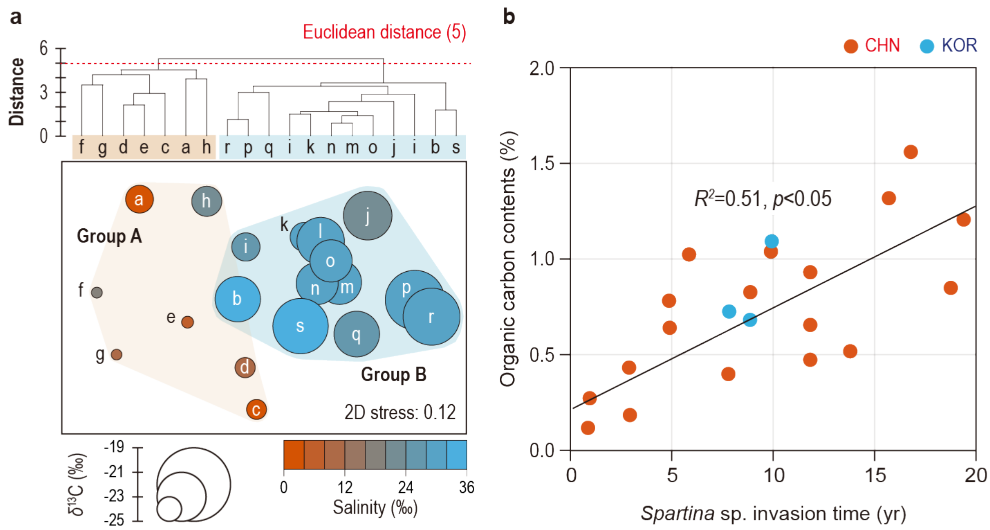

Figure 4.3.

Topographical and biological factors affecting complex dynamics of sedimentary organic carbon in the Yellow Sea. (a) Cluster analysis and non-metric multidimensional scaling (nMDS) ordination of environmental condition groups, (b) Relationships between *Spartina* invasion time and TOC in sediments.

Table 4.2.
Influence of *Spartina alterniflora* invasion time on the TOC contents in the 0-30 cm sediment layer in the Yellow Sea.

Location	Latitude	Longitude	Core depth (cm)	*Spartina* invasion year	TOC (%)	Reference
China						
Yancheng, Jiangsu	33°30'-33°40'N	120°30'-120°35'E	20	1	0.24	Mao et al. (2010)
				3	0.40	
				5	0.61	
				19	0.83	
	33°35'-33°38'N	120°30'-120°40'E	20	1	0.08	Wang et al. (2013)
				3	0.16	
				5	0.76	
				12	0.64	
	32°36'-34°28'N	119°51'-121°05'E	30	6	1.01	Yang et al. (2016b)
				10	1.03	
				17	1.56	
				20	1.19	
Sheyang, Jiangsu	33°30'00.0"N	120°38'00.0"E	30	9	0.81	Xiang et al. (2015)
				12	0.92	
				16	1.30	
Wanggang River estuary, Jiangsu	33°08'-33°10'N	120°45'-120°50'E	10	8	0.37	Zhang et al. (2010)
				12	0.45	
				14	0.49	
Korea						
Ganghwa, Incheon	37˚35'42.58"N	126˚27'48.28"E	30	8	0.68	This study
				9	0.67	
				10	1.07	

4.3.2. Effects of *Spartina alterniflora* invasion on sedimentary organic carbon

Data on sedimentary organic carbon stock per unit in the 19 coastal regions generally indicated a varied spatial distribution in the Yellow Sea (Figure 4.2b; c). The results showed that, for South Korea, organic carbon stocks ranged from 1 to 145 Mg C ha^{-1} (mean: 47 Mg C ha^{-1}) in bare tidal flats and 4 to 161 Mg C ha^{-1} (mean: 53 Mg C ha^{-1}) in salt marshes. For China, organic carbon stocks ranged 5 to 116 Mg C ha^{-1} (mean: 39 Mg C ha^{-1}) in bare tidal flats and 18 to 170 Mg C ha^{-1} (mean: 76 Mg C ha^{-1}) in salt marshes. Overall, sedimentary organic stocks were generally higher in the salt marshes of China compared to South Korea. Thus, caution is required to evaluate different rates of increase for organic carbon stocks in the sediment of salt marshes in China and South Korea.

In the coastal salt marshes of China, three species of halophytes (*P. australis*, *S. alterniflora*, and *Suaeda salsa*) dominated the vegetation. In contrast, *P. australis* and *S. japonica* were the dominant halophytes in the coastal areas of South Korea, and only *S. alterniflora* was present in Ganghwa and Jindo. Organic carbon sequestration rates in sediments of *S. alterniflora* habitats were 2.63 to 8.78 times higher compared to those of native halophyte habitats (e.g., *P. australis* and *S. salsa*) in Yancheng National Nature Reserve, China (Yuan et al., 2015). Furthermore, data collected from previous and present studies indicated significant relationship between the year of *S. alterniflora* invasion and organic carbon content in sediments ($R^2 = 0.51$, $p < 0.05$, $n = 20$) (Figure 4.3 and Table 4.2). Therefore, the species composition of halophytes contributed to different rates of organic carbon sequestration in the intertidal flats of the Yellow Sea.

After *S. alterniflora* was first introduced to China for ecological engineering purposes in 1979, habitats of this species were first observed in Ganghwa and Jindo of South Korea in 2008 (Figure 4.2) (MOF and KOEM, 2019). After one decade of *S. alterniflora* invasion, several studies reported a 59-fold increase in the coverage of *S. alterniflora* habitats (from 0.05 to 3.12 ha) in Ganghwa, South Korea (Figure 4.4a, b, and Table 4.3). To examine the effect of halophyte species, changes to the rate of organic carbon stocks in three halophyte habitats (*P. australis*, *S.*

alterniflora, and *S. japonica*) was compared to bare tidal flats using transect surveys in Ganghwa. Our results showed that *P. australis* habitats had the highest rate of increase in organic carbon stocks (2.0 times) at the 0–50 cm core sediment depth, followed by *S. alterniflora* habitats (1.9 times) and *S. japonica* habitats (1.6 times), respectively (Figure 4.4c). However, within 0–10 cm depth, *S. alterniflora* habitats had the highest rate of increase in organic carbon stocks (3.4 times), followed by *S. japonica* (2.5 times) and *P. australis* (2.4 times) habitats. Interestingly, our core sediment age dating results by ^{210}Pb analysis showed that 10 cm depth of sediments in Ganghwa was estimated to be 2007 (Figure 4.4c and Table 4.4), which corresponded to the timing of *S. alterniflora* invasion. Thus, invasive C_4 halophytes (*S. alterniflora*) cause a clear increase in sedimentary organic carbon compared to native C_3 halophytes (*P. australis* and *S. japonica*) over the same period. Several studies recently documented that, compared to native C_3 halophytes, *S. alterniflora* contributes to higher carbon accumulation in sediment, due to its greater root biomass, longer growing season, and higher net primary production (Yang et al., 2013; Yang et al., 2017). Thus, *S. alterniflora* invasions could enhance sedimentary organic carbon by changing biogeochemical processes in the coastal regions of the Yellow Sea.

To examine temporal variability in the sources of sedimentary organic carbon, we selected the Yancheng and Ganghwa marshes, which support all three halophytes species (Figure 4.4d). The sediments of both salt marshes in the two regions had relatively higher C/N ratios compared to bare tidal flats, due to the accumulation of carbon-rich organic matter through the decomposition of vascular plants (Lamb et al., 2006). Typical $\delta^{13}C$ of C_3 and C_4 halophyte habitats in sediments were reported to range from -27.0 ‰ to -22.0 ‰ and -18.9 ‰ to -15.8 ‰, reflecting different photosynthetic pathways (Kemp et al., 2012). In the Yacheng and Ganghwa marshes, *P. australis*, *S. salsa,* and *S. japonica* habitats had a signature of C_3 halophyte derived organic carbon, with $\delta^{13}C$ values ranging from -25.0‰ to -23.2‰ (mean: -23.9 ‰) (Figure 4.4d and Table 4.5). Interestingly, *S. alterniflora* habitats in Yancheng during the early invasion stage (1–3 years) represented the origin of C_3 halophyte derived organic carbon, with $\delta^{13}C$ values ranging from -23.2 ‰ to -22.5 ‰ (mean: -22.9 ‰). In contrast, *S. alterniflora* habitats, which invaded over a six-year period, had C_4 halophyte origin with $\delta^{13}C$ values ranging from -18.8 ‰ to -17.5 ‰ (mean: -18.2 ‰). Similarly, the $\delta^{13}C$ values measured in the *S. alterniflora* habitats of Ganghwa, which invaded over a 10-year period, ranged from -19.7 ‰ to -21.2 ‰ (mean: -20.4 ‰). Thus, the origin of sedimentary organic carbon changed from C_3 to C_4 halophyte habitats in parallel with the invasion time of *S. alterniflora* in the coastal regions of the Yellow Sea. Overall, our analysis demonstrated that the distribution and origin of sedimentary organic carbon changed in parallel with the invasion time of *S. alterniflora* in the coastal regions of the Yellow Sea.

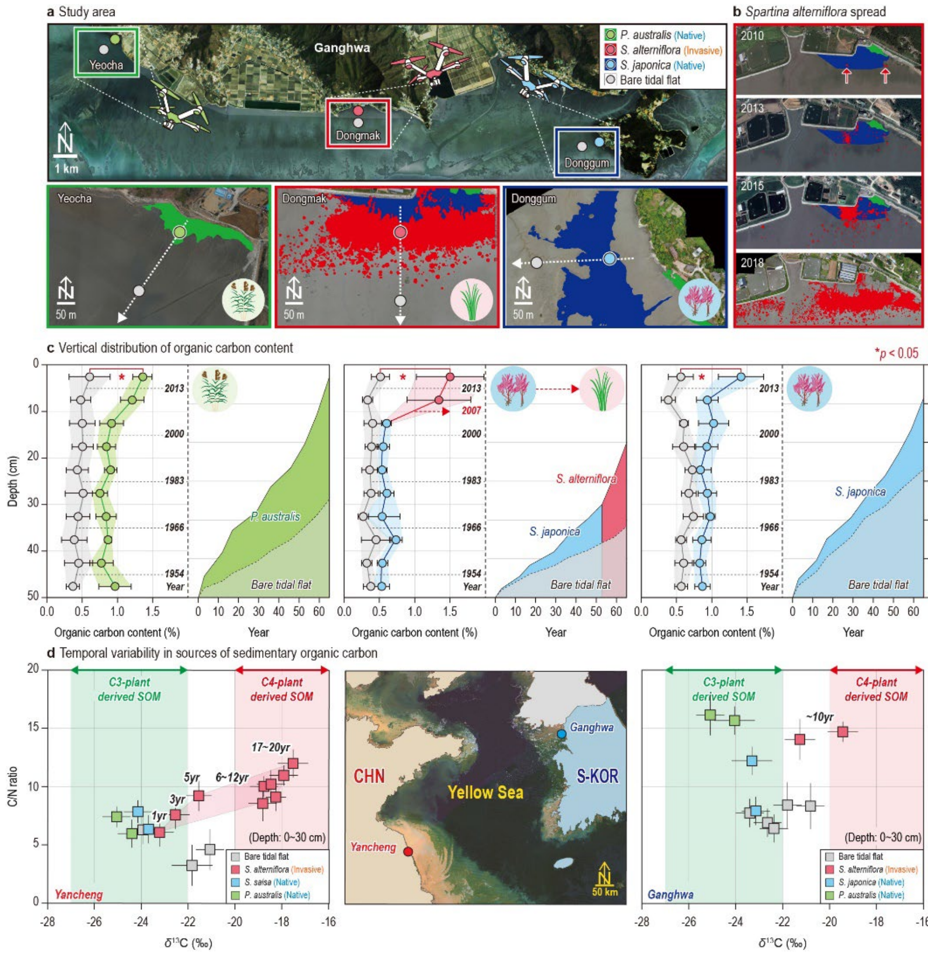

Figure 4.4.
The effect of exotic *Spartina alterniflora* on sedimentary organic carbon in Ganghwa, South Korea. (a) Transect survey of three different halophytes (*P. australis*, *S. alterniflora*, and *S. japonica*) marshes compared to each bare tidal flat in Yeocha, Dongmak, and Donggum, respectively. One transects line consisted of two locations; one location in salt marsh and another location in bare tidal flat (b) *S. alterniflora* spread after the invasion from 2008. (c) Vertical distribution of TOC in core sediments (0–50 cm) (line with shade: mean ± s.d.). (d) Temporal variability in distribution and sources of TOC in core sediments (0–30 cm): A comparative study of China (Yancheng) and South Korea (Ganghwa).

Table 4.3.

The area of three species halophytes species in Yancheng and Ganghwa.

Location	Sampling year	Habitat	Area		Aboveground biomass	Belowground biomass	Reference
			(m^2)	(ha)	($g\ m^{-2}$)	($g\ m^{-2}$)	
China							
Yancheng	2011	*Phragmites australis*	606,000	61	-	-	Zhang et al. (2019)
	2012		-	-	920	2,536	Yang et al. (2015)
	2012		-	-	97	1,763	Yang et al. (2016b)
	2011	*Suaeda salsa*	192,300	19	-	-	Zhang et al. (2019)
	2012		-	-	427	1,128	Yang et al. (2015)
	2012		-	-	106	1,128	Yang et al. (2016b)
	2011	*Spartina alterniflora* (Total)	458,000	46	-	-	Zhang et al. (2019)
	2012	*Spartina alterniflora* (6yr)	-	-	1,777	5,530	Yang et al. (2017)
	2012	*Spartina alterniflora* (10yr)	-	-	1,493	5,808	Yang et al. (2015)
	2012	*Spartina alterniflora* (10yr)	-	-	426	5,808	Yang et al. (2016b)
	2012	*Spartina alterniflora* (10yr)	-	-	1,845	5,808	Yang et al. (2017)
	2012	*Spartina alterniflora* (17yr)	-	-	3,009	5,291	Yang et al. (2017)
	2012	*Spartina alterniflora* (20yr)	-	-	2,330	5,435	Yang et al. (2017)
Korea							
Ganghwa (Yeochari)	2017	*Phragmites australis*	n.a	n.a	1,011	239	This study
	2018		4,776	0	1,716	798	KOEM (2019)
Ganghwa (Donggum)	2017	*Suaeda japonica*	n.a	n.a	478	100	This study
	2018		268,251	27	112	18	KOEM (2019)
Ganghwa (Dongmak)	2008	*Spartina alterniflora* (1yr)	480	0	n.a	n.a	
	2010	*Spartina alterniflora* (3yr)	617	0	n.a	n.a	
	2013	*Spartina alterniflora* (6yr)	3,063	0	n.a	n.a	
	2015	*Spartina alterniflora* (8yr)	12,166	1	4,915	2,055	
	2017	*Spartina alterniflora* (10yr)	22,282	2	n.a	n.a	KOEM (2019)
	2018	*Spartina alterniflora* (11yr)	31,180	3	8,773	3,146	
	2019	*Spartina alterniflora* (12yr)	29,472	3	5,045	1,331	

Table 4.4.
Vertical distribution of excess ^{210}Pb and analysis data using CRS model to calculate the age of core sediment of Ganghwa.

Depth (cm)	Total ^{210}Pb (mBq g^{-1})	Total ^{226}Ra (mBq g^{-1})	Excess ^{210}Pb (mBq g^{-1})	Mass flux (g cm^{-2})	Inventory Excess ^{210}Pb (mBq g^{-1})	Excess ^{210}Pb (sum) (mBq cm^{-2})	Estimated year	Date (year)
0-5	59.4±5.1	43.9±0.7	15.6	5.6	87.8	87.8	6	2013
5-10	44.1±4.3	32.6±0.6	11.6	5.8	66.5	154.3	12	2007
10-15	46.2±4.8	33.7±0.7	12.6	5.4	67.2	221.5	19	2000
15-20	43.1±3.7	29.2±0.5	13.9	5.7	78.9	300.5	29	1990
20-25	39.5±2.8	31.8±0.4	7.7	5.5	42.3	342.7	36	1983
25-30	38.1±2.8	29.9±0.4	8.2	6.1	49.8	392.5	48	1971
30-35	34.3±3.9	31.6±0.5	2.7	5.3	14.0	406.6	53	1966
35-40	35.8±3.9	30.9±0.5	4.9	5.3	26.1	432.7	62	1957
40-45	31.4±2.2	30.2±0.3	1.2	5.2	6.2	438.9	65	1954
45-50	46.9±4.3	29.0±0.6	17.9	3.7	66.0	505.0		

Table 4.5.
C/N ratio and $\delta^{13}C$ measured within 0–30 cm depth in core sediments at Yancheng, Jiangsu.

Location	Latitude	Longitude	Habitat	Invasion time	Core depth (cm)	C/N	$\delta^{13}C$ (‰)	Reference
Yancheng	32°36'-34°28'N	119°51'-121°05'E	Bare tidal flats	-	30	3.05	-21.74	Yang et al. (2015)
				-	30	4.36	-21.11	Yang et al. (2016a)
				-	30	4.36	-21.11	Yang et al. (2017)
				-	20	5.89	-23.93	Wang et al. (2013)
			Phragmites australis	-	30	5.73	-24.32	Yang et al. (2015)
				-	30	7.11	-24.97	Yang et al. (2016a)
			Suaeda salsa	-	30	6.01	-23.69	Yang et al. (2015)
				-	30	7.36	-24.10	Yang et al. (2016a)
			Spartina alterniflora	1	20	5.80	-23.24	Wang et al. (2013)
				3	20	7.11	-22.47	
				5	20	8.80	-21.53	
				6	30	9.69	-18.75	Yang et al. (2017)
				10	30	8.36	-18.77	Yang et al. (2015)
				10	30	9.96	-18.41	Yang et al. (2016a)
				10	30	9.95	-18.41	Yang et al. (2017)
				12	20	8.73	-18.25	Wang et al. (2013)
				17	30	11.47	-17.54	Yang et al. (2017)
				20	30	10.51	-17.94	

4.3.3. Effect of eradication on *Spartina alterniflora* and macrobenthos community

We investigated the communities of *S. alterniflora* and macrobenthos after applying three different physical eradication treatments. The three treatments were: Treatment 1: Mowing only; Treatment 2: Mowing plus tilling; and Treatment 3: Mowing plus tilling together and biological substitution with a native species *S. japonica* (Figure 4.5a, b). Many eradication efforts, including physical and chemical treatments, have been implemented to control *S. alterniflora* habitats, because of their strong adaptability and rapid expansion (Sheng et al., 2014). However, chemical treatments (such as herbicides) might negatively impact the biomass of organisms in marine ecosystems (Relyea, 2005). Thus, physical eradication tends to be preferentially used to control *S. alterniflora* populations (Li and Zhang, 2008).

After eradication treatment, all *S. alterniflora* populations began to sprout during May of the following year, and the maximum growing season was between September and October (Figure 4.5c). The results showed that Treatment 2 and 3 significantly inhibited stem length and the density of *S. alterniflora* compared to the Treatment 1 ($p < 0.05$). Moreover, Treatment 3 was more effective at reducing the stem length of *S. alterniflora* compared to Treatment 2 ($p < 0.05$). Compared to Treatment 1, the biomass of *S. alterniflora* was relatively low in Treatment 2 and 3; however, this difference was not significant ($p > 0.05$). Thus, the biological substitution treatment (transplanting *S. japonica* into the plots pretreated with mowing plus tilling) seemed to be the most effective at inhibiting the growth of *S. alterniflora* habitats over a one-year period. Previously, biological substitution with a native species (*P. australis*) was more effective than other physical disturbance treatments (e.g., mowing and tilling) at controlling the invasion of *S. alterniflora* habitats in Chongming Dongtan Nature Reserve, China (Li and Zhang, 2008). The present study was the first to demonstrate the effectiveness of transplanting *S. japonica* (instead of *P. australis)* to suppress the growth of *S. alterniflora* habitats.

To identify the effects of eradication treatments on the macrobenthos community, we observed the number of species, density, and biomass of macrobenthos (Figure 4.5d). There was no significant difference ($p > 0.05$) in the number of species, density, and biomass of macrobenthos among Treatments 1, 2, 3, and bare tidal flat. Cluster analysis and nMDS were performed to delineate the macrobenthos groups. Three groups (Group I, II, and III) were separated with respect to: (1) eradication treatment and (2) season (Figure 4.5e; f). First, Group I represented Treatment 1 in spring and summer. Group II encompassed Treatment 2, 3, and bare tidal flats, which mostly included summer and fall. Group III also encompassed two eradication treatments (Treatment 2–3) and bare tidal flats, and was mostly represented by spring. *Perinereis linea* was the most dominant species in Group I, and its abundance was recently reported to increase following *S. alterniflora* invasion in Ganghwa, Korea (Shin et al., 2021). *Heteromastus filiformis* dominated Group II, and was previously reported to be widely distributed across the west coasts of South Korea (Park et al., 2014). There was no significant difference in the biodiversity of macrobenthos between *S. alterniflora* habitats in which eradication treatments were applied and bare tidal flats, when considering the number of species, density, and biomass. Of note, the species composition of *S. alterniflora* habitats, in which eradication treatments of tilling and biological substitution were applied, changed to be similar to bare tidal flats. Therefore, eradication treatment seemed to have no negative impacts on the biodiversity of macrobenthos in *S. alterniflora* habitats; however, continuous long-term monitoring is required to manage *S. alterniflora* appropriately in the future.

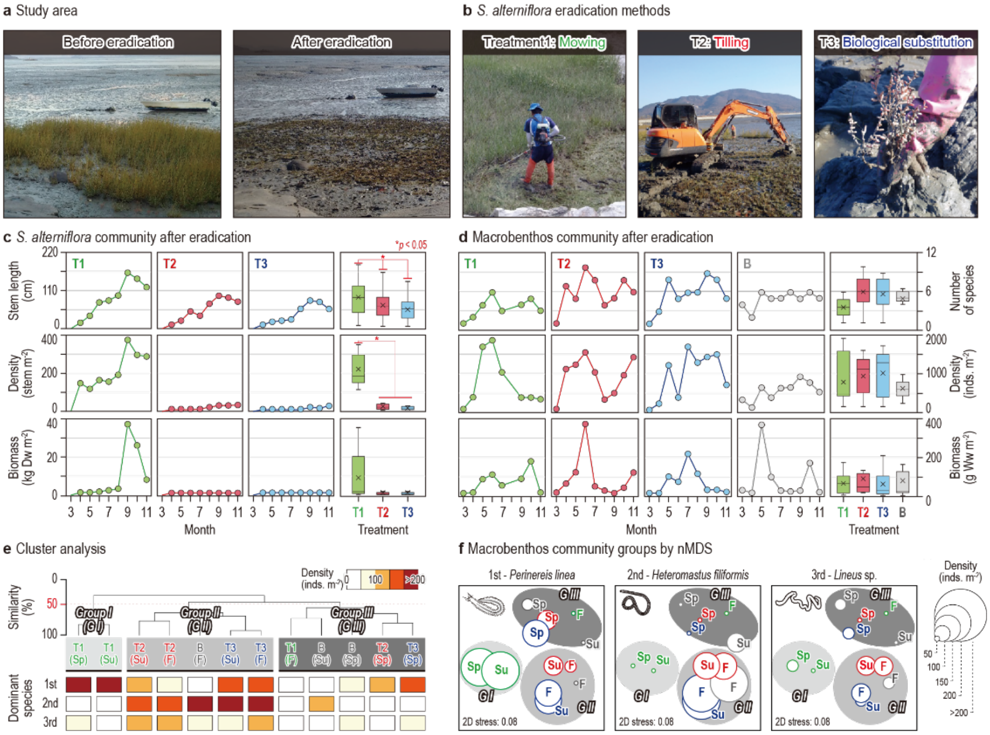

Figure 4.5.

Effect of exotic *Spartina alterniflora* on sedimentary organic carbon in Ganghwa, South Korea. (a) Transect survey of the habitat of three halophyte species (*P. australis*, *S. alterniflora*, and *S. japonica*) compared to bare tidal flats in Yeocha, Dongmak, and Donggum, respectively. One transect line consisted of two locations; specifically, one location in a salt marsh and one location in a bare tidal flat. (b) Spread of *S. alterniflora* following initial invasion in 2008. (c) Vertical distribution of TOC in core sediments (0–50 cm) (line with shading: mean ± s.d.). (d) Temporal variability in the distribution and sources of TOC in the core sediments (0–30 cm) at representative sites in China (Yancheng) and South Korea (Ganghwa).

4.3.4. Comparison of ecological functions among bare tidal flats, native *Phragmites australis*, and invasive *Spartina alterniflora*

To compare ecological functions of bare tidal flats, native *P. australis* marshes, and invasive *S. alterniflora* marshes in intertidal environments, we used four data packages (Data set II–III, V–VI) (Table 4.1). First, the results of greenhouse gases emissions indicated that *S. alterniflora* habitats had the highest CO_2 and CH_4 emissions (3.50 ± 0.32 and 3.88 ± 0.37 g C m^{-2} yr^{-1}), followed by *P. australis* habitats (2.04 ± 0.10 and 0.50 ± 0.01 g C m^{-2} yr^{-1}), and bare tidal flats of Dongmak (0.27 ± 0.13 and 0.13 ± 0.02 g C m^{-2} yr^{-1}) and Yeocha (0.08 ± 0.01 and 0.01 ± 0.00 g C m^{-2} yr^{-1}) (Figure 4.6a). However, when considering how rates had increased compared to bare tidal flats in each region, *P. australis* habitats had higher rates of increased emissions for CO_2 and CH_4 (26 and 51 times) compared to *S. alterniflora* habitats (13 and 30 times). The effects of plant invasion on the emission of greenhouse gases are under debate. Several studies reported that the CO_2 and CH_4 emissions of *S. alterniflora* were higher compared to *P. australis* in Jiangsu, China (Cheng et al., 2007; Yuan et al., 2015). In contrast, the emissions of the two species did not differ in New England, USA (Emery and Fulweiler, 2014). These contrasting results might be attributed to different vegetation biomass (Cheng et al., 2007), soil microbial community (Chen et al., 2012), and methanogenic activity (Kim et al., 2020).

The relative dietary contribution to macrobenthos indicated that microphytobenthos (MPB) had the highest contribution out of all food sources in the *P. australis* habitats ($84 \pm 11\%$) and bare tidal flats of Yeocha ($84 \pm 10\%$) and Dongmak ($88 \pm 9\%$) (Table 4.6). In comparison, halophytes had the highest contribution in *S. alterniflora* habitats ($76 \pm 4\%$). MPB was a major diet for primary consumers in bare tidal flats and native halophyte habitats, supporting previous results in Ganghwa, South Korea (Lee et al., 2021a). Our results showed that invasive *S. alterniflora* might represent a new food source for native macrobenthic fauna. Specifically, the appearance of invasive *S. alterniflora* has altered the diets of native macrobenthos, with it becoming a primary food source (Chen et al., 2018). These data demonstrate that invasive plants can contribute to the diet of native consumers and change their diet patterns.

The results indicated that erosion threshold of sediment was the highest in *P. australis* habitats (0.20–0.45 Pa), followed by *S. alterniflora* habitats (0.10–0.45 Pa) and bare tidal flats of Yeocha (0.10–0.45 Pa) and Dongmak (0.05–0.20 Pa). Considering how rates had increased compared to bare tidal flats in each region, *S. alterniflora* had relative higher rates of increased erosion threshold than *P. australis*. The presence of vegetation in tidal flats reduced water flow from wave action and turbulence and, hence, contributed to protecting sediments (Ha et al., 2018). Moreover, previous studies documented that *S. alterniflora* induced lower sediment erosion than *P. australis* due to higher vegetation density and biomass (Leonard and Croft, 2006; Rahman, 2015). Thus, the highest erosion threshold of *S. alterniflora* habitats seemed to reflect their high above- and belowground biomass, particularly in Ganghwa tidal flats (Table 4.3).

The results of carbon burial rates in Ganghwa showed that *P. australis* habitats had the highest organic carbon sequestration rate (55.38 ± 12.31 g C m^{-2} yr^{-1}), followed by *S. alterniflora* habitats (50.62 ± 21.47 g C m^{-2} yr^{-1}), and the bare tidal flats of Yeocha (22.46 ± 5.22 g C m^{-2} yr^{-1}) and Dongmak (13.10 ± 4.88 g C m^{-2} yr^{-1}). Interestingly, the higher carbon sequestration rates of *P. australis* and *S. alterniflora* habitats showed the opposite trend for greenhouse gases emission data. The carbon sequestration rates were relatively higher for *S. alterniflora* habitats (4 times) compared to *P. australis* habitats (2 times). This higher carbon accumulation in *S. alterniflora* marshes reflected the greater biomass and higher primary productivity of *S. alterniflora* compared to *P. australis* habitats (Yang et al., 2013; Yang et al., 2017).

Overall, invasive *S. alterniflora* marshes could provide various advantages to ecosystems with respect to greenhouse gas emissions, food web, sediment erodibility, and carbon burial compared to native environments. However, the distribution area of *S. alterniflora* marshes is not extensive, and does not appear to have a significant impact on the coastal areas of South Korea. Of note, the rapid eradication program, which was initiated in 2017 by MOF, accelerated the reduction in the distribution area of *S. alterniflora* habitats in South Korea (MOF and KOEM, 2019). Therefore, when considering the positive effects of *S. alterniflora* invasion on coastal environments (Table 4.9), the ecological role of *S. alterniflora* should be assessed holistically.

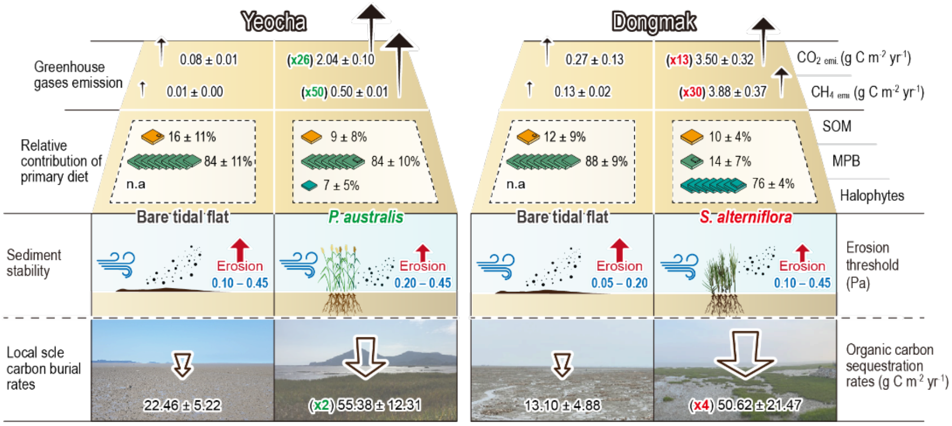

Figure 4.6.
Comparison of ecological functions among bare tidal flats, native *Phragmites australis*, and invasive *Spartina alterniflora*. (a) Overview in local scale by regions (Yeocha and Dongmak) with greenhouse gases emission, relative contribution of primary diet, sediment erodibility, and carbon burial. Black arrows indicate the emissions of CO_2 and CH_4. Yellow, green, and cyan diamonds denote the dietary contribution of SOM, MPB, and halophyte, respectively. Blue arrows denote erosion threshold (Pa). Red arrows denote erosion rates compared to bare tidal flat.

Table 4.6.
The relative contribution of four potential food sources (SOM, MPB, *Phragmites australis*, *Spartina alterniflora*) to the benthic organisms in Ganghwa island, based on stable carbon and nitrogen isotopic signatures. Contributions are reported as means with standard deviations (mean ± SD).

Location	**Halophyte species**	**Food source**			
		SOM	**MPB**	***Phragmites australis***	***Spartina alterniflora***
Korea					
Ganghwa (Yeochari)	Bare tidal flat	0.16 ± 0.11	**0.84 ± 0.11**	-	-
	Phragmites australis	0.09 ± 0.08	**0.84 ± 0.10**	0.07 ± 0.05	-
Ganghwa (Dongmak)	Bare tidal flat	0.12 ± 0.09	**0.88 ± 0.09**	-	-
	Spartina alterniflora	0.10 ± 0.04	0.14 ± 0.07	-	**0.76 ± 0.04**

Table 4.7.
Erosion threshold for sediments in bare tidal flat, *Phragmites australis*, and *Spartina alterniflora* at Ganghwa, South Korea.

Location	Date (yyyy/mm)	Habitat	Erosion threshold (Pa)	Reference
Korea				
Ganghwa (Yeochari)	2017/04	Bare tidal flat	0.10–0.20	Ha et al. (2018)
	2017/12		0.30–0.45	
	2017/04	*Phragmites australis*	0.20–0.30	
	2017/12		0.30–0.45	
Ganghwa (Dongmak)	2020/05	Bare tidal flat	0.10–0.20	Seo et al. (2021)
	2020/11		0.05–0.10	
	2020/05	*Spartina alterniflora*	0.30–0.45	
	2020/11		0.10–0.20	

Table 4.8.
Total area of bare tidal flats, *Phragmites australis* marshes, and *Spartina alterniflora* marshes in South Korea.

Location	Sampling year	Distribution area			Reference
		(m^2)	(km^2)	(ha)	
Korea					
Bare tidal flat	2021	2,490,725,921	2,491	249,073	Lee et al. (2021)
Phragmites australis	2017–2018	1,135,546	1.14	114	Lee et al. (2019)
Spartina alterniflora	2019	29,668	0.03	3	MOF and KOEM (2019)

Table 4.9
The positive and negative effects by *Spartina alterniflora* invasion in coastal environments.

Category	Content	Positive	Negative
Biodiversity (amensalism)	Excluding habitats for certain macrobenthos (shellfish)[c]		O
	Excluding habitats for native halophytes and seagrasses[a,c]		O
Biodiversity (commensalism)	Providing habitats for certain macrobenthos (ragworms, crab)[a]	O	
	Providing habitats for migratory shore birds[a,c]	O	
Primary production	Reducing microphytobenthos productivity[c]		O
	Enhancing net primary production by *S. alterniflora*[b,c]	O	
Sedimentation	Enhancing sedimentation rate[a,c]	O	
	Enhancing sediment stability[a,c]	O	
Carbon burial	Enhancing carbon sequestration rate[a,b,c]	O	

[a]Grosholz et al. (2009); [b]Rout and Callaway (2009); [c]Wan et al. (2009).

CHAPTER 5.

SPATIOTEMPORAL DYNAMICS OF SEDIMENTARY ORGANIC CARBON IN THE COASTAL AREAS OF THE YELLOW SEA

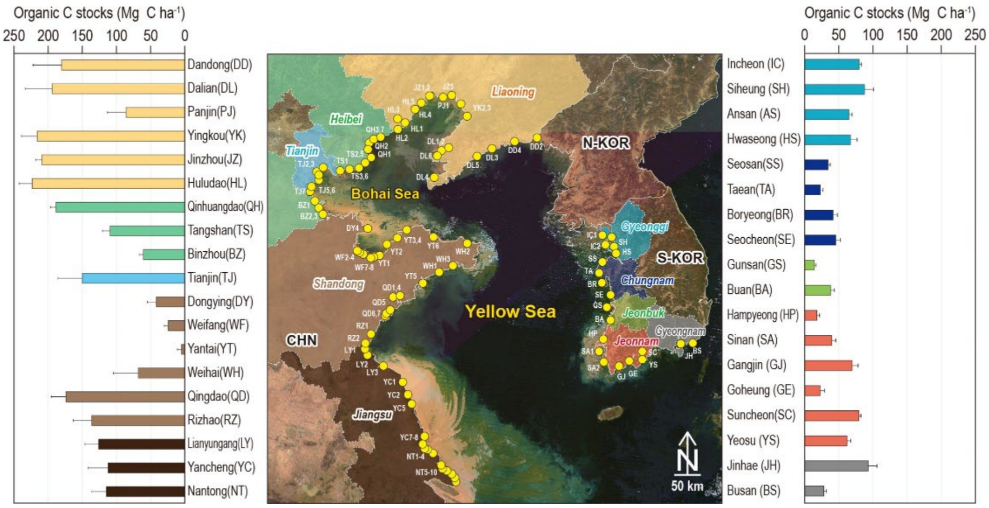

This chapter is in preparation.

5.1. Introduction

Intertidal flats between marine and terrestrial environments provide various ecosystem services to humans, including food production, biodiversity, and nutrient cycling (Costanza et al., 1997). Vegetated habitats, including salt marshes, mangroves, and seagrasses, have been highlighted for their high carbon sequestration under global warming (Chmura et al., 2003; Mcleod et al., 2011; Kelleway et al., 2016). Although these habitats are widely studied for their role as highly efficient CO_2 sinks, information remains limited on carbon sink capacity and its controlling factors in tidal flats (Lin et al., 2020). Globally, tidal flats cover 127,921 km^2, of which about 44% occur in Asia (56,051 km^2) (Murray et al., 2019). However, tidal flats have been threatened by intensifying anthropogenic development (e.g., aquaculture, reclamation) over the last three decades (Chen et al., 2016). Consequently, between 1984 and 2016, the global area of tidal flats has declined by 16% (Murray et al., 2019). In the Yellow Sea, around 36% of tidal flats (~3,800 km^2) were lost between 1980 and 2010, due to changes in land cover through reclamation (Yim et al., 2018).

Sedimentary organic carbon in coastal environments varies depending on terrestrial and marine sources (Graham et al., 2001; Lamb et al., 2006). In addition, anthropogenic inputs (e.g., aquaculture, industrial, and municipal sewage) likely contribute to its burial or organic matter accumulation in coastal areas (Rumolo et al., 2011; Pradhan et al., 2014). Although previous studies reported the dynamics of organic matter from rivers to coastal ecosystems, this process remains subject to debate (Krishna et al., 2013).

In general, sediment characteristics (e.g., mud content; silt + clay) represent environmental parameters that affect the distribution of sedimentary organic carbon stock in coastal ecosystems (Serrano et al., 2016; Lee et al., 2019; Lee et al., 2021). For example, mud-dominated sediment, which are composed of silt and clay, traps more organic carbon compared to sand-dominated sediments, due to greater adsorption capacity with larger surface areas (Keil and Hedges, 1993; Burdige, 2007). Moreover, fine grained sediments could enhance the preservation of organic carbon by reducing remineralization rates and/or redox potential (Hedges and Keil, 1995; Dauwe et al., 2001; Burdige, 2007).

Recently, tidal flats in the Yellow Sea have been threatened by the invasion of *Spartina alterniflora*, which could change the dynamics of sedimentary organic matter and the benthic community (Li et al., 2009). Although several studies have reported the negative effects of this species (e.g., biodiversity diminishment, aquaculture damage), *S. alterniflora* marshes have positive effects in terms of carbon fixation (Wan et al., 2009; Rout and Callaway, 2009). *Spartina alterniflora* marshes could contribute to more carbon accumulation in tidal flats through higher primary production and longer growing seasons compared to native halophyte marshes (*Phragmites australis*, *Suaeda japonica*) (Yang et al., 2013; Yang et al., 2017). Under both anthropogenic impacts and climate change, it is necessary to quantify the capacity of carbon burial in tidal flats, and elucidate associated regulating factors.

The present study investigated how various factors influence the spatial distribution of organic carbon stock in coastal sediments along the Yellow Sea. The targeted endpoints included total organic carbon (TOC), organic carbon stock, organic carbon sequestration rate, mud content, carbon stable isotope ratio ($\delta^{13}C$), and carbon to nitrogen ratio (C/N) in core sediments. The specific objectives were to: (1) investigate the spatial distribution of organic carbon stock per unit area; (2) evaluate environmental parameters affecting organic carbon stock; (3) elucidate the sources of sedimentary organic carbon; and (4) identify sedimentary organic carbon stocks and sequestration rates in the Yellow Sea.

5.2. Materials and methods

5.2.1. Study area

This study focused on the coastal regions of the Yellow Sea Large Marine Ecosystem (YSLME), encompassing both China and South Korea. China has five provinces; Liaoning (Dandong, Dalian, Panjin, Yingkou, Jinzhou, Huludao), Heibei (Qinhuangdao, Tangshan, Binzhou), Tianjin, Shandong (Dongying, Weifang, Yantai, Weihai, Qingdao, Rizhao), and Jiangsu (Lianyungang, Yancheng, Nantong). South Korea includes also has five provinces; Gyeonggi (Incheon, Siheung, Ansan, Hwaseong), Chungnam (Seosan, Taean, Boryeong, Seocheon), Jeonbuk (Gunsan, Buan), Jeonnam (Hampyeong, Sinan, Gangjin, Goheung, Suncheon, Yeosu), and Gyeongnam (Jinhae, Busan). Core sediment samples were collected in 2018 from major rivers and estuaries in 19 coastal regions of China and 18 coastal regions of South Korea. To identify the geographic distribution and quantity of carbon in tidal flats, these 37 coastal regions were selected to monitor tidal flats along the Yellow Sea (Figure 5.1). Target regions were selected based on certain environmental conditions, including latitude, longitude, land-use type, vegetation, temperature, geography, morphology, and sediment type.

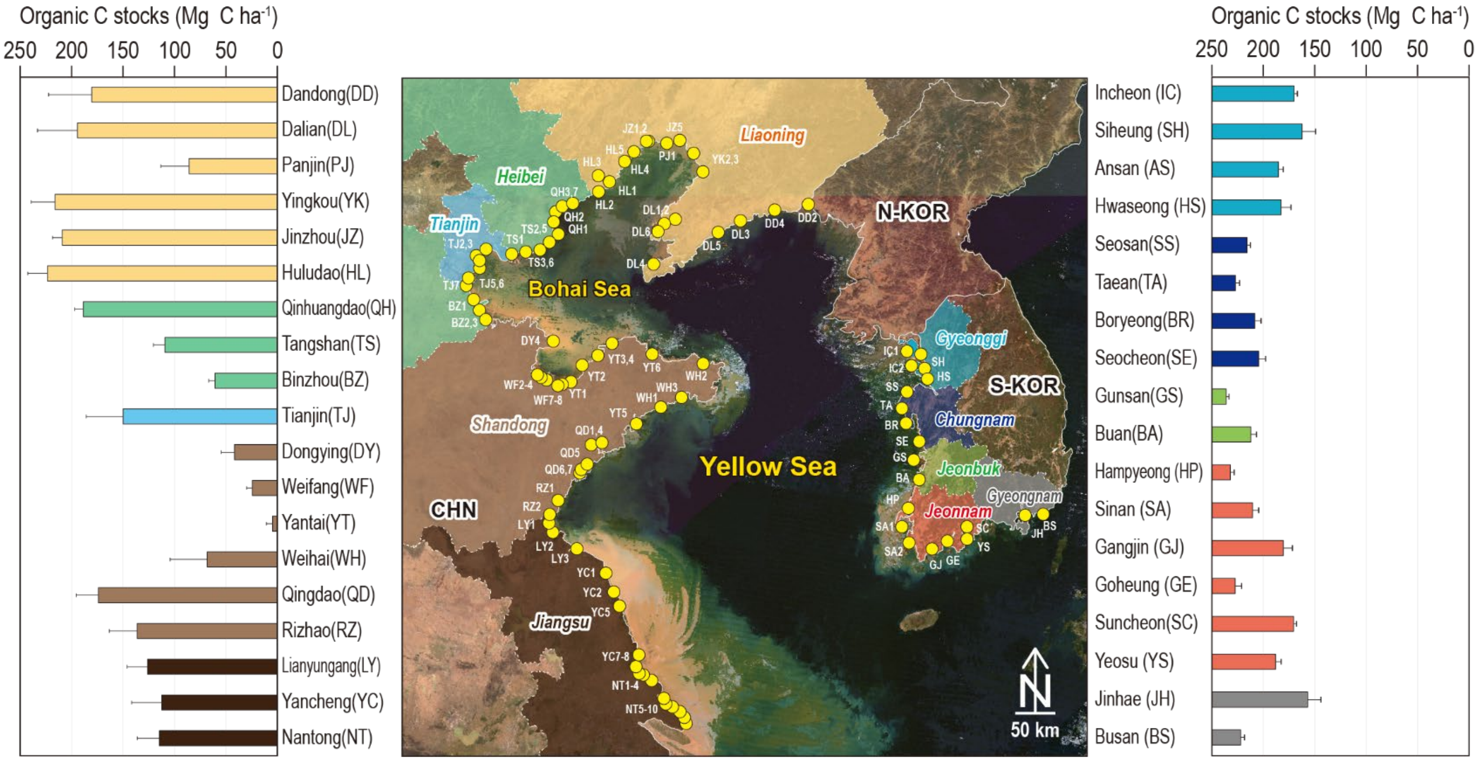

Figure 5.1.
Map showing the sampling sites along the Yellow Sea. Spatial distribution of organic carbon stocks in the core sediments of 37 region of the Yellow Sea. Core sediments were collected from Dangdong (n = 3), Dalian (n = 6), Panjin (n = 2), Yingkou (n = 3), Jinzhou (n = 4), Huludao (n = 5), Qinhuangdao (n = 5), Tangshan (n = 6), Qingdao (n = 5), Rizhao (n = 2), Weihai (n = 3), Yantai (n = 6), Weifang (n = 5), Dongying (n = 4), Binzhou (n = 6), Tianjin (n = 6), Lianyungang (n = 4), Yancheng (n = 5), Nantong (n = 9), Incheon (n = 48), Siheung (n = 8), Ansan (n = 8), Hwaseong (n = 8), Seosan (n = 36), Taean (n = 8), Boryeong (n = 8), Seocheon (n = 10), Gunsan (n = 8), Buan (n = 4), Hampyeong (n = 10), Sinan (n = 25), Gangjin (n = 12), Goheung (n = 6), Suncheon (n = 32), Yeosu (n = 12), Jinhae (n = 10), Busan (n = 33).

5.2.2. Sampling and laboratory analyses

To sample core sediments, we used a stainless steel can-corer (60 cm x 10 cm x 2 cm). Core sediments (50 cm; subsampled at 5 cm intervals) from the 19 regions along the coast of the Yellow Sea were collected from salt marshes and bare tidal flats in 2018. Detailed information on organic carbon stocks in China is provided in Table 5.1. Detailed information on organic carbon stocks and carbon sequestration in the coastal areas of Korea are provided in Table 3.1 (Chapter 3).

To analyze sediment properties, sediment samples were stored in plastic bags to prevent evaporation, and were then transferred to the laboratory. Details on the procedures used to analyze sediment properties, total organic carbon, carbon stable isotopic ration, and radioactive isotope ratio are provided in Figure 5.2. A MasterSizer 3000 (Malvern Panalytical Ltd., UK) was used to analyze the mud content of sediment after removing organic matter, using diluted hydrogen peroxide (H_2O_2). Sediment to analyze TOC was freeze-dried, homogenized, and powdered using a Planetary Ball Mill 100 (Retsch Ltd., Germany). TOC was analyzed using an Elemental Analyzer-Isotope Ratio Mass Spectrometer (EA-IRMS) (Elementar, Gmbh, Hanau, Germany). To date the age of core sediments, we used the constant rate of supply (CRS) model for the vertical profiles of excess ^{210}Pb activity (Appleby and Oldfieldz, 1983). The sedimentation rate was calculated from the age dating data (Appleby, 2001). The sedimentation rate of core sediments at the sampling stations in China is provided in Figure 5.3. Through analyzing the TOC and sedimentation rate, we assessed the organic carbon stocks and carbon sequestration rates of the sediment in tidal flats along the coasts of the Yellow Sea. Detailed information on the assessment of organic carbon stocks and sequestration rates is provided in Chapter 3.

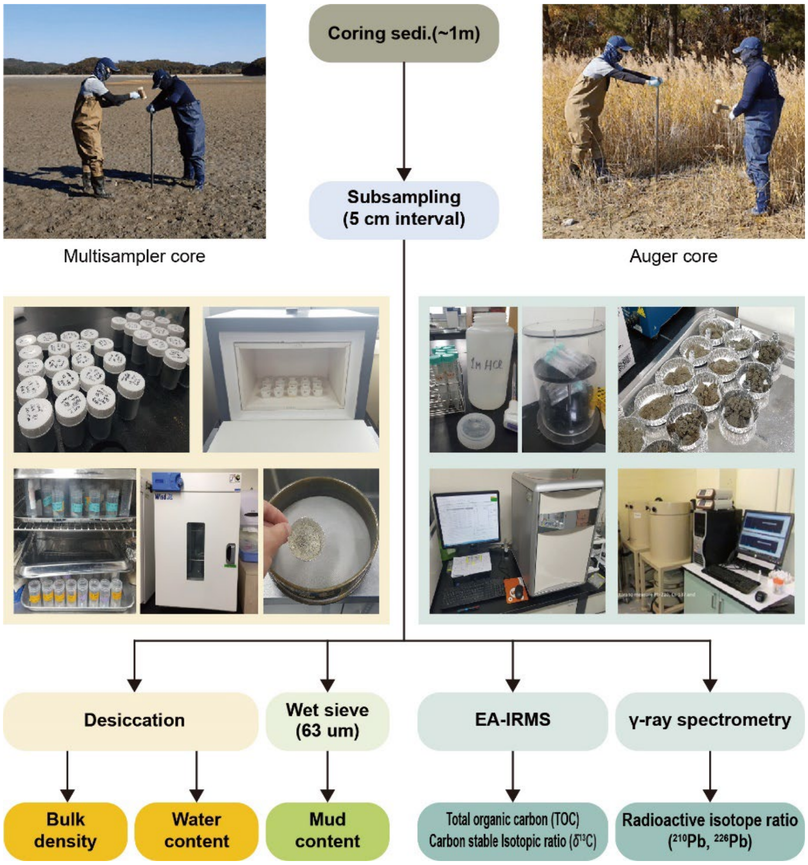

Figure 5.2.
Analysis procedure of sediment properties, total organic carbon, carbon stable isotopic ratio, and radioactive isotope ratio

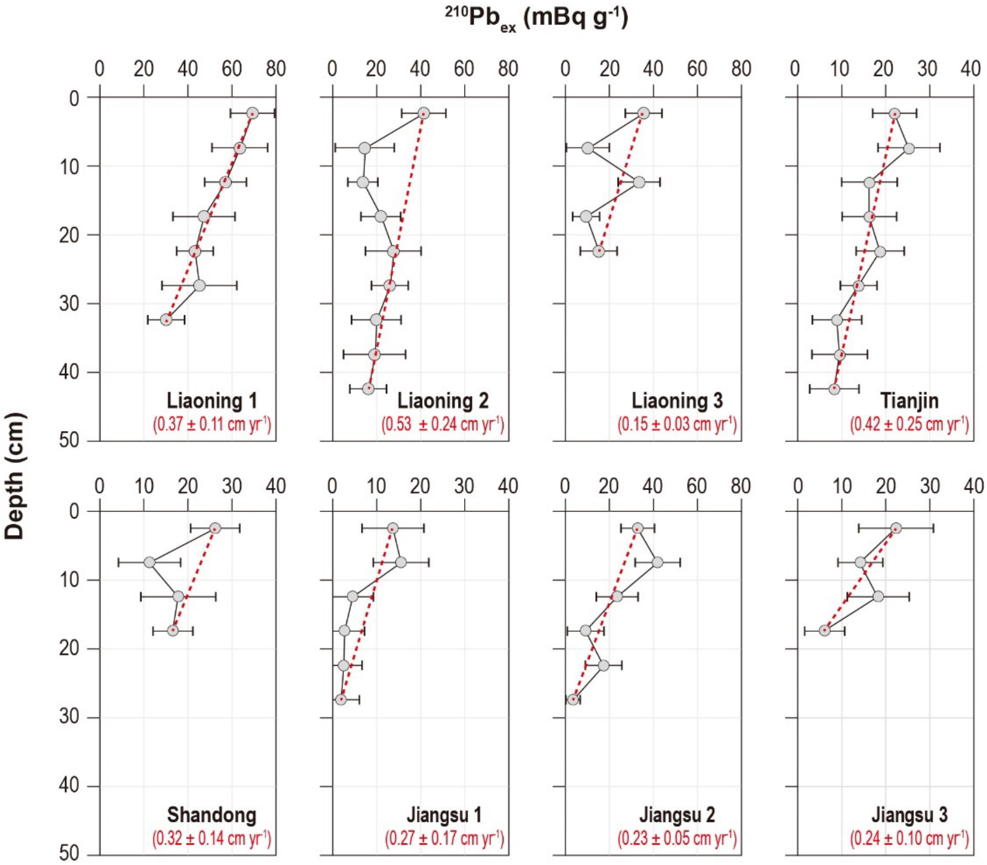

Figure 5.3.

Depth profiles of unsupported ^{210}Pb ($^{210}Pb_{ex}$) and sedimentation rate of core sediments at Liaoning, Tianjin, Shandong, Jiangsu.

Table 5.1.
Organic carbon content in the coastal sediments (salt marshes and bare tidal flats) of China.

Location	Sampling year	Latitude	Longitude	[a]Habitat	Dominant halophyte	Core depth (cm)	Organic carbon stock (Mg C ha^{-1})	[b]Organic carbon stock (Mg C ha^{-1})	Reference
Dandong, Liaoning	2018	39.9436	124.2828	B	Bare	50	125	250	This study
	2018	39.8383	123.6528	SM	*Suaeda* sp.	50	89	178	
Dalian, Liaoning	2018	39.6208	121.5214	B	Bare	50	16	31	
	2018	39.6947	121.7400	SM	*Spartina* sp.	50	32	64	
	2018	39.6633	122.9939	SM	*Spartina* sp.	50	88	175	
	2018	38.9844	121.5103	B	Bare	50	51	102	
	2018	39.4817	122.5592	SM	*Suaeda* sp.	50	162	324	
	2018	39.5058	121.4033	B	Bare	50	230	460	
Panjin, Liaoning	2018	40.8822	121.5714	B	Bare	50	56	112	
Yingkou, Liaoning	2018	40.6900	122.1292	B	Bare	50	143	286	
	2018	40.4250	122.2844	B	Bare	50	98	197	
Jinzhou, Liaoning	2018	40.9242	121.1867	B	Bare	50	99	197	
	2018	40.9181	121.2436	B	Bare	50	113	225	
	2018	40.9092	121.8192	SM	*Suaeda* sp.	50	100	200	
Huludao, Liaoning	2018	40.2697	120.4622	SM	*Suaeda* sp.	50	96	193	
	2018	40.1747	120.2614	B	Bare	50	97	195	
	2018	40.3703	120.2583	B	Bare	50	93	185	
	2018	40.7469	120.9347	B	Bare	50	167	333	
	2018	40.5919	120.7694	B	Bare	50	101	201	
Qinhuangdao, Hebei	2018	39.6789	119.2911	B	Bare	50	111	221	
	2018	39.7814	119.4136	B	Bare	50	88	177	
	2018	39.8394	119.5133	SM	*Phragmites* sp.	50	89	178	
	2018	39.9653	119.7694	B	Bare	50	89	177	
Tangshan, Hebei	2018	39.0203	117.4578	B	Bare	50	55	110	
	2018	39.1522	118.5342	B	Bare	50	53	106	
	2018	39.0436	118.3642	B	Bare	50	50	100	
	2018	39.4308	119.2800	B	Bare	50	54	108	
	2018	39.4607	119.1341	SM	*Phragmites* sp.	50	48	96	
Binzhou, Hebei	2018	38.2637	117.8511	B	Bare	50	30	61	
	2018	38.2006	118.0047	B	Bare	50	32	64	
	2018	38.1460	118.0528	B	Bare	50	22	43	
Tianjin	2018	39.1640	117.6623	SM	*Spartina* sp.	50	54	107	

Table 5.1. (Continued)

Location	Sampling year	Latitude	Longitude	[a]Habitat	Dominant halophyte	Core depth (cm)	Organic carbon stock (Mg C ha^{-1})	[b]Organic carbon stock (Mg C ha^{-1})	Reference
Tianjin	2018	39.0938	117.7298	B	Bare	50	43	85	
	2018	38.9695	117.7315	SM	*Spartina* sp.	50	49	98	
	2018	38.7667	117.5694	B	Bare	50	123	246	
Dongying, Shandong	2018	37.7615	119.1706	SM	*Phragmites* sp.	50	27	53	
	2018	38.6547	117.5447	SM	*Phragmites* sp.	50	31	62	
Weifang, Shandong	2018	37.1354	119.2870	B	Bare	50	6	12	
	2018	37.1401	119.1434	B	Bare	50	9	19	
	2018	37.0765	119.4793	SM	*Spartina* sp.	50	18	37	
	2018	37.0921	119.5599	SM	*Spartina* sp.	50	11	21	
	2018	37.1330	119.1860	B	Bare	50	21	42	
Yantai, Shandong	2018	37.1286	119.7277	B	Bare	50	4	8	
	2018	37.4017	119.9493	B	Bare	50	5	10	
	2018	37.5518	120.2482	B	Bare	50	11	21	
	2018	37.7493	120.5242	SM	*Suaeda* sp.	50	2	4	
	2018	37.5753	121.2966	B	Bare	50	4	8	
Weihai, Shandong	2018	36.8266	121.4636	SM	*Spartina* sp.	50	70	140	
	2018	37.4296	122.2754	B	Bare	50	11	21	
	2018	36.9321	121.8657	B	Bare	50	19	37	
Qingdao, Shandong	2018	36.2609	120.3259	SM	*Spartina* sp.	50	90	180	
	2018	36.2353	120.1206	SM	*Spartina* sp.	50	86	172	
	2018	35.8568	120.0477	B	Bare	50	81	162	
	2018	35.7684	119.9262	B	Bare	50	79	157	
	2018	35.7405	119.9111	B	Bare	50	93	186	
Rizhao, Shandong	2018	35.2980	119.4482	SM	*Spartina* sp.	50	74	148	
	2018	35.0782	119.3033	SM	*Spartina* sp.	50	80	160	
Lianyungang, Jiangsu	2018	34.9023	119.1961	SM	*Spartina* sp.	50	43	86	
	2018	34.7963	119.2244	SM	*Spartina* sp.	50	91	181	
	2018	34.5026	119.7720	B	Bare	50	51	103	
Yancheng, Jiangsu	2018	34.1128	120.3239	B	Bare	50	33	67	
	2018	33.8160	120.4768	SM	*Spartina* sp.	50	96	193	
	2018	33.7400	120.5499	SM	*Spartina* sp.	50	40	79	
	2018	32.8821	120.9646	SM	*Spartina* sp.	50	42	83	

Table 5.1. (Continued)

Location	Sampling year	Latitude	Longitude	[a]Habitat	Dominant halophyte	Core depth (cm)	Organic carbon stock (Mg C ha^{-1})	[b]Organic carbon stock (Mg C ha^{-1})	Reference
Yancheng, Jiangsu	2018	32.6933	120.8959	SM	*Spartina* sp.	50	51	103	
Nantong, Jiangsu	2018	32.6031	120.9437	B	Bare	50	41	82	
	2018	32.5577	121.0457	SM	*Spartina* sp.	50	47	93	
	2018	32.4919	121.2226	B	Bare	50	20	40	
	2018	32.2016	121.3851	B	Bare	50	30	60	
	2018	32.1535	121.4562	SM	*Spartina* sp.	50	67	133	
	2018	32.1014	121.6039	B	Bare	50	60	120	
	2018	32.0292	121.7411	SM	*Spartina* sp.	50	60	119	
	2018	31.9337	121.8257	SM	*Spartina* sp.	50	110	220	
	2018	31.8490	121.8521	B	Bare	50	52	103	

[a]SM: Salt marsh, B: Bare tidal flat
[b]Organic carbon stock normalized to the amount for 1 m depth

5.2.3. Data analysis

We used SPSS 23.0 (SPSS Inc., Chicago, IL, USA) to perform the statistical analyses. To estimate variation in geography, salinity, land-use, vegetation, and halophyte species, we performed *t*-tests. Pearson correlation analysis was used to test for significant relationships with organic carbon stocks and mud content. To estimate site-specific variation in organic carbon stocks, we performed ANOVA with Tukey's post-hoc test to determine the mean difference in organic carbon stocks among the 10 provinces bordering the Yellow Sea (Liaoning, Tianjin, Hebei, Jiangsu, Shandong, Gyeonggi, Jeonnam, Gyeongam, Chungnam, and Jeonbuk). Before the analysis, Levene's test was used to evaluate homogeneity of variance. The same statistical method was used to investigate the mean difference in carbon stable isotopic ratios ($\delta^{13}C$) and carbon to nitrogen ratios (C/N) of three halophyte species (*P. australis*, *S. japonica*, and *S. alterniflora*).

5.3. Results and discussion

5.3.1. Spatial distribution of organic carbon stocks per unit area

The spatial distributions of sedimentary organic carbon stocks per unit in the 37 coastal regions varied in general (Figure 5.1). By province, Liaoning had the greatest organic carbon stock per unit area (206 ± 25 Mg C ha^{-1}), followed by Tianjin (146 ± 50 Mg C ha^{-1}), Hebei (141 ± 24 Mg C ha^{-1}), Jiangsu (115 ± 14 Mg C ha^{-1}), Gyeonggi (77 ± 3 Mg C ha^{-1}), Jeonnam (55 ± 3 Mg C ha^{-1}), Shandong (52 ± 18 Mg C ha^{-1}), Gyeongnam (43 ± 6 Mg C ha^{-1}), Chungnam (36 ± 2 Mg C ha^{-1}), and Jeonbuk (20 ± 4 Mg C ha^{-1}) (Figure 5.4). Of note, tidal flats along the coast of China had relatively higher sedimentary organic carbon stock (138 ± 13 Mg C ha^{-1}) compared to those of South Korea (53 ± 2 Mg C ha^{-1}).

The concentration of organic carbon tends to fluctuate in relation to natural and anthropogenic sources (Lee et al., 2019; Lee et al., 2021). Carbon in coastal areas originates from both marine and terrestrial sources; consequently, its composition changes depending source. In the present study, Liaoning had the highest organic carbon stocks of China. This province is strongly affected by anthropogenic inputs from industrial and municipal areas (Yoon et al., 2020). Riverine inputs of anthropogenic organic matter (e.g., sewage) could contribute to organic carbon burial in sediments (Bae et al., 2017; Lee et al., 2019; Lee eat al., 2021). For instance, the relatively higher organic carbon stocks in China might reflect greater exposure to pollution from aquaculture, municipal, and industrial sewage discharge (Lim et al., 2006; Seo et al., 2014; Yoon et al., 2020).

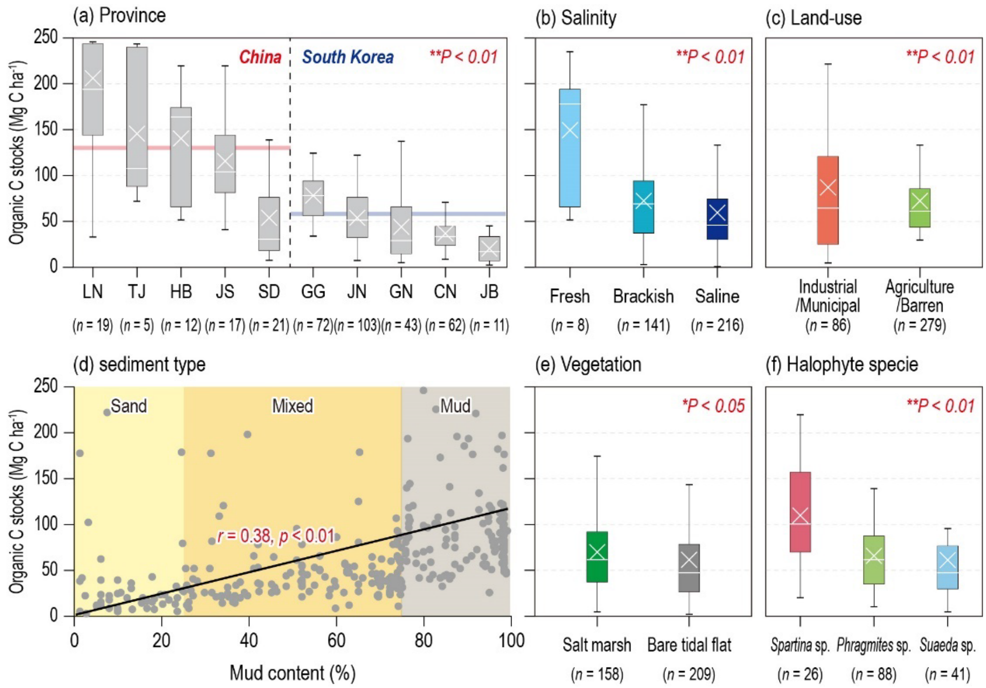

Figure 5.4.

Distribution of organic carbon stocks in core sediment with respect to (a) province, (b) salinity, (c) land-use, (d) sediment type, (e) vegetation, (f) halophyte specie. Panels: (a) LN (Liaoning) (n = 19), TJ (Tianjin) (n = 5), HB (Hebei) (n = 12), JS (Jiangsu) (n = 17), SD (Shandong) (n = 21), GG (Gyeonggi) (n = 72), JN (Jeonnam) (n = 103), GN (Gyeongnam) (n = 43), CN (Chungnam) (n = 62), and JB (Jeonbuk) (n = 11). (b) Fresh (n = 8), Brackish (n = 141), Saline (n = 216). (c) Industrial/Municipal (n = 86) and Agriculture/Barren (n = 279). (d) Sand (mud content: 0–25%) (n = 53), Mixed (25–75%) (n = 136), and Mud (75–100%) (n = 154). (e) Salt marsh (n = 158) and Bare tidal flat (n = 209). (f) *Spartina* sp. (n = 26), *Phragmites* sp. (n = 88), and *Suaeda* sp. (n = 41). Relationship between organic carbon stocks and mud content of 365 core sediments of South Korea.

5.3.2. Environmental factors affecting the complex dynamics of sedimentary organic carbon stocks

Organic carbon stocks in the sediments of tidal flats along the Yellow Sea differed significantly with respect to environmental characteristics, including geography, salinity, land-use type, vegetation, halophyte specie, and mud content (Figure 5.4). Higher organic carbon stocks at freshwater stations seemed to be influenced by anthropogenic inputs from municipal and/or industrial sources.

Interestingly, organic carbon stocks were significantly correlated with mud content ($r = 0.38$, $p < 0.01$) at all sampling stations (Figure 5.4 and Figure 5.5). In general, fine-grained sediments (e.g., mud) provide larger surface areas to capture organic matters compared to coarse grained sediments (e.g., sand) (Keil and Hedges, 1993; Mayer, 1994; Burdige, 2007; Serrano et al., 2016). As expected, organic carbon stock was greater in mud-dominated sediment (92 ± 4 Mg C ha^{-1}), compared to mixed sediment (49 ± 4 Mg C ha^{-1}) and sand-dominated sediment (32 ± 6 Mg C ha^{-1}). Previous studies reported positive relationships between mud content and organic carbon stocks (Serrano et al., 2016; Lee et al., 2019; Lee et al., 2021). Therefore, mud content could be used to predict sedimentary organic carbon stocks in tidal flats, and is already used as a universal proxy in the intertidal flats of the Yellow Sea.

The organic carbon stocks of salt marshes were significantly higher compared to bare tidal flat, indicating that organic matter originates from halophytes (e.g., *S. alterniflora*, *P. australis*, *S. japonica*). Salt marshes are key carbon reservoirs in coastal environment because they serve as highly efficient CO_2 sinks through primary production (Duarte et al., 2013; Spivak et al., 2019). Salt marshes absorb CO_2 from the atmosphere, and then sequester organic carbon in aboveground (stems, leaves), belowground (roots), non-living biomass (litter), and sediments (Mcleod et al., 2011). Because salt marshes are vegetated, they are able to trap organic matter in sediments that originates from vegetation biomass. Overall, higher sedimentary organic carbon stocks in salt marshes results from carbon inputs through vegetated ecosystems.

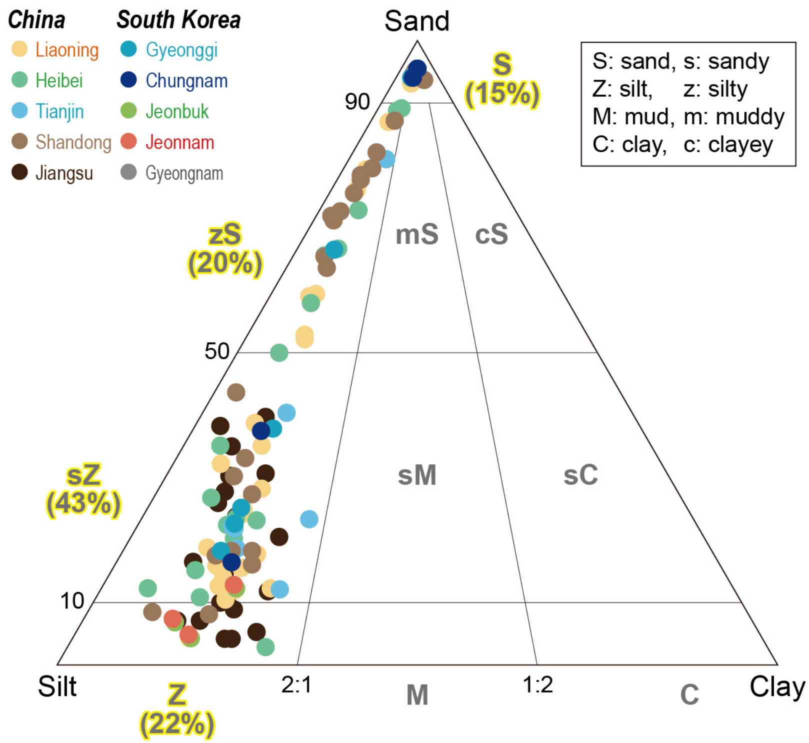

Figure 5.5.
Sediment facies in the representative tidal flats of the Yellow Sea

5.3.3. Halophyte species-specific variability in the sources of sedimentary organic matter

The habitats of *P. australis* and *S. japonica* had the signature of C_3 plant derived organic carbon, with $\delta^{13}C$ values ranging from –26.2‰ to –21.0‰ (mean: –23.7‰) (Figure 5.5). In comparison, habitats of *S. alterniflora* were of C_4 plant origin, with $\delta^{13}C$ values of –22.9‰ to –17.8‰ (mean: –21.7‰). Through different photosynthetic pathways, the typical $\delta^{13}C$ signature of C_4 and C_3 plant habitats intertidal flats has been reported to range from –18.9‰ to –15.8‰ and –27.0‰ to –22.0‰, respectively (Kemp et al., 2006).

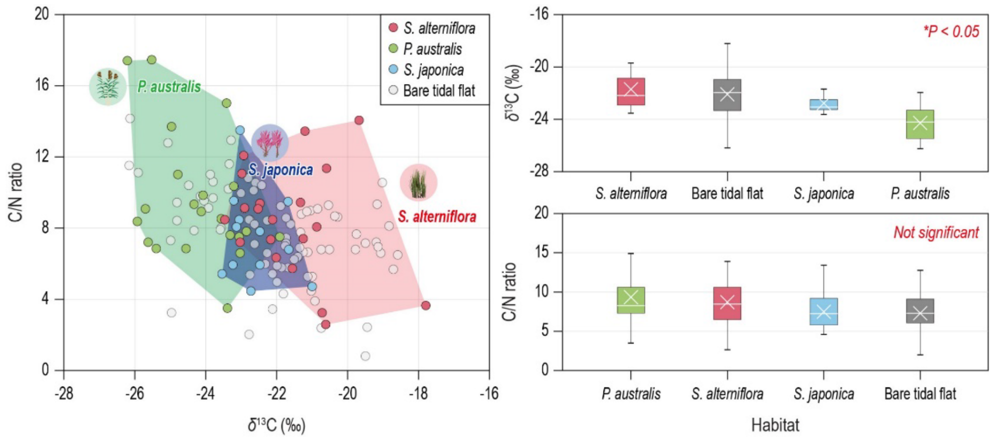

Figure 5.6.
Biplot of stable carbon isotopic ratio (δ^{13}C) and carbon to nitrogen ratio (C/N) of sediments by halophyte species (*S. alterniflora*, *P. australis, S. japonica*) and bare tidal flat.

5.3.4. Organic carbon stocks and carbon sequestration rates in the coastal areas of the Yellow Sea

Through integrating organic carbon stock per unit area with tidal flat area, we estimated the organic carbon stocks and sequestration rates of the coastal areas of the Yellow Sea (Table 5.2 and 5.3). Jiangsu had the greatest organic carbon stocks (9,885–54,014 Gg C), followed by Liaoning (2,292–33,787 Gg C), Shandong (1,676–32,937 Gg C), Gyeonggi (2,890–16,157 Gg C), Hebei (2,371–12,157 Gg C), Jeonnam (538–10,729 Gg C), Tianjin (1,566–4,518 Gg C), Gyeongnam (119–4,254 Gg C), Chungnam (299–2,818 Gg C), and Jeonbuk (2–54 Gg C) (Table 5.5). The organic carbon sequestration of all provinces in the Yellow Sea was also estimated from sedimentation rates. The total organic carbon stocks of tidal flats in the Yellow Sea were 20,637–171,423 Gg C, while sequestration rates were 81–613 Gg C yr^{-1} and 297–678 Gg CO_2 eq. yr^{-1}. However, the present study only estimated values on tidal flats, without distinguishing salt marshes and bare tidal flats; thus, more focused analyses are required in the future.

Table 5.2.
Total organic carbon (%) and bulk density (g cm^{-3}) in the Chinese coastal regions.

Country	**Province**	**Total organic carbon (%)**	**Bulk density (g cm^{-3})**
China	Liaoning	1.20 (± 0.17)	1.80 (± 0.07)
	Hebei	0.67 (± 0.15)	2.10 (± 0.09)
	Tianjin	0.80 (± 0.34)	1.90 (± 0.14)
	Shandong	0.24 (± 0.10)	2.70 (± 0.16)
	Jiangsu	0.59 (± 0.09)	2.00 (± 0.05)

Table 5.3.
Organic carbon stock (Mg C ha^{-1}) and carbon sequestration rate (Mg C ha^{-1} yr^{-1}) in the Chinese coastal regions.

Country	Province	Organic carbon stock per unit area (Mg C ha^{-1})	Organic carbon sequestration rate per unit area (Mg C ha^{-1} yr^{-1})
China	Liaoning	206 (± 25)	1.47 (± 0.18)
	Hebei	129 (± 24)	0.91 (± 0.17)
	Tianjin	146 (± 52)	1.04 (± 0.36)
	Shandong	52 (± 18)	0.40 (± 0.14)
	Jiangsu	115 (± 14)	0.81 (± 0.10)

Table 5.4
Organic carbon stock (Gg C) and organic carbon sequestration rate (Gg C yr^{-1}) in the coastal regions along the Yellow Sea (1 Gg = 10^9 g)

Country	Province	Area (km^2)	Sedimentation rate (cm yr^{-1})	Organic carbon stocks (Gg C)	Organic carbon sequestration rate (Gg C yr^{-1})
China	Liaoning	734[a]	0.35 ± 0.18	2,292 – 33,787	8 – 118
	Hebei	550[a]	0.42 ± 0.25	2,371 – 12,157	10 – 51
	Tianjin	184[a]	0.42 ± 0.25	1,566 – 4,518	7 – 19
	Shandong	1,912[a]	0.32 ± 0.14	676 – 32,937	7 – 105
	Jiangsu	2,450[a]	0.25 ± 0.11	9,885 – 54,014	25 – 135
	Subtotal	**5,830**		**16,789 – 137,412**	**56 – 429**
South Korea	Gyeonggi	920[b]	0.71 ± 0.19	2,890 – 16,157	21 – 116
	Chungnam	378[b]	0.41 ± 0.13	299 – 2,818	1 – 11
	Jeonbuk	12[b]	0.49 ± 0.22	2 – 54	0.1 – 0.3
	Jeonnam	876[b]	0.39 ± 0.12	538 – 10,729	2 – 42
	Gyeongnam	296[b]	0.36 ± 0.11	119 – 4,254	1 – 15
	Subtotal	**2,482**		**3,848 – 34,011**	**25 – 185**
Total		**8,312**		**20,637 – 171,423**	**81 – 613**

[a]Yim et al. (2018)
[b]Lee et al. (2021)

CHAPTER 6.

CONCLUSIONS

6.1. Summary

The present study investigated the spatiotemporal distribution and fate of sedimentary organic carbon in the tidal flat ecosystem of the Yellow Sea. This section presents a summary the major findings of the present study.

Chapter 2 demonstrated the spatiotemporal distributions and sources of sedimentary organic matter in the typical coastal waters of Korea. The results indicated that large variation in time and space existed depending on source and origin across natural and altered coastal environments. The results showed that, first, terrestrial input considerably influenced the sediment dynamics, with direct strong impacts from fresh water discharge. Second, mud content was a key environmental factor regulating the dynamics of sedimentary organic matter in the coastal environment. Third, elevated sedimentary organic matter recorded in typical tidal flats of certain seasons generally closely mirrored MPB blooms that occurred in winter to spring. Fourth, the combined impacts of terrestrial and marine-derived forcing on sediment dynamics were evidenced in the altered environment. Fifth, the origin and sources of sedimentary organic matter in the coastal environment significantly varied in time and space. The factors affecting spatiotemporal variation in sedimentary organic matter included mud content, algal biomass, and water content.

Chapter 3 presented the organic carbon stocks and sequestration rates in tidal flats at the national scale of Korea, based on extensive field surveys combined with state of the are remote sensing technology. The results showed that, first, major variation exists with respect to spatio-physiographic characteristics and terrestrial sources across the coastal environment. Second, terrestrial input appeared to influence the dynamics of sedimentary organic carbon, particularly in coastal areas adjacent to metropolitan areas. Third, vegetation and mud content were key environmental factors regulating the spatiotemporal distributions of sedimentary organic carbon in the coastal waters of Korea. Fourth, organic carbon stocks and sequestration rates were evaluated along the entire tidal flat of South Korea.

Chapter 4 examined the effects of *S. alterniflora* invasion on the coastal ecosystem using multiple parameters, including temperature anomaly, sedimentary organic carbon, macrobenthos community, greenhouse gas emission, food web, and sediment erodibility. The results confirmed that, first, elevated temperatures have affected the spread of *S. alterniflora* along the coasts of the Yellow Sea during 1980–2020. Second, invasive *S. alterniflora* accumulated more carbon compared to native C_3 plants (e.g., *P. australis*, *S. japonica*), due to its greater biomass, longer growing season, and higher primary production. Third, the stem length and density of *S. alterniflora* were affected by eradication treatments, but they did not affect the biodiversity of macrobenthos during the one–year monitoring period. Fourth, in comparison to native *P. australis* and bare tidal flats, the ecological functions of *S. alterniflora* invasion was evaluated with respect to greenhouse gas emissions, the food web, sediment erodibility, and carbon burial.

Chapter 5 provided comprehensive information about the spatiotemporal dynamics of sedimentary organic carbon in the coastal areas of the Yellow Sea. The results showed that, first, the riverine inputs of anthropogenic organic matter from aquaculture, municipal, and industrial areas contributed to the burial of sedimentary organic carbon. Second, sediment mud content represents a reliable proxy for estimating sedimentary organic carbon stocks. Third, *S. alterniflora* marshes enhance carbon sequestration more than other halophyte species (*P. australis* and *S. japonica*). Fourth, total organic carbon stocks (21–171 Tg C) and sequestration rates (0.08–0.61 Tg C yr^{-1}; 0.29–2.24 Tg CO_2 eq. yr^{-1}) were evaluated in the Yellow Sea.

Overall, the present study demonstrated the spatiotemporal distribution and fate of sedimentary organic carbon of the tidal flat ecosystem in the Yellow Sea. The results showed that variation in time and space existed, and were related to different sources and origins across coastal regions. Spatially, tidal flats had relatively higher organic carbon stocks and sequestration rates in China compared to Korea, in association with different geomorphological features. Temporally, organic carbon stocks were generally stable over the four-year period within 1 m sediment depth. In contrast, TOC varied more broadly over a one-year period within 0.05 cm depth. Regardless of location, vegetation and mud content were key environmental factors regulating the distribution of sedimentary organic carbon, with mud content being positively correlated with organic carbon. In conclusion, the origin and sources of sedimentary organic carbon in the coastal environment varied in time and space, and the factors affecting these spatiotemporal variations included mud content and vegetation. The data provided in the present study is expected to serve as baseline information on the carbon dynamics of coastal sediments along the Yellow Sea, contributing to the global database of "Blue Carbon" science.

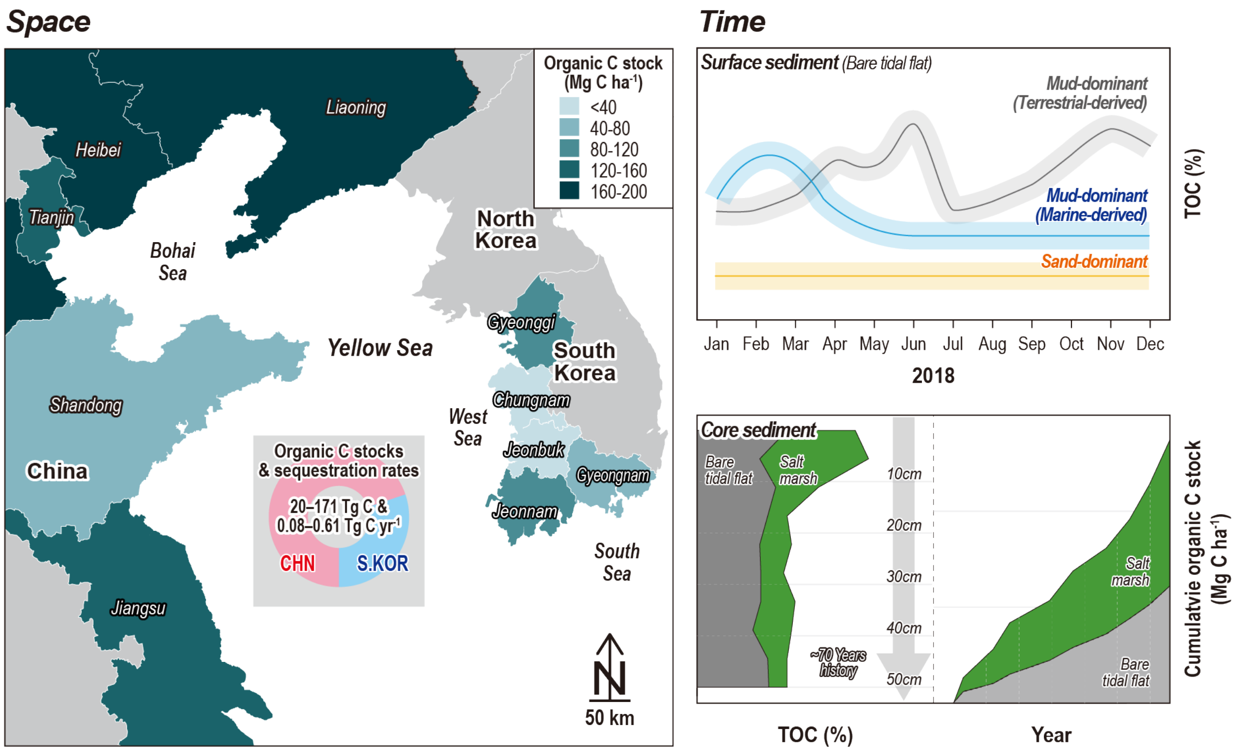

Figure 6.1.

Spatiotemporal distribution of sedimentary organic carbon of tidal flat in the Yellow Sea. **(Left)** Spatial distribution of organic carbon stocks in core sediments of 74 regions. Yellow circles denote five monitoring regions (Ganghwa, Garolim, Sinan, Suncheon, and Nakdong River estuary) in South Korea. **(Right)** Monthly variation of TOC (%) in surface sediment of five regions in 2018. Vertical distribution of TOC in and cumulative organic carbon stock (Mg C ha^{-1}) of core sediments (0–50 cm) of bare tidal flat and salt marsh, respectively.

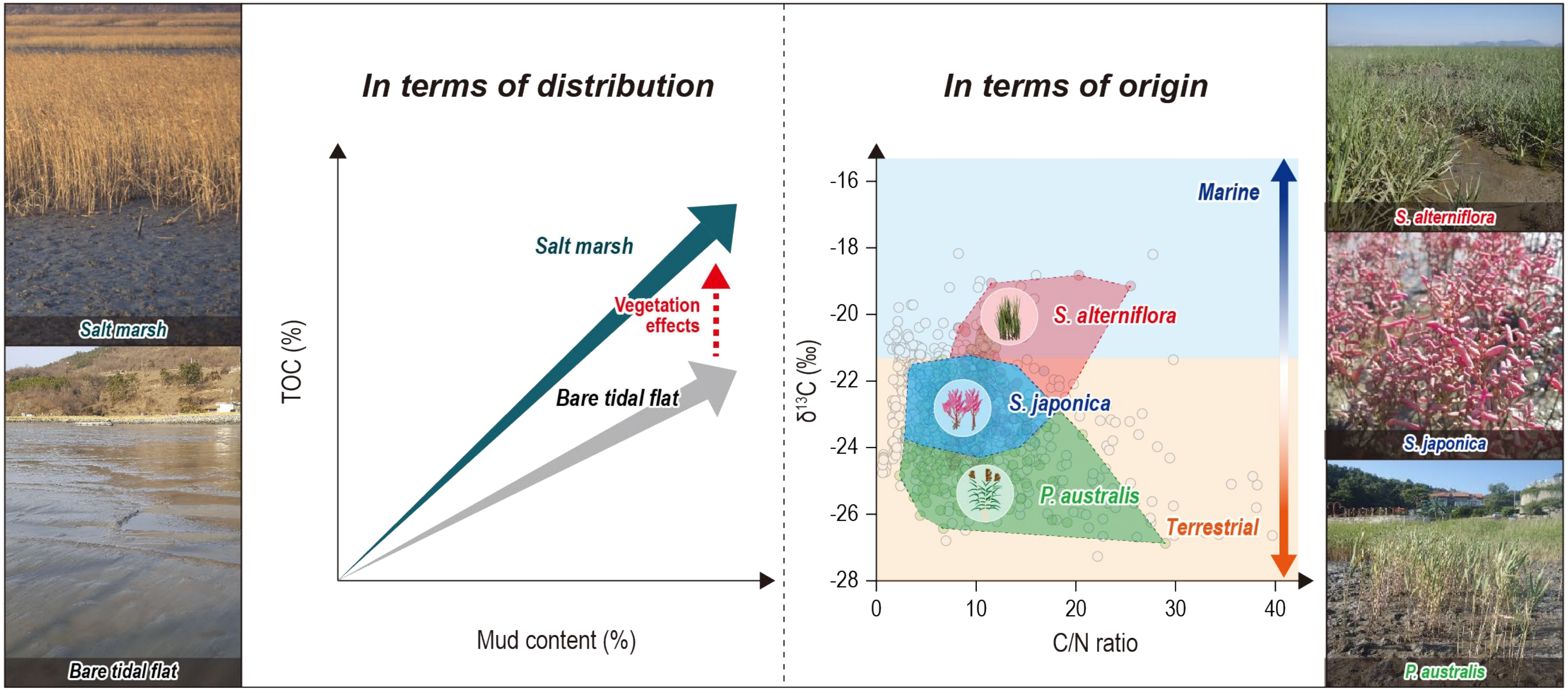

Figure 6.2.
Research summary and key findings in the present study. (Left) Relationships between mud content and TOC in sediment of tidal flats in the Yellow Sea. Grey and Dark green arrow denote bare tidal flat and salt marsh. (Right) Scatter plots of carbon isotopic composition ($\delta^{13}C$) and carbon to nitrogen (C/N) ratio of sediments.

6.2. Ecological implications and limitations

One of the greatest challenges of this study was related to assessing tidal flats as Blue Carbon Ecosystems (BCEs) using a number of core sediment samples in the Yellow Sea region. Because research on the ability of tidal flats to fix CO_2 remains limited, this system had not been previously recognized as a blue carbon sink in comparison to recognized BCEs (mangroves, salt marshes, and seagrasses) (Nellemann et al., 2009). In particular, to recognize tidal flats as blue carbon sinks, they must: 1) perform large scale GHG removal and/or emissions, and 2) store fixed CO_2 over long periods (>100 years) (Lovelock and Duarte, 2019).

To verify the first point, high levels of organic carbon stocks and carbon sequestration rates must be confirmed using field data in coastal ecosystems. In the tidal flats of the Yellow Sea region, organic carbon stocks per unit area ranged from 18 to 206 Mg C ha^{-1} (mean: 79 Mg C ha^{-1}), and carbon sequestration rates ranged from 0.07 to 1.47 Mg C ha^{-1} yr^{-1} (mean: 0.50 Mg C ha^{-1} yr^{-1}) (Table 3.8, 3.10, and 5.3). Out of BCEs, mangroves have the highest organic carbon stocks and carbon sequestration rates (251 Mg C ha^{-1} and 1.26 Mg C ha^{-1} yr^{-1}), followed by salt marshes (168 Mg C ha^{-1} and 0.39 Mg C ha^{-1} yr^{-1}), and seagrasses (112 Mg C ha^{-1} and 0.36 Mg C ha^{-1} yr^{-1}). Compared to conventional BCEs, tidal flats had similar organic carbon stocks and sequestration rates. Furthermore, the global area of tidal flats (~128,000 km^2) is comparable to conventional BCEs (Seagrasses: ~400,000 km^2, Salt marshes: ~300,000 km^2, Mangroves: 140,000 km^2) (Table 3.14); thus, tidal flats represent important carbon sinks that should be recognized.

To verify the second point, evidence that fixed organic carbon is stored for longer than 100 years is required. The current study confirmed that the storage of organic carbon stocks in tidal flats was stably maintained for at least four years in South Korea (Figure 3.1). In addition, core sediments collected from 50 cm depth were dated back to 70 years ago, and the concentration of organic carbon at 50 cm depth was relatively similar to surface sediment (Figure 4.4). Thus, sedimentary organic carbon was confirmed to be stable in tidal flats for 4–70 years. However, information on the long-term (over 100 years) storage of carbon stocks in tidal flats needs to be collected. Thus, further studies are necessary through continued monitoring. Overall, the present study provides baseline information on carbon dynamics in tidal flats, demonstrating its potential to be recognized as Blue carbon. Furthermore, other countries globally with tidal flats could also add to carbon reduction sources base on these results. Now that global warming is accelerating due to climate change, studies on tidal flats contribute vital information towards realizing net-zero carbon globally.

Nevertheless, the present study had limitations. This study focused on identifying organic carbon stocks and carbon sequestration rates, which might be limited by the process of carbon dynamics in tidal flats. To understand and predict the fate of sedimentary carbon in tidal flats, four biogeochemical mechanisms should be considered: 1) allochthonous deposition, 2) tidal flushing, 3) redox condition, and 4) plant-microbe interaction (Spivak et al., 2019). Tidal flat ecosystems, including tidal flats, are distinct from marine and terrestrial ecosystems, but have commonalities. For example, marine environments have typical conditions in that sediments are saturated with redox and diffusional gradients, whereas terrestrial soils are oxygenated and well-drained, except during heavy precipitation. In comparison, water content and chemistry vary among tidal flat ecosystems and over sediment elevation gradients, reflecting local hydrology. Furthermore, plant rhizosphere interactions between microbes and plants contribute to the dynamics of geochemical environments, and change spatially and temporally. Because of these differences, to estimate the fate of carbon in tidal flats, additional data on carbon considering these four mechanisms are required in future studies.

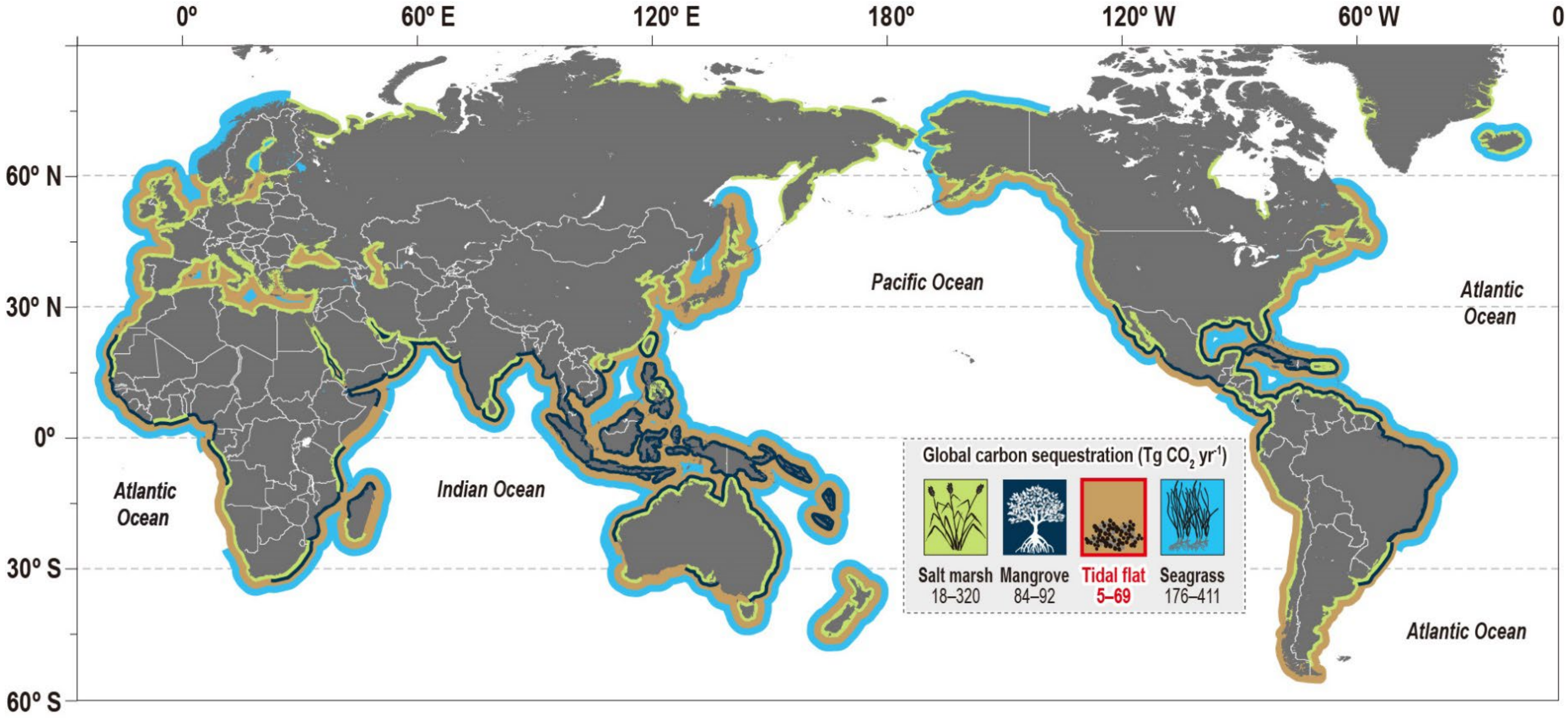

Figure 6.3.
Ecological implications and limitations in the present study. Red box denotes the estimated organic carbon sequestration rates (Tg CO_2 yr^{-1}) of tidal flat in Global scale.

6.3. Future research directions

This study examined the spatiotemporal distribution and fate of sedimentary organic carbon of tidal flat ecosystems in the Yellow Sea. The scale used in the present study was effective for assessing organic carbon stocks and carbon sequestration rates in coastal sediments. However, the involved mechanisms must be investigated to elucidate the fate of carbon in tidal flat ecosystems. To elucidate the fate of carbon, four biogeochemical mechanisms should be studied, including allochthonous deposition, tidal flushing, redox condition, and plant-microbe interactions in tidal flat ecosystem.

The deposition of allochthonous particles increases the elevation of the area, and enhances tidal flat resilience against sea-level rise, while stabilizing organic matter against decomposition (Yang et al., 2014). Deposited terrestrial and marine particles contribute different quantities of organic matter, mineral, and microbial communities to sediments, thus increasing complexity. Deposited organic matter increases sedimentary carbon and stimulates respiration in surface sediments, reducing aerobic decomposition.

Tidal flushing, including water content and movement, influences decomposition by changing the geochemical environment (Liu and Lee, 2006). In tidal flats, the water level and chemistry change across the elevation gradients of intertidal flats, with flushed sediments occurring near creekbanks and drier conditions. Tides and evapotranspiration affect sediment moisture and salinity, thus influencing the extent to which organic matter decomposes. Higher water content in sediments causes desorption and increases microbial access to organic matter; however, the accumulation of metabolites in flushing tides inhibits activity.

Redox conditions vary with tidal inundation across elevation gradients in intertidal wetlands (Freeman et al., 2004). Oscillating redox conditions affect surface sediment in tidal flats ecosystems. Pore-water advection, root oxygen loss, and bioturbation enhance the depth of oxygen penetration, increasing decomposition through aerobic respiration. Deeper sediments are more anaerobic, favoring preservation.

Plant communities accumulate sedimentary organic carbon via sediment trapping and primary production, and affect decomposition by creating dynamic environments (Spivak et al., 2019). As a result, plant communities influence the composition of organic matter available to microbes, as well as the chemical and physical environment. Microbes incorporating plant root-derived organic carbon or oxygen contribute to carbon decomposition in different ways, including nutrient mineralization. Although plant-microbe interactions are limited to the plant rooting zone, their effects on the transformation of organic matter might determine whether deposited organic carbon is stored for millennia. When considering these four biogeochemical mechanisms, it is necessary to investigate three key carbon sequestration processes in tidal flats: 1) burial of halophyte litter, 2) lateral transport between ecosystems, and 3) heterotrophic respiration (Figure 6.4).

Current knowledge gaps limit the development of realistic carbon flux models between sedimentary organic carbon and the ecosystem. Methodological and computational advances are required to advance scientific understanding of how sedimentary organic carbon is characterized in terms of its reactivity and sources. To build knowledge, specific steps are required, such as adopting standardized field methodologies (e.g., Blue Carbon Initiative), contextualizing sediment (e.g., grain size and mineralogy), biogeochemical (e.g., organic matter decomposition and pore-water chemistry), and ecological (e.g., plant-microbe interactions) properties. Such steps would allow us to synthesize climatic, environmental, and disturbance gradients more effectively, facilitating the evaluation of organic carbon. The involved biogeochemical mechanisms must first be elucidated to improve carbon cycle models and, therefore, support ecosystem management efficiently. BCEs provide ecosystem services by buffering communities from storms, providing habitats that support recreational and commercial fisheries, and sequestering CO_2 in sediments (Macreadie et al., 2021). Thus, accordingly, it is necessary to examine the biogeochemical mechanisms affecting the carbon dynamics in tidal flat ecosystem, which have potential as a BCEs, as demonstrated in this thesis.

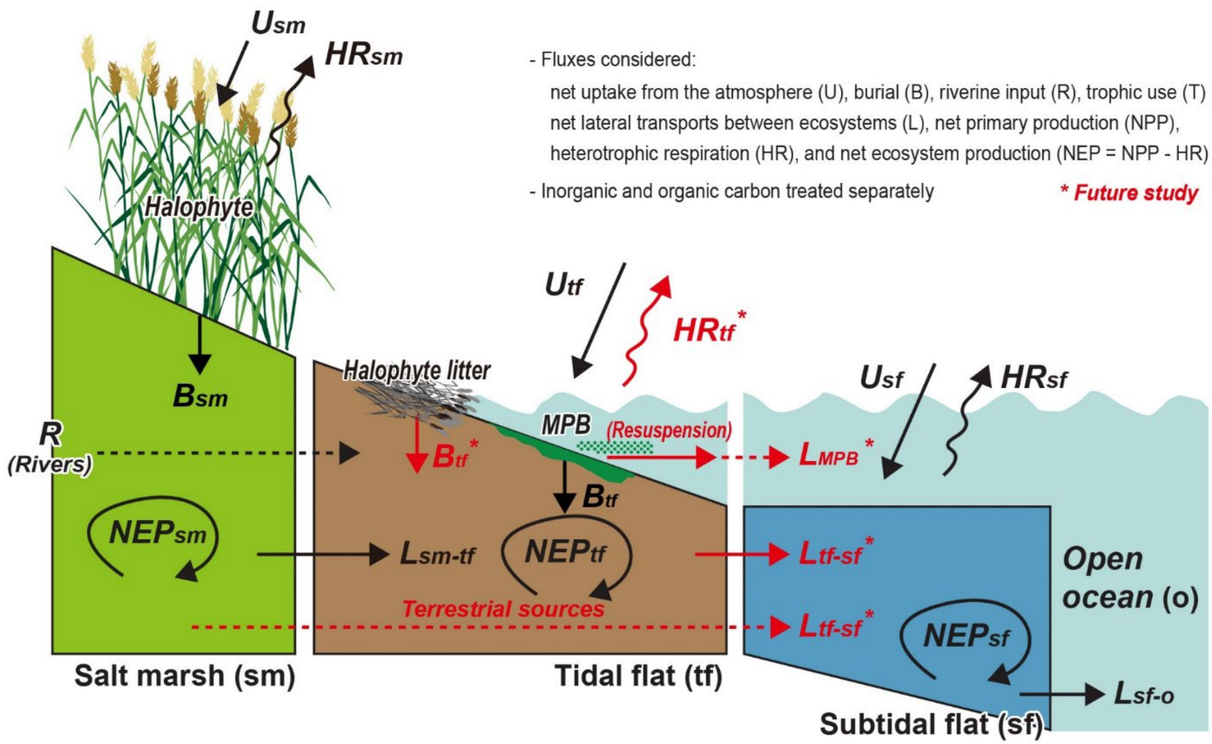

Figure 6.4.
Future directions of the present study. Conceptual diagram for carbon balance of coastal ecosystem. The relevant fluxes are uptake of atmosphere (U), burial (B), riverine input (R), trophic use (T), net lateral transports (L) between ecosystems. Subscripts sm, tf, and sf represent salt marsh, tidal flat, and subtidal flat, respectively.

BIBLIOGRAPHY

Alongi, D. M., Carbon cycling and storage in mangrove forests. *Ann. Rev. Mar. Sci.* 2014, **6**, 195–219.

Anderson, K., Peters, G. The trouble with negative emissions. *Science.* 2016, **354** (6309), 182−183.

Appleby, P. G., Oldfieldz, F. The assessment of ^{210}Pb data from sites with varying sediment accumulation rates. *Hydrobiologia.* 1983, **103**, 29–35.

Ayres, D. R., Smith, D. L., Zaremba, K., Klohr, S., Strong, D. R. Spread of exotic cordgrasses and hybrids (*Spartina* sp.) in the tidal marshes of San Francisco Bay, California, USA. *Biol. Invasions.* 2004, **6**, 221-231.

Bae, H., Lee, J. H., Song, S. J., Park, J., Kwon, B. -O., Hong, S., Ryu, J., Choi, K., Khim, J. S. Impacts of environmental and anthropogenic stresses on macrozoobenthic communities in Jinhae Bay, Korea. *Chemosphere.* 2017, **171**, 681–691.

Barbier, E. B., Hacker, S. D., Kennedy, C., Koch, E. W., Stier, A. C., Silliman, B. R. The value of estuarine and coastal ecosystem services. *Ecol. Monogr.* 2011, **81(2)**, 169−193.

Barth, J. A., Veizer, J., Mayer, B. Origin of particulate organic carbon in the upper St. Lawrence: isotopic constraints. *Earth Planet. Sci. Lett.* 1998, **162,** 111–121.

Bergamaschi, B. A., Tsamakis, E., Keil, R. G., Eglinton, T. I., Montluçon, D. B., Hedges, J. I. The effect of grain size and surface area on organic matter, lignin and carbohydrate concentration, and molecular compositions in Peru Margin sediments. *Geochim. Cosmochim. Acta.* 1997, **61,** 1247–1260.

Bohlin, H. S., Mörth, C. -M., Holm, N. G. Point source influences on the carbon and nitrogen geochemistry of sediments in the Stockholm inner archipelago, Sweden. *Sci. Total Environ.* 2006, **366**, 337–349.

Bouillon, S., Borges, A. V., Castañeda-Moya, E., Diele, K., Dittmar, T., Duke, N. C., Kristensen, E., Lee, S.Y., Marchand, C., Middelburg, J. J., Rivera-Monroy, V. H. Mangrove production and carbon sinks: a revision of global budget estimates. *Global Biogeochem. Cycles.* 2008, **22 (2)**.

Bu, N. S., Qu, J. F., Li, G., Zhao, B., Zhang, R. J., Fang, C. M. Reclamation of coastal salt marshes promoted carbon loss from previously-sequestered soil carbon pool. *Ecol. Eng.* 2015, **81**, 335–339.

Buchanan, J. B. Sediment analysis. In: Holme, N.A., McIntyre, A.D. (Eds.), Methods for the Study of Marine Benthos. *Blackwell, Oxford.* 1984, 41–65.

Buckley, Y. M., Han, Y. Managing the side effects of invasion control. *Science.* 2014, **344**, 975–976.

Burdige, D. J. Preservation of organic matter in marine sediments: controls, mechanisms, and an imbalance in sediment organic carbon budgets? *Chem. Rev.* 2007, **107**, 467–485.

Caccia, V. L., Boyer, J. N. A nutrient loading budget for Biscayne Bay, Florida. *Mar. Pollut. Bull.* 2007, **57 (7)**, 994–1008.

Cha, H. J., Lee, C. B., Kim, B. S., Choi, M. S., Ruttenberg, K.C. Early diagenetic redistribution and burial of phosphorus in the sediments of the southwestern East Sea (Japan Sea). *Mar. Geol.* 2005, **216 (3)**, 127–143.

Chausson, A., Turner, B., Seddon, D., Chabaneix, N., Girardin, C. A., Kapos, V., Seddon, N. Mapping the effectiveness of nature-based solutions for climate change adaptation. *Glob Chang Biol.* 2020, **26(11)**, 6134−6155.

Chen, J., Wang, D., Li, Y., Yu, Z., Chen, S., Hou, X., White, J.R., Chen, Z. The carbon stock and sequestration rate in tidal flats from coastal china. *Global Biogechem. Cycles.* 2020, **34 (11)**, e2020GB006772.

Chen, J., Wang, L., Li, Y., Zhang, W., Fu, X., Le, Y. Effect of *Spartina alterniflora* invasion and its controlling technologies on soil microbial respiration of a tidal wetland in Chongming Dongtan, China. *Ecol. Eng.* 2012, **41**, 52-59.

Chen, Q., Xu, G., Zhang, S., Ma, K. Consumption of an exotic plant (*Spartina alterniflora*) by the macrobenthic fauna in a mangrove wetland at Zhanjiang, China. *Wetlands*. 2018, **38**, 327-335.

Chen, S., Chmura, G. L., Wang, Y., Yu, D., Ou, D., Chen, B., Ye, Y., Chen, G. Benthic microalgae offset the sediment carbon dioxide emission in subtropical mangrove in cold seasons. *Limnol. Oceanogr.* **2019**, 64, 1297–1308,

Chen, W., Ge, Z. -M., Fei, B. -L., Zhang, C., Liu, Q. -X., Zhang, L. -Q. Soil carbon and nitrogen storage in recently restored and mature native *Scirpus* marshes in the Yangtze Estuary, China: Implications for restoration. *Ecol. Eng.* 2017, **104**, 150–157.

Chen, Y., Dong, J., Xiao, X., Zhang, M., Tian, B. O., Zhou, Y., Ma, Z. Land claim and loss of tidal flats in the Yangtze Estuary. *Sci Rep.* 2016, **6 (1)**, 24018.

Cheng, X., Peng, R., Chen, J., Luo, Y., Zhang, Q., An, S., Li, B. CH_4 and N_2O emissions from *Spartina alterniflora* and *Phragmites australis* in experimental mesocosms. *Chemosphere*. 2007, **68**, 420–427

Chmura, G. L., Anisfeld, S. C., Cahoon, D. R., Lynch, J. C. Global carbon sequestration in tidal, saline wetland soils. *Global Biogeochem. Cycles*. 2003, **17(4)**.

Cho, J. H., Park, N. J., Kim, K. H. Distributions and pollution history of heavy metals in Nakdong estuary sediments. *Ocean Sci. J.* 2000, **5 (4)**, 285–294.

Choi, J.-K., Eom, J., Ryu, J.-H. Spatial relationships between surface sedimentary facies distribution and topography using remotely sensed data: Example from the Ganghwa tidal flat, Korea. *Mar. Geol.* 2011, **280**, 205–211,

Choi, K. Morphology, sedimentology and stratigraphy of Korean tidal flats–Implications for future coastal managements. *Ocean. Coast. Manag.* 2014, **102**, 437–448,

Choi, Y.R. Modernization, development and underdevelopment: reclamation of Korean tidal flats, 1950s–2000s. Ocean Coast. Manage. 2014, **102**, 426–436.

Chuine, I., Morin, X., Sonié, L., Collin, C., Fabreguettes, J., Degueldre, D., Roy, J. Climate change might increase the invasion potential of the alien C_4 grass *Setaria parviflora* (Poaceae) in the Mediterranean Basin. *Divers. Distrib.* 2012, **18**, 661–672.

Ciais, P., Sabine, C., Govindasamy, B., Bopp, L., Brovkin, V., Canadell, J., Chhabra, A., DeFries, R., Galloway, J., Heimann, M., Jones, C., Le Quéré, C., Myneni, R., Piao, S., and Thornton, P. Chapter 6: Carbon and Other Biogeochemical Cycles. In: *Climate Change 2013 The Physical Science Basis*, Stocker, T., Qin, D., and Platner, G.-K., *Cambridge University Press, Cambridge*. 2013.

Civille, J. C. Invasion ecology and pattern assessed through remote sensing: *Spartina alterniflora* in Willapa Bay, Washington. *University of California, Davis*. 2006.

Collins, D. S., Avdis, A., Allison, P.A., Johnson, H.D., Hill, J., Piggott, M.D., Hassan, M.H.A., Damit, A.R. Tidal dynamics and mangrove carbon sequestration during the Oligo–Miocene in the South China Sea. *Nat. Commun.* 2017, **8 (1)**, 1–12.

Couch, C. A. Carbon and nitrogen stable isotopes of meiobenthos and their food resources. Estuar. *Coast. Shelf Sci.* 1989, **28**, 433-441.

Dalrymple, R. W., Choi, K.S. Sediment transport by tides, in Middleton, G.V., ed., Encyclopedia of Sediments and Sedimentary Rocks: Kluwer Academic Publishers, 2003, 606–609.

Danovaro, R., Fabiano, M., Boyer, M. Seasonal changes of benthic bacteria in a seagrass bed (*Posidonia oceanica*) of the Ligurian Sea in relation to origin, composition and fate of the sediment organic matter. *Mar. Biol.* 1994, **119**, 489–500.

Dauwe, B., Middelburg, J.J., Herman, P.M. Effect of oxygen on the degradability of organic matter in subtidal and intertidal sediments of the North Sea area. *Mar. Ecol. Prog. Ser.* 2001, **215**, 13−22.

Davidson, N. C., Finlayson, C. M. Updating global coastal wetland areas presented in Davidson and Finlayson (2018). *Mar. Freshw. Res.* 2019, **70** (8), 1195–1200.

Dlugokencky, E. and Tans, P. Trends in atmospheric carbon dioxide, National Oceanic & Atmospheric Administration. *Earth System Research Laboratory (NOAA/ESRL)*. 2019.

Duarte, C. M., Losada, I. J., Hendriks, I. E., Mazarrasa, I., Marbà, N. The role of coastal plant communities for climate change mitigation and adaptation. *Nat Clim Chang.* 2013, **3** (11), 961−968.

Duarte, C. M., Marbà, N., Gacia, E., Fourqurean, J. W., Beggins, J., Barrón, C., Apostolaki, E. T. Seagrass community metabolism: Assessing the carbon sink capacity of seagrass meadows. *Global Biogeochem. Cycles.* 2010, **24**.

Duarte, C. M., Middelburg, J. J., Caraco, N. Major role of marine vegetation on the oceanic carbon cycle. *Biogeosciences.* 2005, **2**, 1–8.

EI-Hussieny, S. A., Ismail, I. M. Role of *Avicennia marina* (Forssk.) Vierh. of South Sinai, Egypt in atmospheric CO_2 sequestration. *Int. J. Sci. Res.* 2015, **6**, 1935–1946.

Emery, H. E., Fulweiler, R. W. *Spartina alterniflora* and invasive *Phragmites australis* stands have similar greenhouse gas emissions in a New England marsh. *Aquat. Bot.* 2014, **116**, 83-92.

Flemming, B. W. A revised textural classification of gravel-free muddy sediments on the basis of ternary diagrams. *Cont. Shelf Res.* 2000, **20 (10–11)**, 1125–1137.

Flemming, B. W., Delafontaine, M.T. Mass physical properties of muddy intertidal sediments: some applications, misapplications and non-applications. *Cont. Shelf Res.* 2000, **20 (10–11)**, 1179–1197.

Freeman, C., Ostle, N. J., Fenner, N., Kang, H. A regulatory role for phenol oxidase during decomposition in peatlands. *Soil Biol. Biochem.* 2004, **36**, 1663–1667.

Friedlingstein, P., Jones, M. W., O'sullivan, M., Andrew, R. M., Hauck, J., Peters, G. P., Zaehle, S. Global carbon budget 2019. *Earth Syst. Sci. Data*. 2019, **11** (4), 1783–1838.

Friess, D. A., Yando, E. S., Alemu, J. B., Wong, L. W., Soto, S. D., Bhatia, N. Ecosystem services and disservices of mangrove forests and salt marshes. *Oceanogr. Mar. Biol.* 2020.

Galy, V., France-Lanord, C., Beyssac, O., Faure, P., Kudrass, H., Palhol, F. Efficient organic carbon burial in the Bengal fan sustained by the Himalayan erosional system. *Nature.* 2007, **450(7168)**, 407.

Graham, M., Eaves, M., Farmer, J., Dobson, J., Fallick, A. A study of carbon and nitrogen stable isotope and elemental ratios as potential indicators of source and fate of organic matter in sediments of the Forth Estuary, Scotland. *Estuar. Coast. Shelf Sci.* 2001, **52**, 375–380.

Gust, G., Mueller, V. Interfacial hydrodynamics and entrainment functions of currently used erosion devices. In Cohesive Sediments: 4th Nearshore and Estuarine Cohesive Sediment Transport Conference (eds. Parker, R., Watts, J., Burt, N.). *Wiley, USA*. 1997, 149-174.

Ha, H. K., Ha, H. J., Seo, J. Y., Choi, S. M. Effects of vegetation and fecal pellets on the erodibility of cohesive sediments: Ganghwa tidal flat, west coast of Korea. *Environ. Pollut.* 2018, **241**, 468–474.

Heaton, T. H. Isotopic studies of nitrogen pollution in the hydrosphere and atmosphere: a review. *Chem. Geol. Isot. Geosci. Sect.* 1986, **59**, 87–102,

Hedges, J. I., Clark, W. A., Quay, P. D., Richey, J. E., Devol, A. H., Santos, M. Compositions and fluxes of particulate organic material in the Amazon River. *Limnol. Oceanogr.* 1986, **31**, 717–738.

Hedges, J. I., Keil, R. G. Sedimentary organic matter preservation: an assessment and speculative synthesis. *Mar. Chem.* 1995, **49**, 81–115.

Hedges, J. I., Keil, R. G., Benner, R. What happens to terrestrial organic matter in the ocean? *Org. Geochem.* 1997, **27**, 195–212.

Hedges, J. I., Parker, P. L., 1976. Land-derived organic matter in surface sediments from the Gulf of Mexico. Geochim. Cosmochim. Acta. 40: 1019-1029,

Heiri, O., Lotter, A. F., Lemcke, G. Loss on ignition as a method for estimating organic and carbonate content in sediments: reproducibility and comparability of results. *J. Paleolimnol.* 2001, **25**, 101-110.

Hersbach, H., Bell, B., Berrisford, P., Biavati, G., Horányi, A., Muñoz Sabater, J., Thépaut, J. N. ERA5 monthly averaged data on single levels from 1979 to present. *Copernicus Climate Change Service (C3S) Climate Data Store (CDS)*. 2019.

Himes-Cornell, A., Grose, S. O., Pendleton, L. Mangrove ecosystem service values and methodological approaches to valuation: where do we stand? *Front. Mar. Sci.* 2018, **376**.

Hong, S., Khim, J. S., Park, J., Kim, M., Kim, W. -K., Jung, J., Hyun, S., Kim, J. -G., Lee, H., Choi, H. J. In situ fate and partitioning of waterborne perfluoroalkyl acids (PFAAs) in the Youngsan and Nakdong River Estuaries of South Korea. *Sci. Total Environ.* 2013, **445**, 136–145.

Hong, S., Lee, Y., Yoon, S. J., Lee, J., Kang, S., Won, E. -J., Hur, J., Khim, J.s., Shin, K. -H. Carbon and nitrogen stable isotope signatures linked to anthropogenic toxic substances pollution in a highly industrialized area of South Korea. *Mar. Pollut. Bull.* 2019, **144**, 152–159.

Hovenden, M., Newton, P. Plant responses to CO_2 are a question of time. Science. 2018, **360**, 263–264.

Howard J, Sutton-Grier A, Herr D, Kleypas J, Landis E, Mcleod E, Simpson S. Clarifying the role of coastal and marine systems in climate mitigation. *Front. Ecol. Environ.* 2017, **15**, 42–50.

Howard, J., Hoyt, S., Isensee, K., Telszewski, M., Pidgeon, E. Coastal blue carbon: methods for assessing carbon stocks and emissions factors in mangroves, tidal salt marshes, and seagrasses. *International Union for Conservation of Nature (IUCN)*. 2014.

IPCC (Intergovernmental Panel on Climate Change). Climate change 2007: the physical science basis. In: *Contribution of Working Group I to the Fourth Assessment Report of the Intergovernmental Panel on Climate Change*. Solomon S, Qin D, Manning M. *Cambridge University Press*. 2007.

Jeong, K. S., Cho, J. H., Lee, J. H., Kim, K. H. Accumulation history of anthropogenic heavy metals (Cu, Zn, and Pb) in Masan Bay sediments, southeastern Korea: A role of chemical front in the water column. *Geosci. J.* 2006, **10 (4)**, 445–455.

Joh, G. Species diversity of the old genus *Navicula Bory* (Bacillariophyta) on intertidal sand-flats in the Nakdong River estuary, Korea. *J. Ecol. Environ.* 2013, **36(4)**, 371−390.

Joos, F., Spahni, R. Rates of change in natural and anthropogenic radiative forcing over the past 20,000 years. *Proc. Natl. Acad. Sci. U.S.A.* 2008, **105** (5), 1425–1430.

Kang, C. K., Kang, Y. S., Choy, E. J., Kim, D. S., Shim, B. T., Lee, P. Y. Condition, reproductive activity, and gross biochemical composition of the Manila clam, *Tapes philippinarum* in natural and newly created sandy habitats of the southern coast of Korea. *J. Shellfish Res*. 2007, **26 (2)**, 401−413.

Kang, C. K., Kim, J. B., Lee, K. S., Kim, J. B., Lee, P. Y., Hong, J. S. Trophic importance of benthic microalgae to macrozoobenthos in coastal bay systems in Korea: dual stable C and N isotope analyses. *Mar. Ecol. Prog. Ser.* 2003, **259**, 79–92.

Kang, C. K., Lee, Y. W., Choy, E. J., Shin, J. K., Seo, I. S., Hong, J. S. Microphytobenthos seasonality determines growth and reproduction in intertidal bivalves. *Mar. Ecol. Prog. Ser.* 2006, **315**, 113–127.

Kang, X., Song, J., Yuan, H., Li, X., Li, N., Duan, L. The sources and composition of organic matter in sediments of the Jiaozhou Bay: implications for environmental changes on a centennial time scale. *Acta. Oceanol. Sin.* 2017, **36**, 68–78.

Keil, R. G., Hedges, J. I. Sorption of organic matter to mineral surfaces and the preservation of organic matter in coastal marine sediments. *Chem. Geol.* 1993, **107 (3–4)**, 385–388.

Keil, R. G., Tsamakis, E., Giddings, J. C., Hedges, J. I. Biochemical distributions (amino acids, neutral sugars, and lignin phenols) among size-classes of modern marine sediments from the Washington coast. *Geochim. Cosmochim. Acta.* 1998, **62**, 1347–1364.

Kelleway, J. J., Saintilan, N., Macreadie, P. I., Ralph, P. J. Sedimentary factors are key predictors of carbon storage in SE Australian saltmarshes. *Ecosystems.* 2016, **19 (5)**, 865–880.

Kemp, A. C., Vane, C. H., Horton, B. P., Engelhart, S. E., Nikitina, D. Application of stable carbon isotopes for reconstructing salt-marsh floral zones and relative sea level, New Jersey, USA. *J. Quat. Sci.* 2012, **27**, 404–414.

Kennedy, H., Beggins, J., Duarte, C.M., Fourqurean, J.W., Holmer, M., Marbà, N., Middelburg, J.J. Seagrass sediments as a global carbon sink: Isotopic constraints. *Global. Biogeochem. Cycles.* 2010, **24**.

Kim, J., Lee, J., Yun, J., Yang, Y., Ding, W., Yuan, J., Kang, H. Mechanisms of enhanced methane emission due to introduction of *Spartina anglica* and *Phragmites australis* in a temperate tidal salt marsh. *Ecol. Eng.* 2020, **153**, 105905.

Kim, Y. H., Hong, S., Song, Y. S., Lee, H., Kim, H. -C., Ryu, J., Park, J., Kwon, B.-O., Lee, C.-H., Khim, J.S. Seasonal variability of estuarine dynamics due to freshwater discharge and its influence on biological productivity in Yeongsan River Estuary, Korea. *Chemosphere.* 2017, **181**, 390-399.

Koh, C. H., Khim, J. S. The Korean tidal flat of the Yellow Sea: Physical setting, ecosystem and management. *Ocean Coast. Manage.* 2014, **102**, 398–414.

Korea Marine Environment Management Corporation (KOEM). Korea Marine Environment Preservation-Restoration of Marine Ecosystem. 2019.

Krause-Jensen, D., Duarte, C. M. Substantial role of macroalgae in marine carbon sequestration. *Nat. Geosci.* 2016, **9**, 737–742.

Krishna, M. S., Naidu, S. A., Subbaiah, C. V., Sarma, V. V. S. S., Reddy, N. P. C. Distribution and sources of organic matter in surface sediments of the eastern continental margin of India. *J. Geophys. Res.* 2013, **118 (4)**, 1484–1494.

Krishnaswamy, S., Lal, D., Martin, J. M., Meybeck, M. Geochronology of lake sediments. *Earth Planet. Sc. Lett.* 1971, **11**, 407–414.

Kubo, A., Kanda, J. Seasonal variations and sources of sedimentary organic carbon in Tokyo Bay. *Mar. Pollut. Bull.* 2017, **114 (2)**, 637–643.

Kwon, B. -O., Kim, H. -C., Koh, C. -H., Ryu, J., Son, S., Kim, Y. H., Khim, J. S. Development of temperature-based algorithms for the estimation of microphytobenthic primary production in a tidal flat: A case study in Daebu mudflat, Korea. *Environ. Pollut.* 2018, **241**, 115–123.

Kwon, B. -O., Kim, H., Noh, J., Lee, S. Y., Nam, J., Khim, J. S. Spatiotemporal variability in microphytobenthic primary production across bare intertidal flat, saltmarsh, and mangrove forest of Asia and Australia. Mar. Pollut. Bull. 2020, **151**, 110707.

Lamb, A. L., Wilson, G. P., Leng, M. J. A review of coastal palaeoclimate and relative sea-level reconstructions using $\delta^{13}C$ and C/N ratios in organic material. *Earth-Sci. Rev.* 2006, **75**, 29–57.

Lampert, A., Hastings, A., Grosholz, E. D., Jardine, S. L., Sanchirico, J. N. Optimal approaches for balancing invasive species eradication and endangered species management. *Science.* 2014, **344**, 1028−1031.

Lee, I. O., Noh, J., Lee, J., Kim, B., Hwang, K., Kwon, B. O., Khim, J. S. Stable isotope signatures reveal the significant contributions of microphytobenthos and saltmarsh-driven nutrition in the intertidal benthic food webs. *Sci. Total Environ.* 2021, **756**, 144068.

Lee, J., Park, K.-T., Lim, J.-H., Yoon, J.-E., Kim, I.-N., 2018. Hypoxia in Korean coastal waters: a case study of the natural Jinhae Bay and artificial Shihwa Bay. Front. Mar. Sci. 5, 70

Lee, J., Kwon, B.-O., Kim, B., Noh, J., Hwang, K., Ryu, J., Park, J., Hong, S., Khim, J. S. Natural and anthropogenic signatures on sedimentary organic matters across varying intertidal habitats in the Korean waters. *Environ. Int.* 2019, **133**, 105166.

Lee, J., Kim, B., Noh, J., Lee, C., Kwon, I., Kwon, B. O., Ryu, J., Park, J., Hong, S., Lee, S., Kim, S. -G., Son, S., Yoon, H. J., Yim, J., Nam, J., Choi, K., Khim, J. S. The first national scale evaluation of organic carbon stocks and sequestration rates of coastal sediments along the West Sea, South Sea, and East Sea of South Korea. *Sci. Total Environ.* 2021, **793**, 148568.

Lee, M., Kim, S., Jung, H. Distribution patterns of halophytes in the coastal area in Korea. *Ocean Sci. J.* 2019, **24**, 139-159.

Lee, Y., Hong, S., Kim, M. S., Kim, D., Choi, B. H., Hur, J., Khim, J. S., Shin, K. H. Identification of sources and seasonal variability of organic matter in Lake Sihwa and surrounding inland creeks, South Korea. *Chemosphere.* 2017, **177**, 109–119.

Leonard, L. A., Croft, A. L. The effect of standing biomass on flow velocity and turbulence in *Spartina alterniflora* canopies. *Estuar. Coast. Shelf Sci.* 2006, **69**, 325–336.

Li, H., Zhang, L. An experimental study on physical controls of an exotic plant *Spartina alterniflora* in Shanghai, China. *Ecol. Eng.* 2008, **32**, 11–21.

Liao, C., Peng, R., Luo, Y., Zhou, X., Wu, X., Fang, C., Li, B. Altered ecosystem carbon and nitrogen cycles by plant invasion: a meta-analysis. *New Phytol.* 2008, **177**, 706–714.

Lim, D. I., Jung, H. S., Kim, K. T., Shin, H. H., Jung, S. W. Sedimentary records of metal contamination and eutrophication in Jinhae-Masan Bay, Korea. *Mar. Pollut. Bull.* 2012, **64 (11)**, 2542–2548.

Lim, H. S., Diaz, R. J., Hong, J. S., Schaffner, L. C. Hypoxia and benthic community recovery in Korean coastal waters. *Mar. Pollut. Bull.* 2006, **52 (11)**, 1517–1526.

Lin, W. J., Wu, J., Lin, H. J. Contribution of unvegetated tidal flats to coastal carbon flux. *Glob Chang Biol*. 2020, **26 (6)**, 3443–3454.

Liu, J., Zhou, H., Qin, P., Zhou, J. Effects of *Spartina alterniflora* salt marshes on organic carbon acquisition in intertidal zones of Jiangsu Province, China. *Ecol. Eng.* 2007, **30**, 240–249.

Liu, J. E., Han, R. M., Su, H. R., Wu, Y. P., Zhang, L. M., Richardson, C. J., Wang, G. X. Effects of exotic *Spartina alterniflora* on vertical soil organic carbon distribution and storage amount in coastal salt marshes in Jiangsu, China. *Ecol. Eng.* 2017, **106**, 132–139.

Liu, M., Mao, D., Wang, Z., Li, L., Man, W., Jia, M., Zhang, Y. Rapid invasion of *Spartina alterniflora* in the coastal zone of mainland China: new observations from Landsat OLI images. *Remote Sens.* 2018, **10**, 1933.

Liu, M., Hou, L., Xu, S., Ou, D., Yang, Y., Yu, J., Wang, Q. Organic carbon and nitrogen stable isotopes in the intertidal sediments from the Yangtze Estuary, China. *Mar. Pollut. Bull.* 2006, **52**, 1625–1633.

Liu, S., Jiang, Z., Zhang, J., Wu, Y., Lian, Z., Huang, X. Effect of nutrient enrichment on the source and composition of sediment organic carbon in tropical seagrass beds in the South China Sea. *Mar. Pollut. Bull.* 2016, **110 (1)**, 274–280.

Liu, Z., Lee, C. Drying effects on sorption capacity of coastal sediment: the importance of architecture and polarity of organic matter. *Geochim. Cosmochim. Acta.* 2006, **70**, 3313–3324.

Lorenzen, C. J. Determination of chlorophyll and pheo-pigments: spectrophotometric equations. *Limnol. Oceanogr.* 1967, **12**, 343–346.

Lovelock, C. E., Atwood, T., Baldock, J., Duarte, C. M., Hickey, S., Lavery, P. S., Steven, A. Assessing the risk of carbon dioxide emissions from blue carbon ecosystems. *Front. Ecol. Environ.* 2017, **15**, 257–265.

Lovelock, C. E., Duarte, C. M. Dimensions of blue carbon and emerging perspectives. *Biol. Lett.* 2019, **15** (3), 20180781.

Lu, Q., Bai, J., Zhang, G., Zhao, Q., Wu, J. Spatial and seasonal distribution of carbon, nitrogen, phosphorus, and sulfur and their ecological stoichiometry in wetland soils along a water and salt gradient in the Yellow River Delta, China. *Phys. Chem. Earth.* 2018, **104**, 9–17.

Macreadie, P. I., Atwood, T. B., Seymour, J. R., Fontes, M. S., Sanderman, J., Nielsen, D. A., Connolly, R. M. Vulnerability of seagrass blue carbon to microbial attack following exposure to warming and oxygen. *Sci. Total Environ.* 2019, **686**, 264–275.

Macreadie, P. I., Costa, M. D., Atwood, T. B., Friess, D. A., Kelleway, J. J., Kennedy, H., Duarte, C. M. Blue carbon as a natural climate solution. *Nat. Rev. Earth Environ.* 2021, **2** (12), 826–839.

Magni, P., Montani, S. Development of benthic microalgal assemblages on an intertidal flat in the Seto Inland Sea, Japan: effects of environmental variability. *La mer.* 1997, **35**, 137–148.

Maksymowska, D., Richard, P., Piekarek-Jankowska, H., Riera, P. Chemical and isotopic composition of the organic matter sources in the Gulf of Gdansk (Southern Baltic Sea). *Estuar. Coast. Shelf Sci.* 2000, **51 (5)**, 585-598.

Mao, R., Ye, S. -Y., Zhang, X. -H. Soil-aggregate-associated organic carbon along vegetation zones in tidal salt marshes in the Liaohe Delta. *Clean (Weinh).* 2018, **46**, 1800049.

Mao, Z., Gu, X., Liu, J., Ren, L., Wang, G. Distribution of the soil enzyme activities in different vegetation zones and farms in Yancheng coastal wetland. *Acta. Ecol. Sin.* 2010, **30**, 5043–5049.

Mayer, L. M. Relationships between mineral surfaces and organic carbon concentrations in soils and sediments. *Chem. Geol.* 1994, **114**, 347–363.

Mayer, L. M. Surface area control of organic carbon accumulation in continental shelf sediments. *Geochim. Cosmochim. Ac.* 1994, **58 (4)**, 1271–1284.

McLaren, D. A comparative global assessment of potential negative emissions technologies. *Process Saf. Environ. Prot.* 2012, **90** (6), 489–500.

Mcleod, E., Chmura, G. L., Bouillon, S., Salm, R., Björk, M., Duarte, C. M., Lovelock, C. E., Schlesinger, W. H., Silliman, B. R. A blueprint for blue carbon: toward an improved understanding of the role of vegetated coastal habitats in sequestering CO_2. *Front. Ecol. Environ.* 2011, **9 (10)**, 552–560.

Meyers, P. A. Preservation of elemental and isotopic source identification of sedimentary organic matter. *Chem. Geol.* 1994, **114**, 289–302.

Middelburg, J. J., Nieuwenhuize, J. Carbon and nitrogen stable isotopes in suspended matter and sediments from the Schelde Estuary. *Mar. Chem.* 1998, **60**, 217–225.

Milliman, J. D., Qinchun, X., Zuosheng, Y. Transfer of particulate organic carbon and nitrogen from the Yangtze River to the ocean. *Am. J. Sci.* 1984, **284**, 824–834.

Mohamed, E. S., Abu-hashim, M., AbdelRahman, M. A., Schütt, B., Lasaponara, R. Evaluating the effects of human activity over the last decades on the soil organic carbon pool using satellite imagery and GIS techniques in the Nile Delta Area, Egypt. *Sustainability.* 2019, **11 (9)**, 2644.

Montani, S., Magni, P., Abe, N. Seasonal and interannual patterns of intertidal microphytobenthos in combination with laboratory and areal production estimates. *Mar. Ecol. Prog. Ser.* 2003, **249**, 79-91.

Mou, X. -J., Sun, Z. -G., Liu, X. -T. Storage and vertical distribution characteristics of carbon and nitrogen in different *Suaeda salsa* marsh soils of the Yellow River estuary. Chinese Journal of Soil Science. 2012, **43**, 1444–1449.

Murray, N. J., Phinn, S. R., DeWitt, M., Ferrari, R., Johnston, R., Lyons, M. B., Fuller, R. A. The global distribution and trajectory of tidal flats. *Nature*, 2019, **565 (7738)**, 222–225.

National Atlas of Korea II (NGII). Gyeonggi-do, Korea: National Geographic Information Institute (NGII), 2016, 166–183.

Nellemann, C., Corcoran, E., Duarte, C. M., De Young, C., Fonseca, L. E., Grimsdith, G. Blue carbon: the role of healthy oceans in binding carbon. 2010

Nesshöver, C., Assmuth, T., Irvine, K. N., Rusch, G. M., Waylen, K. A., Delbaere, B., Wittmer, H. The science, policy and practice of nature-based solutions: An interdisciplinary perspective. *Sci. Total Environ.* 2017, **579**, 1215–1227.

Noh, J., Yoon, S. J., Kim, H., Lee, C., Kwon, B. -O., Lee, Y., Hong, S., Kim, J., Ryu, J., Khim, J. S. Anthropogenic influences on benthic food web dynamics by interrupted freshwater discharge in a closed Geum River estuary, Korea. *Environ. Int.* 2019, **131**, 104981

Park, H.J., Kwak, J.H., Kang, C.K., 2015. Trophic consistency of benthic invertebrates among diversified vegetational habitats in a temperate coastal wetland of Korea as determined by stable isotopes. Estuar. Coast. 38(2): 599-611.,

Park, H. J., Kwak, J. H., Lee, Y. -J., Kang, H. Y., Choy, E. J., Kang, C. -K. Trophic Structures of Two Contrasting Estuarine Ecosystems With and without a Dike on the Temperate Coast of Korea as Determined by Stable Isotopes. *Estuar. Coast.* 2019, **43(3)**, 560–577.

Park, J., Song, S. J., Ryu, J., Kwon, B. O., Hong, S., Bae, H., Khim, J. S. Macrozoobenthos of Korean tidal flats: A review on species assemblages and distribution. *Ocean Coast. Manag.* 2014, **102**, 483–492.

Park, J., Kwon, B. -O., Kim, M., Hong, S., Ryu, J., Song, S. J., Khim, J. S. Microphytobenthos of Korean tidal flats: A review and analysis on floral distribution and tidal dynamics. *Ocean. Coast. Manag.* 2014, 102, 471–482.

Park, S. C., Lee, K. W. Modern sedimentary environment of Jinhae Bay, SE Korea. *Ocean Sci. J.* 1996, **31 (2)**, 43–54.

Park, S. -C., Yoo, D. -G., Lee, K. -W., Lee, H. -H. Accumulation of recent muds associated with coastal circulations, southeastern Korea Sea (Korea Strait). *Quat. Int.* 1999, **19 (5)**, 589–608.

Pendleton, L., Donato, D. C., Murray, B. C., Crooks, S., Jenkins, W. A., Sifleet, S., Baldera, A. Estimating global "blue carbon" emissions from conversion and degradation of vegetated coastal ecosystems. *PloS one.* 2012, **7 (9)**, e43542.

Percival, H. J., Parfitt, R. L., Scott, N. A. Factors controlling soil carbon levels in New Zealand grasslands is clay content important? *Soil. Sci. Soc. Am. J.* 2000, **64**, 1623−1630.

Peters, K., Sweeney, R., Kaplan, I. Correlation of carbon and nitrogen stable isotope ratios in sedimentary organic matter. *Limnol. Oceanogr.* 1978, **23**, 598−604.

Pidgeon, E., Austin, W., Cifuentes-Jara, M., Comstock, M., Crooks, S., Duarte, C., Elverum, C., Fourqurean, J., Hamilton, J., Herr, D., Hickey, T., Howard, J., Isensee, K., Kennedy, H., Lovelock, C., Megonigal, P. Blue carbon integrating ocean ecosystems in global climate action. *Conservation International.* 2021.

Pires, J. C. M. Negative emissions technologies: a complementary solution for climate change mitigation. *Sci. Total Environ.* 2019, **672**, 502–514.

Pradhan, U., Wu, Y., Shirodkar, P., Zhang, J., Zhang, G. Sources and distribution of organic matter in thirty-five tropical estuaries along the west coast of India-a preliminary assessment. *Estuar. Coast. Shelf Sci.* 2014, **151**, 21-33.

Qing, W. A. N. G., Shu-Qing, A. N., Zhi-Jun, M. A., Bin, Z. H. A. O., Jia-Kuan, C. H. E. N., Bo, L. I. Invasive *Spartina alterniflora*: biology, ecology and management. *J Syst Evol*. 2006, **44**, 559.

Qiu, J. China's cordgrass plan is 'overkill'. *Nature*. 2013, 499.

Rahman, A. Cliff erosion of salt marshes: experimental evaluation of the effect of vegetation characteristics and sediment properties of erodibility. *University of Twente Enschede*. 2015.

Relyea, R. A. The impact of insecticides and herbicides on the biodiversity and productivity of aquatic communities. *Ecol. Appl.* 2005, **15**, 618–627.

Riera, P., Stal, L., Nieuwenhuize, J. Heavy δ^{15}N in intertidal benthic algae and invertebrates in the Scheldt Estuary (The Netherlands): effect of river nitrogen inputs. *Estuar. Coast. Shelf Sci.* 2000, **51**, 365–372.

Rohmer, T., Kerr, D. San Francisco Estuary Invasive *Spartina* Project 2015-2016 Monitoring and Treatment Report. 2018.

Rout, M. E., Callaway, R. M. An invasive plant paradox. *Science*. 2009, **324**, 734-735.

Rumolo, P., Barra, M., Gherardi, S., Marsella, E., Sprovieri, M. Stable isotopes and C/N ratios in marine sediments as a tool for discriminating anthropogenic impact. *J. Environ. Monit.* 2011, **13**, 3399-3408.

Sage, R. F., Kubien, D. S. Quo vadis C_4? An ecophysiological perspective on global change and the future of C_4 plants. *Photosynth. Res.* 2003, **77**, 209–225.

Sanchez-Cabeza, J. A., Ruiz-Fernández, A. C. ^{210}Pb sediment radiochronology: an integrated formulation and classification of dating models. *Geochim. Cosmochim. Ac.* 2012, **82**, 183–200.

Savage, C., Leavitt, P. R., Elmgren, R. Distribution and retention of effluent nitrogen in surface sediments of a coastal bay. *Limnol. Oceanogr.* 2004, **49**, 1503–1511.

Seo, J. Y., Lim, H. S., Choi, J. W. Threshold value of Benthic Pollution Index (BPI) for a muddy healthy benthic faunal community and its application to Jinhae Bay in the southern coast of Korea. *Ocean Sci. J.* 2014, **49 (3)**, 313–328.

Seo, J. Y., Choi, S. M. Ha, H. K. Assessment of potential impact of invasive vegetation on cohesive sediment erodibility in intertidal flats. *Sci. Total Environ.* 2021, **766**, 144493.

Serrano, O., Lavery, P., Duarte, C., Kendrick, G. A., Calfat, A. M., York, P. H., Steven, A. D., Macreadie, P. I. Can mud (silt and clay) concentration be used to predict soil organic carbon content within seagrass ecosystems? *Biogeosciences.* 2016, **13**, 4915–4926.

Sheng, Q., Zhao, B., Huang, M., Wang, L., Quan, Z., Fang, C., Wu, J. Greenhouse gas emissions following an invasive plant eradication program. *Ecol. Eng.* 2014, **73**, 229−237.

Sherr, E. B. Carbon isotope composition of organic seston and sediments in a Georgia salt marsh estuary. *Geochim. Cosmochim. Acta.* 1982, **46**, 1227-1232.

Shin, W. *Spartina anglica* settlement and effect on macrofauna in the west coast of Korea. *Seoul National University.* 2018.

Sippo, J. Z., Lovelock, C. E., Santos, I. R., Sanders, C. J., Maher, D. T. Mangrove mortality in a changing climate: an overview. *Estuar. Coast. Shelf Sci.* 2018, **215**, 241–249.

Song, B., Yi, S., Nahm, W. -H., Lee, J. -Y., Yang, Z., Yang, X. Holocene environmental changes of the Songji lagoon, South Korea, and its linkage to sea level and ENSO changes. *Quat. Int.* 2019, **503**, 32–40.

Spivak, A. C., Sanderman, J., Bowen, J. L., Canuel, E. A., Hopkinson, C. S. Global-change controls on soil-carbon accumulation and loss in coastal vegetated ecosystems. *Nat. Geosci.* 2019, **12 (9)**, 685–692.

Suh, Y. J., Shin, K. -H. Size-related and seasonal diet of the manila clam (*Ruditapes philippinarum*), as determined using dual stable isotopes. *Estuar. Coast. Shelf. Sci.* 2013, **135**, 94−105.

Takai, N., Yorozu, A., Tanimoto, T., Hoshika, A., Yoshihara, K. Transport pathways of microphytobenthos-originating organic carbon in the food web of an exposed hard bottom shore in the Seto Inland Sea, Japan. *Mar. Ecol. Prog. Ser.* 2004, **284**, 97−108.

Tao, B., Wang, Y., Yu, Y., Li, Q., Luo, C., Zhang, B. Interactive effects of nitrogen forms and temperature on soil organic carbon decomposition in the coastal wetland of the Yellow River Delta, China. *Catena.* 2018, **165**, 408–41.

The Korea Ministry of Environment (KOEM). A study for ecological restoration of the Nakdong River estuary. 2015.

Thornton, S., McManus, J. Application of organic carbon and nitrogen stable isotope and C/N ratios as source indicators of organic matter provenance in estuarine systems: evidence from the Tay Estuary, Scotland. *Estuar. Coast. Shelf Sci.* 1994, **38**, 219–233.

Van Dover, C.L., Grassle, J., Fry, B., Garritt, R.H., Starczak, V.R. Stable isotope evidence for entry of sewage-derived organic material into a deep-sea food web. *Nature*. 1992, **360**, 153.

Voss, M., Larsen, B., Leivuori, M., Vallius, H. Stable isotope signals of eutrophication in Baltic Sea sediments. *J. Mar. Syst.* 2000, **25**, 287–298.

Voβ, M., Struck, U. Stable nitrogen and carbon isotopes as indicator of eutrophication of the Oder river (Baltic Sea). *Mar. Chem.* 1997, **59**, 35–49.

Wada, E., Minagawa, M., Mizutani, H., Tsuji, T., Imaizumi, R., Karasawa, K. Biogeochemical studies on the transport of organic matter along the Otsuchi River watershed, Japan. *Estuar. Coast. Shelf Sci.* 1987, **25**, 321−336.

Wan, S., Qin, P., Liu, J., Zhou, H. The positive and negative effects of exotic *Spartina alterniflora* in China. *Ecol. Eng.* 2009, **35**, 444–452.

Wang, C., Lv, Y., Li, Y. Riverine input of organic carbon and nitrogen in water-sediment system from the Yellow River estuary reach to the coastal zone of Bohai Sea, China. *Cont. Shelf Res.* 2018, **157**, 1–9.

Wang, G., Yang, W., Wang, G., Liu, J., Hang, Z. The effects of *Spartina alterniflora* seaward invasion on soil organic carbon fractions, sources and distribution. *Acta. Ecol. Sin.* 2013, **33**, 2475–2483.

Wang, G., Yang, W., Wang, G., Liu, J., Hang, Z. The effects of *Spartina alterniflora* seaward invasion on soil organic carbon fractions, sources and distribution. *Acta. Ecol. Sin.* 2013, **33**, 2475–2483.

Wang, J., Bai, J., Zhao, Q., Lu, Q., Xia, Z. Five-year changes in soil organic carbon and total nitrogen in coastal wetlands affected by flow-sediment regulation in a Chinese delta. *Sci. Rep.* 2016, **6**, 21137.

Williams, J.R., Dellapenna, T.M., Lee, G.-h. Shifts in depositional environments as a natural response to anthropogenic alterations: Nakdong Estuary, South Korea. *Mar. Geol.* 2013, **343**, 47−61.

Windham-Myers, L., Crooks, S., Troxler, T. G. A blue carbon primer: the state of coastal wetland carbon science, practice and policy. *CRC Press*. 2018.

Woo, H.J., Cho, J.H., Jeong, K.S., Chung, C.S., Kwon, S.J., Park, S.M. Pollution history of the Masan Bay, southeast Korea, from heavy metals and foraminifera in the subsurface sediments. *J. Korean Earth Sci. Soc.* 2003, **24 (7)**, 635–649.

WSDA. *Spartina* Eradication Program 2017 Progress Report. 2017.

Xiang, J., Liu, D., Ding, W., Yuan, J., Lin, Y. Invasion chronosequence of *Spartina alterniflora* on methane emission and organic carbon sequestration in a coastal salt marsh. *Atmos. Environ.* 2015, **112**, 72–80.

Xiaonan, D., Xiaoke, W., Lu, F., Zhiyun, O. Primary evaluation of carbon sequestration potential of wetlands in China. *Sheng Tai Xue Bao.* 2008, 28, 463–469.

Yamaguchi, H., Montani, S., Tsutsumi, H., Hamada, K. I., Ueda, N. Estimation of particulate organic carbon flux in relation to photosynthetic production in a shallow coastal area in the Seto Inland Sea. *Mar. Pollut. Bull.* 2003, **47(1–6)**, 18–24.

Yang, J., Gao, J., Liu, B., Zhang, W. Sediment deposits and organic carbon sequestration along mangrove coasts of the Leizhou Peninsula, southern China. *Estuar. Coast. Shelf Sci.* 2014, **136**, 3–10.

Yang, W., Zhao, H., Chen, X., Yin, S., Cheng, X., An, S. Consequences of short-term C_4 plant *Spartina alterniflora* invasions for soil organic carbon dynamics in a coastal wetland of Eastern China. Ecol. Eng. 2013, **61**, 50-57.

Yang, W., An, S., Zhao, H., Fang, S., Xia, L., Xiao, Y., Qiao, Y., Cheng, X. Labile and recalcitrant soil carbon and nitrogen pools in tidal salt marshes of the Eastern Chinese coast as affected by short-term C_4 plant *Spartina alterniflora* invasion. *Clean-Soil Air Water.* 2015, **43**, 872–880.

Yang, W., An, S., Zhao, H., Xu, L., Qiao, Y., Cheng, X. Impacts of *Spartina alterniflora* invasion on soil organic carbon andnitrogen pools sizes, stability, and turnover in a coastal salt marsh of eastern China. *Ecol. Eng.* 2016, **86**, 174–182.

Yang, W., Jeelani, N., Leng, X., Cheng, X., An, S. *Spartina alterniflora* invasion alters soil microbial community composition and microbial respiration following invasion chronosequence in a coastal wetland of China. *Sci. Rep.* 2016, **6**, 26880.

Yang, W., Zhao, H., Leng, X., Cheng, X., An, S. Soil organic carbon and nitrogen dynamics following *Spartina alterniflora* invasion in a coastal wetland of eastern China. Catena. 2017, **156**, 281–289.

Yim, J., Kwon, B.-O., Nam, J., Hwang, J.H., Choi, K., Khim, J.S. Analysis of forty years long changes in coastal land use and land cover of the Yellow Sea: The gains or losses in ecosystem services. *Environ. Pollut.* 2018, **241**, 74–84.

Yuan, J., Ding, W., Liu, D., Kang, H., Freeman, C., Xiang, J., Lin, Y. Exotic *Spartina alterniflora* invasion alters ecosystem–atmosphere exchange of CH_4 and N_2O and carbon sequestration in a coastal salt marsh in China. *Glob Chang Biol.* 2015, **21**, 1567–1580.

Yuan, J., Liu, D., Ji, Y., Xiang, J., Lin, Y., Wu, M., Ding, W. *Spartina alterniflora* invasion drastically increases methane production potential by shifting methanogenesis from hydrogenotrophic to methylotrophic pathway in a coastal marsh. *J. Ecol.* 2019, **107**, 2436–2450.

Zhang, D., Hu, Y., Liu, M., Chang, Y., Yan, X., Bu, R., Li, Z. Introduction and spread of an exotic plant, *Spartina alterniflora*, along coastal marshes of China. *Wetlands*. 2017, **37**, 1181–1193.

Zhang, H., Wu, F., Zhang, Y., Han, S., Liu, Y. Spatial and temporal changes of habitat quality in Jiangsu Yancheng Wetland National Nature Reserve-Rare birds of China. *Appl. Ecol. Environ. Res.* 2019, **17**, 4807−4821.

Zhang, T., Chen, H., Cao, H., Ge, Z., Zhang, L. Combined influence of sedimentation and vegetation on the soil carbon stocks of a coastal wetland in the Changjiang estuary. *Chin. J. Oceanol. Limnol.* 2017, **35**, 833–843.

Zhang, Y., Ding, W., Luo, J., Donnison, A. Changes in soil organic carbon dynamics in an Eastern Chinese coastal wetland following invasion by a C– plant *Spartina alterniflora*. *Soil Biol. Biochem.* 2010, **42**, 1712–1720.

Zhao, Q., Bai, J., Liu, Q., Lu, Q., Gao, Z., Wang, J. Spatial and seasonal variations of soil carbon and nitrogen content and stock in a tidal salt marsh with Tamarix chinensis, China. Wetlands. 2016, **36**, S145–S152.

Zhao, Q., Bai, J., Lu, Q., Zhang, G. Effects of salinity on dynamics of soil carbon in degraded coastal wetlands: Implications on wetland restoration. *Phys. Chem. Earth.* 2017, **97**, 12–18.

Zhao, Q., Bai, J., Lu, Q., Zhang, G., Jia, J., Wang, W., Wang, X. Effects of water and salinity regulation measures on soil carbon sequestration in coastal wetlands of the Yellow River Delta. *Geoderma.* 2018, **319**, 219–229.

Zhou, C., Zhao, H., Sun, Z., Zhou, L., Fang, C., Xiao, Y., Deng, Z., Zhi, Y., Zhao, Y., An, S. The invasion of *Spartina alterniflora* alters carbon dynamics in China's Yancheng Natural Reserve. *Clean (Weinh)*. 2015, **43**, 159–165.

Zhou, H.-X., Liu, J.-E., Zhou, J., Qin, P. Effect of an alien species *Spartina alterniflora* loisel on biogeochemical processes of intertidal ecosystem in the Jiangsu coastal region, China. *Pedosphere.* 2008, **18**, 77–85.

ABSTRACT (IN KOREAN)

전 세계적으로 염습지, 맹그로브, 잘피를 포함한 블루카본 생태계는 지구온난화가 가속화되는 상황에서 높은 이산화탄소 흡수율로 기후 변화를 완화하는데 중요한 역할을 한다. 그러나 기존의 블루카본 생태계의 이산화탄소 흡수 능력에 대해 많은 연구가 진행되었으나, 잠재적 탄소흡수원인 갯벌의 탄소 저장 능력과 그 조절 요인에 대한 연구는 미비한 실정이다. 이에 본 연구에서는 황해 갯벌 퇴적물내 유기탄소의 시공간분포와 거동요인에 미치는 영향을 평가하였다.

첫째로, 한국 조간대 표층퇴적물내 총유기탄소의 시공간적 분포와 거동을 평가하였다. 조간대 환경의 대표성과 객관적 비교를 담보하기 위해 전형적 자연 갯벌 4개소와 닫힌 하구 1개소를 대상으로 2018년 1월부터 12월까지 월별 조사를 수행하였다. 조사 및 분석결과, 총 유기탄소 함량은 퇴적물 입자크기(입도)를 대변하는 니질 함량에 따라 결정됨이 확인되었다. 가로림만과 순천만 퇴적물은 저서미세조류 대발생에 기인하여 겨울철 총 유기탄소 함량이 높았고, 특히 $\delta^{13}C$ 값이 크게 증가했다. 반면 낙동강 하구 퇴적물은 장마철(9–10월)에 육상으로부터의 담수방류 영향으로 인해 $\delta^{13}C$와 $\delta^{15}N$ 값이 감소하는 것이 확인되었다.

둘째로, 한국 전 연안 갯벌 퇴적물내 유기탄소 저장량과 유기탄소 침적률의 산정을 위해 현장조사 자료와 원격탐사 기법을 활용하였다. 조사지역은 동서남해 7개 시도(경기, 충남, 전북, 전남, 경남, 경북, 강원) 내 21개 지역이었으며, 2017년부터 2020년까지 코어퇴적물을 분석하였고, 원격탐사기법을 통해 갯벌의 퇴적물 성상과 면적을 산정하였다. 염생식물이 서식하는 염습지에서는 식물의 일차생산을 통한 높은 탄소고정 능력으로 인해, 비식생 갯벌보다 상대적으로 높은 유기탄소 저장량을 보였다. 현장조사 자료와 원격탐사 기법을 통해, 국가 수준에서 한국 전 연안의 조간대 갯벌의 총 유기탄소 저장량 및 연간 유기탄소 침적률을 산정하였다.

셋째로, 외래식물 갯끈풀과 토착식물 갈대, 칠면초가 유기탄소 증가에 미치는 영향을 비교하기 위해 염생식물 종별 유기탄소 저장량 증가율을 분석하였다. 중국 7개지역과 한국 12개지역을 대상으로, 각 지역의 염생식물이

서식하는 염습지와 비식생 갯벌에서 조사를 실시하였다. 외래식물 갯끈풀이 우점하는 중국 염습지가 토착식물 갈대와 칠면초가 우점하는 한국 염습지보다 높은 유기탄소 저장량을 보였다. 동일 기간 동안 갯끈풀의 유기탄소 저장량 증가율은 칠면초와 갈대에 비해 높았으며, 이는 상대적으로 높은 일차생산량과 지하부 뿌리 생물량으로 인한 것으로 나타났다. 또한 갯끈풀 서식지는 비식생 갯벌과 갈대 서식지에 비해 온실가스 배출, 대형저서동물 먹이망, 퇴적물 안정도, 탄소침적의 관점에서 이점이 있는 것으로 확인되었다.

끝으로, 대규모 현장조사를 통해 황해 전 연안 갯벌의 유기탄소 저장량과 유기탄소 침적률을 산정하였다. 조사지역은 중국 5개 시도(랴오닝성, 허베이성, 톈진시, 산둥성, 장쑤성)내 19개 지역, 한국 5개 시도(경기, 충남, 전북, 전남, 경남)내 18개 지역에서 코어퇴적물을 채집하였다. 분석결과, 양식장, 도시 및 산업단지로부터 강을 통한 유기물질의 유입이 유기탄소 침적에 기여하는 것이 확인되었다. 황해 갯벌 퇴적물내 유기탄소 함량은 퇴적물 입도와 염생식물의 유무에 따라 결정되는 것으로 나타났다. 단위면적당 유기탄소 저장량과 갯벌 면적자료를 기반으로 황해 전 연안 갯벌의 총 유기탄소 저장량 21–171 Tg C과 연간 유기탄소 침적률 0.08–0.61 Tg C yr^{-1}; 0.29–2.24 Tg CO_2 eq. yr^{-1}을 추정하였다.

기존의 블루카본 생태계와 비교하였을 때 갯벌은 상대적은 낮은 단위면적당 유기탄소 저장량과 침적률을 보이나, 전 세계적으로 광활한 면적과 해당 서식지의 일차생산자인 저서미세조류를 고려할 때 갯벌도 또한 중요한 탄소흡수원임을 시사한다. 이상의 연구결과를 종합 요약하면, 황해 갯벌 퇴적물내 유기탄소 분포는 퇴적물 입도와 식생의 유무에 의해 가장 많은 영향을 받으며, 유기탄소 기원은 염생식물 종과 육상-해양기원 유기물 유입에 따라 변화되는 것이 확인되었다. 결과적으로, 본 연구는 황해 갯벌의 블루카본 잠재성과 이에 영향을 미치는 생태학적 특성에 대한 정보를 제공하며, 향후 황해 갯벌 퇴적물내 탄소순환 연구에 대한 중요한 기초자료로 활용될 수 있음을 시사한다.

주제어: 총 유기탄소, 유기탄소 저장량, 유기탄소 침적률, 블루카본, 탄소중립, 갯벌생태계, 황해

학 번: 2017-24161